DINUSH SHAYAMAN PRIYANKER BADDAVIDANA

Assessment of wave overtopping at Praia da Vitória, Terceira, Azores, with SWASH model

Faculdade de Ciências e Tecnologia

2025

DINUSH SHAYAMAN PRIYANKER BADDAVIDANA

Assessment of wave overtopping at Praia da Vitória, Terceira, Azores, with SWASH model

Master's in Coastal Hazards, Risks, Climate Change Impacts and Adaptation

Work performed under the supervision of:

Dr. Liliana Pinheiro (LNEC)
Dr. Juan L. Garzon (UALg)
Dr.Ana Catarina Zózimo(LNEC)

Faculdade de Ciências e Tecnologia

2025

Declaração de autoria de trabalho

Declaration of Authorship of work

Assessment of wave overtopping at Praia da Vitória, Terceira, Azores, with the SWASH model

Declaro ser o autor deste trabalho, que é original e inédito. Autores e trabalhos consultados estão devidamente citados no texto e constam da listagem de referências incluída.

I declare to be the author of this work, which is original and unpublished. Authors and works consulted are duly cited in the text and are included in the list of references.

Dinush Shayaman Priyankera Baddavidana

Lisbon, 24 July 2025

COPYRIGHT

ACKNOWLEDGEMENT

I would like to express my deepest gratitude to everyone who has supported and guided me throughout the course of this thesis.

First and foremost, I would like to thank my supervisor, Dr. Liliana Pinheiro, for her invaluable guidance, encouragement, and expertise. Her insightful feedback and constant support have been instrumental in the successful completion of this thesis.

I am also deeply grateful to Dr. Juan L. Garzon and Dr. Ana Catarina Zózimo for their valuable input and assistance during the research process.

A special thanks to the COASTHazar Programme coordinators: Prof. Javier López Lara, Prof. Óscar Ferreira, and Dr. Álvaro Semedo, as well as to all the professors, instructors, mentors, and staff from IHE Delft Institute for Water Education, Universidad de Cantabria, and Universidade do Algarve, for their ongoing support and guidance throughout my academic journey.

I would also like to acknowledge the "LIFE-GARACHICO Project—Coastal Flooding Adaptation to Climate Change through Flexible Strategies in Macaronesian Urban Areas" (LIFE20 CCA/ES/001641, 2021–2026), CNCA (National Center for Advanced Computing) for providing computational resources, the National Laboratory for Civil Engineering for their support during my internship and for providing data related to the physical model tests, and the project "RISK - Gestão do Risco em Infraestruturas Marítimas / LNEC 0603/1102/24209" for their contributions.

I want to extend my heartfelt appreciation to my family, especially my mother, my wife Hiranya Sudhari, my daughter Damsi Vinulya, and my son Siluna Damsithu, for their unwavering love, patience, and encouragement. Their belief in me has been a constant source of motivation.

Lastly, I would like to thank all my friends and colleagues for their support, companionship, and assistance in both academic and personal matters. Without their encouragement, this journey would not have been the same.

Thank you all for being part of this journey.

Abstract

The primary objective of this dissertation is to enhance the accuracy of overtopping predictions using the SWASH (Simulating WAves till SHore) model, for inclusion in the Early Warning System (EWS), HIDRALERTA, currently operational in Praia da Vitória. While existing tools within HIDRALERTA offer valuable insights, they have limitations in accurately representing waves and overtopping details. To address these limitations, this research tested the capabilities of the SWASH model by simulating past storm events and typical wave conditions across the two-dimensional model of the entire port and bay areas with complex coastal structures and bathymetry. Outcomes of the simulations were compared to predictions from the NN_OVERTOPPING2 neural network and observed images from extreme events.

In the SWASH model, coastal structures were modelled as impermeable layers, with bottom roughness incorporated to enhance energy dissipation from roughness and seepage. An unstructured triangular mesh was used for the computational domain. Manning's coefficient for the outer slope of the south breakwater, with tetrapod armour units, was calibrated using a physical model test conducted in February 2025 at the National Laboratory of Civil Engineering (LNEC). The model was replicated in SWASH at prototype scale, using two test cases that resulted in overtopping for calibration.

The results demonstrate that the SWASH model effectively simulates wave propagation and overtopping in harbour and bay areas, especially over complex coastal structures. Its accuracy in estimating wave propagation and overtopping is sensitive to wave energy interactions with the bottom and slopes, influenced by the Manning coefficient. While unstructured meshes enable large-domain simulations, the quality of the mesh affects both prediction accuracy and computational time. The model is stable when using implicit time integration but unstable with explicit methods. Despite some simulation instability, most simulations reached the maximum allowed simulation time on the National Distributed Computing Infrastructure (INCD) cluster. The model's accuracy is heavily dependent on bathymetric data, with results generally aligning with NN_OVERTOPPING2 predictions and observed images from extreme events, although underpredictions can occur. Parallel processing is currently limited to structured grids in

SWASH and, there is potential for efficiency improvements with unstructured meshes. Future studies should compare SWASH results with field data to fully assess its performance.

Keywords: Overtopping; Wave Propagation; SWASH ; Numerical modelling; Manning's coefficient

Resumo

Este trabalho contribui para o projeto LIFE-GARACHICO, que se centra na adaptação aos impactos das inundações costeiras e das alterações climáticas, através da aplicação de estratégias flexíveis em áreas urbanas da Macaronésia. A área em questão é o porto e a baía da Praia da Vitória, situados na ilha Terceira, nos Açores. Esta área é vulnerável aos riscos costeiros, que têm sido exacerbados pelas alterações climáticas.

O principal objetivo desta dissertação é aumentar a precisão das previsões de galgamento utilizando o modelo SWASH (Simulating WAves till SHore) ara integrar no Sistema de Alerta Precoce atualmente em funcionamento na Praia da Vitória, designado HIDRALERTA. Atualmente, este sistema depende de um modelo numérico de propagação linear de ondas (DREAMS) e de uma rede neural (NN_OVERTOPPING2), treinada com testes de modelos em escala, para fazer previsões de galgamento. Embora as ferramentas existentes no sistema HIDRALERTA forneçam informações valiosas, apresentam limitações na propagação não linear das ondas e na caracterização do galgamento. O modelo SWASH, baseado nas equações de águas rasas não lineares (NLSW), consegue simular uma vasta gama de ondas e calcular com precisão a rebentação induzida pela profundidade. Oferece representações mais precisas da refração e difração das ondas, especialmente em ambientes costeiros complexos, como portos e baías. Para abordar as limitações referidas, o presente estudo avaliou a capacidade do modelo em simular todo o porto e a baía, que apresentam estruturas costeiras complexas e uma batimetria variada, recorrendo à simulação de eventos de tempestades passadas e de condições de ondas habituais, e valida os resultados recorrendo à rede neural NN_OVERTOPPING2.

No modelo bidimensional SWASH, as estruturas costeiras foram modeladas como camadas impermeáveis, tendo sido incluída a rugosidade do fundo para melhorar a dissipação da energia causada pela mesma e pela infiltração. Foi utilizada uma malha triangular não estruturada como domínio de cálculo. Para calibrar o coeficiente de Manning do talude exterior do molhe sul, composto por blocos de betão do tipo tetrápodes, foi replicado no SWASH, à escala de protótipo, um ensaio em modelo físico realizado em fevereiro de 2025 no Laboratório Nacional de Engenharia Civil (LNEC) para uma secção transversal. Cada simulação foi executada

durante três horas, um tempo semelhante ao do teste de modelo físico. Dois casos de teste com o mesmo nível de maré, que resultaram em galgamento, foram utilizados para calibrar o coeficiente de Manning neste quebra-mar.

Os resultados mostraram que o desempenho do modelo SWASH (versão 11.01A) na estimativa do galgamento é sensível à calibração do coeficiente de Manning para o talude exterior do quebra-mar. Após a calibração, o modelo produziu bons resultados com um esforço computacional reduzido.

Para a preparação da batimetria no âmbito da simulação do modelo SWASH para o porto e a baía inteiros, estavam disponíveis dados de alta resolução de LiDAR para o quebra-mar sul e dados de levantamento batimétrico para a bacia do porto. No entanto, não existiam dados batimétricos para o quebra-mar norte, as séries de quebra-mares ou o muro de defesa costeira frontal. Por conseguinte, recorreram-se a desenhos de construção do repositório LNEC para determinar os níveis dessas estruturas costeiras.

As condições das ondas no Porto da Praia da Vitória e na baía foram caracterizadas com base em dados de reanálise ERA5 hindcast (1989-2024), disponibilizados pelo Centro Europeu de Previsões Meteorológicas de Médio Prazo (ECMWF). Para a simulação SWASH de todo o porto e baía, foram selecionados dois conjuntos de condições de ondas: eventos mais frequentes (MF) e eventos extremos (ST). Foram escolhidos diferentes cenários de altura das ondas, período, direção e nível de maré com base nos registos de dados horários.

O processo de validação incluiu parâmetros espectrais de ondas em várias localizações próximas das estruturas, bem como os caudais médios instantâneos de galgamento das ondas sobre essas mesmas estruturas. Foram simulados um total de nove cenários de teste, cobrindo eventos de tempestades passadas selecionados e as condições de ondas mais frequentes com base no regime de ondas. Os resultados mostraram que o modelo SWASH simula efetivamente a propagação de ondas em áreas portuárias e na baía, incluindo o galgamento sobre estruturas costeiras complexas. A sua precisão na estimativa da propagação das ondas e do galgamento foi sensível à interação da energia das ondas com o fundo e as encostas, que foi influenciada pelo coeficiente de Manning. Embora as malhas não estruturadas permitam a simulação de

grandes domínios, a qualidade da malha afeta tanto as previsões como o tempo de processamento. A estabilidade é crucial para o modelo, que é instável com integração explícita no tempo, mas estável ao utilizar métodos implícitos. O efeito da série temporal da altura das ondas nos volumes de galgamento diminui com a duração da simulação. A precisão do modelo depende fortemente dos dados batimétricos e os resultados geralmente coincidem com as previsões do NN_OVERTOPPING2, embora possam ocorrer subestimações.

Como ferramenta de previsão, o SWASH mostrou ser fiável, embora os tempos de processamento da CPU não sejam compatíveis com as necessidades diárias do HIDRALERTA. Atualmente, o processamento paralelo está limitado às malhas estruturadas, mas existe potencial para melhorar a eficiência com malhas não estruturadas.

Por conseguinte, será necessário desenvolver um substituto com base em pré-execuções extensivas do modelo e em algoritmos de aprendizagem automática. Este trabalho contribuiu para estabelecer uma configuração numérica eficaz para o efeito. Além disso, para avaliar definitivamente o desempenho do modelo SWASH, é necessário comparar os resultados com dados de campo em estudos futuros.

Palavras-chave: galgamento; propagação de ondas; modelo SWASH; modelação numérica; coeficiente de Manning

Table of Contents

List of figures

List of tables

Equations

List of notations

Symbol	Units	Means
Hs	m	Significant wave height (average of the highest 1/3 of wave heights in a record)
H_{mean}	m	Mean wave height
H_{max}	m	Maximum wave height
L	m	Wave length
L_0	m	Deep water wave length based on T ($=gT^2/(2\pi)$)
k		Wave number
n	$s/m^{1/3}$	Manning's friction coefficient
q	$m^3/s/m$ or l/s/m	Mean overtopping discharge per metre length of structure
$RSPE^{WP}$		Root Square Percentage Error for wave parameter
$RSPE^{V}$		Root Square Percentage Error for cumulative overtopping volume
RMSE	Unit of data	Root Mean Square Error

(Continued to next page)

List of notations

Symbol	Units	Means
t	s	• Time • Total duration of the test
T	s	Wave period
T_{max}	s	Maximum wave period
T_P	s	Peak wave period
MSL	m	Mean Sea Level
N_L		Length scale factor
N_P		Pressure scale factor
N_M		Mass scale factor
N_T		Time scale factor
N_V		Volume scale factor

List of acronyms

1D, 2D, 3D	One, two, three-Dimensional
ANN	Artificial Neural Network
CFL	Courant Friedrich Lewy
CLASH	Crest Level Assessment of coastal Structures by full scale monitoring, neural network prediction and Hazard analysis on permissible wave overtopping
CLIMAAT	CLIma e Meteorologia dos Arquipélagos ATlânticos (Climate and Meteorology of the Atlantic Archipelagos)
DREAMS	Diffraction Refraction Elliptic Approximation Mild Slope
ECMWF	European Centre for Medium-Range Weather Forecasts
JFlow	Jeremy Flow model
JONSWAP	JOint North Sea WAve Project
LiDAR	Light Detection And Ranging
LNEC	Laboratório Nacional de Engenharia Civil (National Laboratory for Civil Engineering)
MPI	Message Passing Interface
NLSW	Non-Linear Shallow Water
NN_Overtopping2	Neural Network for Overtopping (Version 2)

(Continued to next page)

List of acronyms

SVSW	Saint Venant Shallow Water
SWAN	Simulating WAves Nearshore
SWASH	Simulating WAves till Shore
TELEMAC	Short for the open TELEMAC-MASCARET system
TUFLOW	Two and one-dimensional Unsteady FLOW model
VARANS	Volume-Averaged Reynolds-Averaged Navier-Stokes
WAM	Wave Action Model
XBeach	eXtreme Beach behaviour model
MSL	Mean Sea Level
SWL	Still-Water-Level
TL	Tide Level
ZH	Zero Hidrográfico

1 Introduction

Coastal zones are home to 41% of the European population and 29% of the world's population. and support essential economic activities such as harbours, industries, and communication infrastructures. This concentration of people in coastal areas is quite significant and has been rising. Predictions suggest that the percentage of the global population living in coastal regions will continue to rise (Neumann *et al.*, 2015). . However, these areas are highly vulnerable to extreme weather events and climate change (European Environment Agency, 2015). Consequently, the impacts of climate change, including sea level rise and its associated effects, present significant threats to coastal communities, economic activities, and infrastructure, underscoring the increasing importance of safety and resilience in coastal areas.

Overtopping is a crucial phenomenon that significantly impacts the performance of onshore coastal structures, exposed to wave attacks. Overtopping occurs when the waves reach and pass the crest of the protection structure and is frequently measured as the mean overtopping discharge, expressed in litres per second or cubic meters per second per meter width. Safety and resilience of coastal areas depend on the capacity of coastal structures to prevent wave-driven coastal flooding, which is often assessed by measuring the overtopping discharge (Pillai *et al.*, 2016). Being able to predict and estimate the occurrence of overtopping of coastal structures is therefore crucial, and several established methods are available for quantifying it, including analytical methods, empirical methods, physical modelling, numerical modelling, and neural networks. Each method has distinct advantages and disadvantages (EurOtop, 2018). Many researchers have investigated the overtopping behaviour of coastal structures, including vertical walls, dikes, and rubble mound breakwaters, on a global scale (EurOtop, 2007, 2016, 2018; Victor *et al.*, 2012). Considering the limitations of the methods above and advancements in computational capacity, analysing overtopping hazards using numerical models has become a viable alternative(Suzuki *et al.*, 2020).

Recent advancements in numerical modelling and its integration with machine learning techniques have enabled Early Warning Systems (EWSs) to provide reliable hourly data on sea states and sea levels (Papadimitriou *et al.*, 2024). These systems are particularly beneficial in areas with dense infrastructure and high levels of human activity. The United Nations' initiative, "Early Warnings

for All," aims to ensure that everyone has access to early warning systems globally (United Nations, 2022).

Portugal has a coastline that stretches approximately 1,860 km, including the mainland and two archipelagos in the North Atlantic Ocean: the Azores and Madeira. These coastal regions frequently encounter hazards such as wave overtopping, flooding, and navigation difficulties (Pinheiro *et al*., 2023). To mitigate these risks, an EWS known as HIDRALERTA has been implemented as an adaptation measure in several coastal ports(Pinheiro *et al.*, 2023; Poseiro, 2019). This system covers six ports on the mainland and three ports in the Azores archipelago, namely on Terceira Island (Pinheiro *et al.*, 2023).

The HIDRALERTA system integrates various real-time numerical models to propagate waves from deep sea to nearshore, estimate the mean overtopping discharge, and calculate ship motions and mooring forces at three-hour intervals. It operates in real-time, enabling the detection of emergencies in coastal and harbour areas up to 72 hours in advance, with forecasts sent to decision-makers.

The system obtains forecasts (or hindcasts) of regional wind and wave characteristics from the European Centre for Medium-Range Weather Forecasts (ECMWF) and Copernicus Marine Service Forecasts (CMEMS), along with astronomical tide levels using Xtide (Flater, 2024). The SWAN numerical model propagates these deep-water parameters into shallow water (Booij *et al.*, 1999). The DREAMS (Fortes, 2002) numerical model propagates waves from the foreshore to shallow water and sheltered areas. To assess the wave parameters inside the port, either the DREAMS or BOUSS-WMH (Pinheiro *et al.*, 2011) numerical models are employed. This system generate forecasts of overtopping volume, movements, and mooring forces on a three hour basis , using specific models (NN_OVERTOPPING 2 neural network, Coeveld *et al.*, 2005, and MOORNAV numerical tool, Santos 1994) based on the site's bathymetry and structures characteristics along with wave, wind and currents predictions. Finally, these predictions are compared with pre-set threshold values to evaluate the probability of exceedance and determine the related risk level.

1.1 Motivation

To determine overtopping over port structures, the HIDRALERTA system uses DREAMS numerical model to simulate wave propagation from the nearshore into sheltered areas, such as bays, ports, and harbours, coupled with NN_OVERTTOPING2 tool, a neural network trained with measured data from laboratory experiments and field data, to predict the mean overtopping discharges. DREAMS model, developed by LNEC, is based on linear wave theory and represents monochromatic incident waves characterized by a single frequency and direction. Therefore, DREAMS model does not fully capture the complex interactions of actual sea state conditions and their propagation in the nearshore area. NN_OVERTOPPING2, developed by WL Delft Hydraulics, was specifically designed to predict mean overtopping discharges. It is built upon a database compiled from physical tests and field data as part of the European Union project CLASH (Crest Level Assessment of Coastal Structures), and utilises hydraulic and structural parameters from the EurOtop manual.

These databases are based on schematized tests conducted worldwide, which, while helpful, do not fully represent real overtopping events in full-scale harbours and bays. To achieve accurate predictions of overtopping using NNs, it is essential to carefully select data that is relevant to the specific application. The performance of these ANN models could be significantly improved if they were trained using overtopping data from full-scale harbours and bays, as this would more accurately reflect the complex coastal structures and bathymetry that influence wave overtopping under real-world conditions.

This research aims to test the capability of the SWASH numerical model to propagate waves from nearshore into shelter areas and produce overtopping on an entire harbour and bay scale, considering complex coastal structures and bathymetry. These findings will be valuable resources for developing a database for Praia da Vitória using the SWASH numerical model. This database will then serve as a crucial resource for creating the training dataset of a NN that can accurately predict both wave characteristics near the structures and the overtopping volumes in Praia da Vitória port and bay area.

1.2 Objectives

In order to improve the accuracy of wave and overtopping predictions in the HIDRALERTA EWS, it is intended to replace the existing coupled models DREAMS-NN_OVERTOPPING2 by a more suited non-linear non-hydrostatic model that can address more accurately the complex behaviour of waves near shore and their interaction with coastal structures. SWASH, which is based on the shallow water equations is a good candidate, among others, namely based ones based Boussinesq-type equations or on Reynolds Averaged Navier-Stokes equations. All these models have the same disadvantage of being very computationally demanding and are still not suited for operational daily multiple runs.

The main objective of this study is to investigate if SWASH is suited to replace the existing models in the HIDRALERTA EWS and implement in SWASH a two-dimensional numerical set-up for the Praia da Vitória full-scale harbour and bay areas.

To do so the study here presented was divided into two main parts:

1. Calibration, validation and sensitivity analysis;
   Firstly a calibration process was done to calibrate Manning's coefficient for the outer slope of the south breakwater by replicating physical model tests (Lemos *et al*., 2025) for a cross section using a two-dimensional SWASH model at prototype scale. using the physical model tests results it was possible to validate SWASH implementation.
   Then, to identify the key factors that influence the accuracy of the two-dimensional SWASH model in simulating overtopping processes, a sensitivity analysis was performed to assess the impact of mesh resolution and quality, as well as seeding number, on computational time, the prediction of cumulative overtopping volume, and the accuracy of wave parameter predictions at specific locations.
2. Simulation of past storm events and typical wave conditions and comparison with HIDRALERTA's results and historical records.
   SWASH model was then run at prototype scale, covering the entire harbour and bay of Praia da Vitória, the model's results were compared with significant wave height

predictions from the DREAMS numerical model, overtopping predictions from the NN_OVERTOPPING2 neural network, and observed images of extreme events.

1.3 Wave overtopping estimation and modelling

Wave overtopping of coastal structures can be divided into two categories: white water overtopping and green water overtopping. Green water overtopping is particularly concerning because it occurs when a continuous sheet of water flows over the crest of the structure, creating a significant hazard. In contrast, white water overtopping occurs when waves break against the structure, generating spray that exceeds its crest, which the momentum of water particles or wind can assist. Both types of overtopping present substantial risks; green water overtopping can cause widespread flooding and damage, while white water overtopping can lead to localised hazards, such as reduced visibility and potential damage to nearby infrastructure (EurOtop, 2018).

The volume of overtopping over a breakwater is influenced by several factors, including characteristics of incoming waves: the incident significant wave height ($H_{mo,\ toe}$) and the spectral period ($T_{m-1,0\ toe}$) at the toe of the structure. Other factors include the geometry of the structure, such as crest freeboard and the seaward slope of the breakwater, as well as the properties of armour layer materials, including the roughness coefficient and its porosity (Altomare *et al.*, 2016). Understanding these factors is crucial, as they directly influence the prediction of overtopping volumes and the associated risks.

Various wave overtopping prediction models consider wave parameters at either the toe of the structure, at the toe of the foreshore, or offshore (Mase *et al.*, 2015). Although parameters measured offshore are often more convenient to define, each method has its advantages and disadvantages (Altomare *et al.*, 2016). Hedges & Reis (2004) argue that using offshore wave parameters may overlook significant factors, such as energy dissipation due to wave-current interaction, wave energy spreading during propagation, and wave interaction with the structure. Furthermore, they explain that it is difficult to separate the influence of the foreshore and the structure, as they function as a single entity when offshore wave parameters are defined.

Overtopping is inherently a random process, and the velocity of overtopping discharge, flow thickness, wave-by-wave volume, and spatial distribution are crucial for understanding its impacts (EurOtop, 2018; Van Der Meer *et al.*, 2022). The behaviour of these parameters is primarily influenced by the materials used behind the crest of the breakwater. For example, if permeable materials like rocks or grass are employed, some overtopping discharge may be absorbed, which can reduce the impact on people, infrastructure, and vegetation behind the crest. Conversely, if impermeable materials are used, the risks associated with overtopping increase.

Over recent decades, methods for predicting overtopping at coastal structures have evolved, increasing their applicability while addressing the complexities of the overtopping phenomenon. Accurate estimation of wave overtopping is crucial for designing effective coastal structures and assessing the risk levels of existing structures and surrounding communities (EurOtop, 2018). The following sections will provide a detailed discussion of overtopping prediction methods, including empirical formulas, neural networks, and numerical modelling.

1.3.1 Empirical Formulae

Empirical formulae are commonly used in coastal engineering, particularly for predicting overtopping, due to their ease of application. These formulae simplify the overtopping process and rely heavily on field observation data as well as physical model data obtained in laboratory settings. They incorporate key parameters such as overtopping discharge, wave characteristics, and structural features. The coefficients within these equations are adjusted to align with actual field measurements and laboratory results (EurOtop, 2018).

Owen (1980) introduced a formula to predict the overtopping discharge of seawalls, highlighting its importance for design engineers who need to evaluate existing coastal structures and design new seawalls with allowable overtopping discharges in mind. This study examined overtopping discharge using physical models of both simple and berm seawalls, considering the effects of wave obliqueness and the roughness of the structure's slope under irregular wave conditions.

Goda (1985) developed six distinct graphs to represent wave overtopping for vertical smooth walls and vertical walls topped with rubble mounds. This research examined three different wave steepness values: 0.012, 0.017, and 0.036, alongside two foreshore slopes of 1:30 and 1:10. The dimensionless overtopping discharge is denoted as $Q^{\#G}$, which refers to the volume of overtopping. In the graphs, $Q^{\#G}$ is plotted against the ratio h/H_{so}, where H_{so} is the significant wave height and h represents the water depth at the toe of the structure. However, since these graphs are created for a limited range of offshore wave steepness values, their applicability heavily relies on the interpolation process, which is seen as a significant drawback of this method (Besley, 1999).

Herbert (1993) built upon the graphs created by Goda (1985). After conducting a series of physical model tests, Herbert (1993) expanded the scope of Goda's graphs to include wave climates, tidal ranges, and structural designs commonly seen in the UK coastal environment.

Later research conducted by De Waal & Van Der Meer (1992), which involved 200 tests in wave flumes and about 160 tests in wave basins, led to the development of a new expression for overtopping, specifically addressing both breaking waves and non-breaking waves. This study compared the reliability of overtopping discharge and crest freeboard as proposed by TAW (1974) and Owen (1980). The findings facilitated the derivation of an expression based on the exponential functions introduced by Owen (1980). In this formula, two slopes,1:1.5 and 1:8, were examined, and key wave parameters, such as wave height and peak wave period at the toe of the structure, were considered. The analysis also considered factors influencing these parameters, including slope roughness, shallow water conditions, obliqueness of incident waves, and the presence of a berm.

Van der Meer & Janssen (1994) expanded upon the work of De Waal & Van Der Meer (1992) by incorporating the complexities of the wave spectrum into their analysis. They introduced the concept of an equivalent peak wave period, calculated as a weighted average of all the peaks within the spectrum. This method was later adopted in the EurOtop 2018 manual, which established the idea of the spectrum wave period. Furthermore, Van Gent (1999) demonstrated that the spectrum period is a more accurate parameter for predicting overtopping compared to the peak wave period.

Empirical formulae are valuable tools during the design phase of coastal structures; however, they also have limitations. One significant limitation is that these formulae assume the water depth

continuously decreases as it approaches the structure. However, this assumption does not accurately reflect real-world conditions. To address this issue, Mase *et al.* (2013) introduced a formula for calculating wave runup and wave overtopping for seawalls constructed on land or in very shallow foreshore areas. They define an imaginary slope and use the calculated expected runup to estimate the overtopping discharge. However, uncertainties in calculating the depth of wave breaking and directional spreading between the offshore area and the toe of the structure impose limitations on the application of this formula.

Altomare *et al.* (2016) developed a new formula that introduces equivalent slopes and different coefficients; however, it has limitations for shallow and very shallow areas. Lashley *et al.* (2021) further explored this topic. They introduced a concept for capturing the foreshore effect by utilising the foreshore slope and the relative water level at the toe of the structure, based on deep-water wave characteristics. However, Lashley *et al.* (2021) emphasise the necessity for further development of this expression to cover a broader range of foreshore slopes and shallow water depths.

1.3.2 Neural Networks

Artificial Neural Networks (ANNs) are powerful tools used in coastal engineering to predict wave overtopping discharge. These models are trained on large datasets collected from both experimental and field data.

The European Union project CLASH developed a comprehensive database compiled from both physical model tests and field data. This database includes overtopping data collected from physical model tests and prototype investigations for various coastal structures around the globe, enabling researchers to create ANNs for predicting overtopping. The NN_OVERTOPPING2 model (Coeveld *et al.*, 2005) was developed at WL Delft Hydraulics specifically to predict overtopping discharge. The model considers 15 input parameters that describe both the hydraulic and structural characteristics of coastal defences. The parameters that were considered in structural analysis included the wave attack angle (β) relative to the normal of the structure (°) and the water depths surrounding the structure, specifically the water depth in front of the structure (h), at the

toe (h_t), and on the berm (h_b). The widths of key structural components included the toe width (B_t), the berm width (B), and the berm slope ($\tan \alpha_B$). The characteristics of the crest consisted of the crest width (G_c), the armour crest freeboard (A_c), and the crest freeboard (R_c). In terms of wave dynamics, significant wave height ($H_{m0,toe}$) and mean wave period ($T_{m-1,toe}$) at the toe of the structure were considered. Additionally, the structural features included the downward slope of the berm ($\cot \alpha_d$), the upward slope of the berm ($\cot \alpha_u$), and the roughness or permeability of the structure (γ_f). Figure 1.1 illustrates the input parameters.

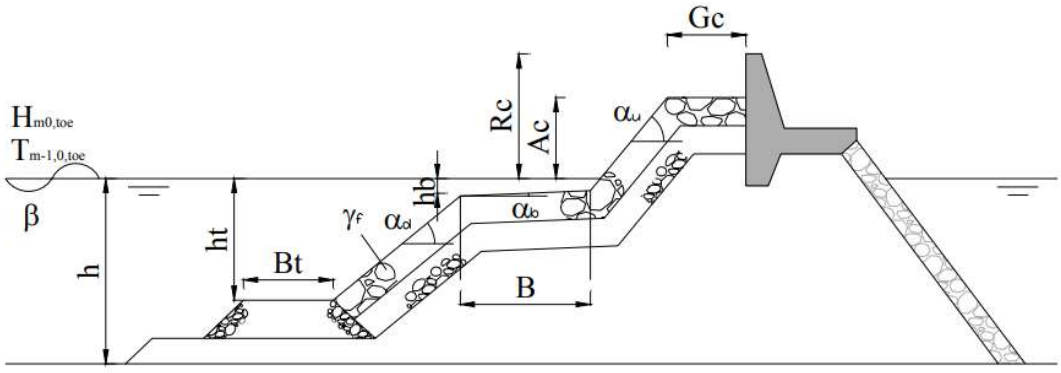

Figure 1.1- Input parameters used in NN_OVERTOPPING2 for estimating wave overtopping discharge at coastal structures.

This ANN was based on the multi-layer perceptron (MLP) architecture, which is a widely used model for regression tasks. The model was trained using a large dataset comprising 8,372 input-output combinations collected from various international research institutes worldwide. In this model, the output parameter is the mean overtopping discharge, which is further detailed into several quantiles: $q_{2.5\%}$, $q_{5\%}$, $q_{25\%}$, $q_{50\%}$, $q_{75\%}$, $q_{95\%}$, and $q_{97.5\%}$. These quantiles help to illustrate the uncertainty associated with the overtopping prediction.

Zanuttigh *et al.* (2014) developed a new ANN based on the original CLASH model (Van Gent *et al.*, 2007), focusing on wave overtopping discharge and the ANN created by Zanuttigh *et al.* (2013) for estimating wave reflection. This new ANN can predict parameters associated with wave-structure interactions, including wave overtopping discharge, wave reflection, and wave transmission. The authors observed that overtopping discharge tends to be overestimated for small overtopping events ($q < 10^{-5}$ $m^3/s/m$). They also noted that the most significant variability in the data occurs in scenarios with zero freeboard, while the error diminishes as the ratio of R_c/H_{m0}

increases. Thus, they concluded that variability is primarily influenced by the R_c/H_{m0} ratio, which is a critical factor in determining overtopping discharge.

In a later study, Zanuttigh *et al.* (2016) improved the NN developed by Zanuttigh *et al.* (2014). This enhancement focused on better predicting overtopping discharge for both extremely low values ($q < 10^{-6}$ m³/s/m) and extremely high values ($q > 10^{-3}$ m³/s/m). The study aimed to increase the accuracy of predicting very low overtopping discharge values by refining and intensifying the training process, as noted by Van Gent *et al.* (2007). Verhaeghe *et al.* (2008) primarily focused on training ANNs for overtopping discharge values greater than 10^{-6} m³/s/m. They indicated that only laboratory data was used to train the ANN, which confined scale and model effects to laboratory conditions. This limitation closely relates to structural properties, such as porosity, permeability, and roughness, as well as hydraulic loads, including wind, currents, and spray Zanuttigh *et al.* (2016). Advancements in ANN-based overtopping prediction models are vital for enhancing the accuracy of safety assessments for coastal structures and for designing more resilient infrastructure in coastal zones.

1.3.3 Numerical Models

Recent advancements in computer hardware and numerical techniques have made the application of numerical models to estimate overtopping increasingly popular. These models, which analyse intermediate and shallow water dynamics, depend on various hydrodynamic equations, each with its strengths and weaknesses based on the specific processes being examined, including wave propagation, overtopping, and flood assessment.

The Saint-Venant Shallow Water (SVSW) equation is often used to simulate large-scale shallow water flows due to its depth-averaging characteristics. Several models based on the SVSW equation have been developed to model coastal processes effectively. Notable examples include LISFLOOD-FP (Bates & De Roo, 2000) and JFlow (Lamb *et al.*, 2009). Furthermore, more advanced models like FUNWAVE-TVD (Shi *et al.*, 2016) improve upon the basic shallow water equations by incorporating higher-order terms that account for wave refraction, breaking, and transformation (Madsen & Sørensen, 1992).

Other models, such as those based on the Volume-Averaged Reynolds-Averaged Navier-Stokes (VARANS) equation, are employed to simulate complex fluid flows. These models effectively capture dynamics such as turbulence and wave-structure interactions (Hsu & Liu, 2004). Several models that utilize the VARANS equation have been developed, including IH2VOF (Lara *et al.*, 2011), OpenFOAM/IHFOAM (Losada *et al.*, 2008), and DualSPHysics (Gomez-Gesteira *et al.*, 2012). However, the high computational costs associated with these models may limit their applicability for predicting overtopping, particularly in real-time simulations.

Models based on the Nonlinear Shallow Water (NLSW) equation are more computationally efficient and easier to use than other methods. The NLSW equation is derived from the Navier-Stokes equation with certain simplifying assumptions: vertical acceleration is negligible, pressure within the water is primarily influenced by hydrostatic pressure, the horizontal length scale is much larger than the vertical scale, and vertical velocity is neglected. As a result, the NLSW equation can accurately simulate shallow water flow. It is commonly used to model wave overtopping and wave propagation over low-crested structures (EurOtop, 2018). Several variants of the NLSW model have been developed for simulating wave overtopping in nearshore environments, including AMAZON-SC (Hu *et al.*, 2000), XBeach (Roelvink *et al.*, 2009), and SWASH (Zijlema et al., 2011). The SWASH model efficiently simulates nearshore wave dynamics with low computational costs. Its integration of wave and flow equations makes it ideal for coastal environments, and it has become a reliable tool for predicting overtopping and conducting coastal studies. Characteristics of the SWASH model will be further discussed in the next chapter.

1.3.3.1 SWASH model

The SWASH (Simulating WAves till SHore) model was developed by Delft University of Technology and is based on the NLSW equation. This model includes features such as non-hydrostatic pressure and shock capturing, enabling it to effectively simulate various phenomena, including wave propagation, wave breaking, wave-structure interaction, wave transmission through structures, wave-induced circulation, and non-linear interactions. The development of this numerical model is attributed to the work of Stelling & Zijlema (2003), Stelling & Duinmeijer (2003), as well as Zijlema & Stelling (2005, 2008) and Zijlema *et al.* (2011).

In the SWASH model, the NLSW equation is deployed to explain the non-hydrostatic, free-surface, and rotational flow. The two-dimensional, depth-averaged shallow water equations are given as follows:

$$\frac{\partial u}{\partial x}+\frac{\partial v}{\partial y}+\frac{\partial \omega}{\partial z}=0 \tag{1}$$

$$\frac{\partial u}{\partial t}+\frac{\partial u^2}{\partial x}+\frac{\partial vu}{\partial y}+\frac{\partial w}{\partial z}+\frac{g}{\rho_0}\frac{\partial \zeta}{\partial x}+C_f\frac{u|u|}{h}=\frac{1}{h}\left(\frac{\partial h\tau_{xx}}{\partial x}+\frac{\partial h\tau_{xy}}{\partial y}\right) \tag{2}$$

$$\frac{\partial v}{\partial t}+\frac{\partial v^2}{\partial y}+\frac{\partial uv}{\partial x}+\frac{\partial wv}{\partial z}+\frac{g}{\rho_0}\frac{\partial \zeta}{\partial y}+C_f\frac{u|u|}{h}=\frac{1}{h}\left(\frac{\partial h\tau_{yx}}{\partial x}+\frac{\partial h\tau_{yy}}{\partial y}\right) \tag{3}$$

$$\frac{\partial w}{\partial z}+\frac{1}{\rho_0}\frac{\partial q}{\partial z}=0 \tag{4}$$

$$\tau_{xx}=2\nu_t\frac{\partial u}{\partial x}\ ,\tau_{xy}=\ \tau_{yx}\ =\ \nu_t\left(\frac{\partial v}{\partial x}+\frac{\partial u}{\partial y}\right)\ ,\tau_{yy}=2\nu_t\frac{\partial v}{\partial y} \tag{5}$$

Where *u, v,* and *w* are depth average flow velocities in x-direction, y-direction, and z-direction, respectively and x, y and z are located at the still water level and z-axis pointing upwards. ζ is the surface elevation, which is measured from the still water level, and *h* is the total depth. *q* is the non-hydrostatic pressure and density has been normalised, g is the gravitational acceleration, C_f is the dimensionless bottom friction coefficient, and V_t is the horizontal eddy viscosity due to wave breaking and sub-grid turbulence. In addition, τ_{xx} , τ_{yy} , τ_{xy} , $and\ \tau_{yx}$ terms express the horizontal turbulent stress in each plane.

Suzuki *et al.* (2014) conducted a study on dike overtopping, effectively validating the SWASH model with in-situ measured data. They developed both one-dimensional and two-dimensional models to compare the performance of the SWASH model during the overtopping process. However, they encountered computational instability in the two-dimensional model when increasing grid resolution, which led them to propose an alternative simulation method. This method employed a two-dimensional model for wave propagation until it reached the toe of the structure, after which a one-dimensional model was used for overtopping calculations. They noted

that overtopping discharge and the frequency of overtopping events were significantly influenced by grid resolution and bottom friction, while wave propagation remained relatively unaffected.

In a subsequent study, Suzuki *et al.* (2017) expanded their investigation into the SWASH model's ability to estimate overtopping for impermeable coastal structures. Their assessment incorporated 124 individual tests across four different physical models, highlighting the model's capability to reproduce key wave parameters, including significant wave height, spectral wave period, wave setup, and the time series of water surface elevation at specific points. They emphasised the critical importance of accurately modelling these parameters at the toe of the structures to estimate overtopping discharge reliably. However, they found that the model struggled to accurately estimate overtopping discharge rates below 1 litre per second per meter at the prototype scale.

While average overtopping discharge and maximum overtopping volume are essential parameters for assessing overtopping impacts, they can often lead to an overestimation of hazard levels. Recognising this, Suzuki *et al.* (2020) emphasised the need to evaluate overtopping velocity and depth over time for a more precise understanding of associated risks. They conducted a two-dimensional vertical SWASH simulation represented by two vertical layers to model frequency dispersion in the vertical direction, effectively capturing the influence of infragravity waves, which are critical to overtopping. Their findings indicated that the presence of a vertical wall at the end of a promenade could lead to increased flow depth and negative flow velocity, thereby heightening the risk of overtopping hazards.

Tuozzo *et al.* (2024) explored the effects of low-frequency waves at the toe of a structure on mean overtopping discharge using the SWASH model. They proposed a formula for calculating mean overtopping discharge for vertical seawalls under shallow water conditions, applicable in both wave-breaking and non-breaking scenarios. Unlike existing formulas that rely on spectral wave parameters such as significant wave height and spectral wave period, their approach utilises the average of the highest one-fourth wave displacement at the toe. The study primarily focused on long-crested waves, emphasising the need for further validation against oblique short-crested waves, which significantly affect mean overtopping discharge.

Modelling permeable structures, such as breakwaters, within the SWASH framework presents challenges in simulating energy dissipation and flow resistance in the porous layers of the

structure. Pés, V.M. (2013) assessed the applicability of SWASH for predicting overtopping in porous structures. The author indicated that when modelling a breakwater as a permeable structure, SWASH calculates average porosity across the structure's width based on its porosity, height, and water depth, assuming the value 1 for water porosity. This calculated porosity is then applied to the total water depth, excluding the breakwater, resulting in the breakwater behaving like a sponge layer that allows continuous flow without overtopping, contrary to impermeable structures.

Furthermore, the porosity reduces the horizontal velocity component but fails to adequately dampen the vertical component in the momentum conservation equation. Consequently, there is a continuous water surface both inside and outside the structure, with no discontinuity at the water-breakwater interface. As waves pass through the breakwater, some of their momentum is dissipated due to increased resistance across its width, while another portion accumulates in front of the structure due to insufficient vertical damping, causing the waves to interact with the breakwater earlier than anticipated.

Salas Pérez (2014) further investigated the performance of the SWASH model on permeable breakwaters, validating his findings against field measurements. The study confirmed that SWASH effectively models overtopping processes for impermeable and low-permeable structures; however, it struggles with highly permeable structures due to limitations in simulating wave dissipation within porous media. Salas Pérez emphasised the need for substantial calibration of the Manning and Forchheimer coefficients, which represent porosity in the model, to improve the accuracy of overtopping predictions for permeable structures using SWASH.

Zhang *et al.* (2020) introduced a novel approach for predicting overtopping at permeable breakwaters, addressing the challenges of simulating wave dissipation in porous structures. In their study, they focused on breakwaters with accropode armour layers. They modelled the breakwater as an impermeable structure and incorporated an apparent friction coefficient to account for wave energy dissipation caused by surface roughness and seepage.

To support their findings, researchers have conducted several simulations based on physical model tests of breakwaters with accropode armour from the CLASH database. They adjusted the Manning coefficient in their numerical model to replicate the mean overtopping discharge obtained in the physical model tests. Additionally, Zhang *et al.* (2020) examined the relationship among the ratio

R_c/H_{m0}, the wave steepness(S_{op}), slope angle, and Manning's coefficients. They proposed an equation to determine the apparent friction coefficient for breakwaters with accropode armour layers. Manz *et al.* (2022) implemented a one-dimensional SWASH model to analyse a breakwater featuring armour layers with antifer and tetrapod, primarily aiming to demonstrate wave overtopping and calibrate the model using predictions from NN_OVERTOPPING2 (Coeveld *et al.*, 2005). The breakwater was treated as an impermeable structure, and an apparent friction coefficient was introduced to account for energy dissipation caused by surface roughness and seepage from the porous layers. To estimate this apparent friction coefficient for breakwaters with antifer and tetrapod armour layers, they developed two equations. They emphasised the necessity of calibrating the model with field data instead of relying solely on predictions from NN_OVERTOPPING2. Additionally, the study highlighted the importance of considering the angle of incident waves alongside parameters such as R_c/H_{mo} and Sop, which were carefully analysed during the research**.**

2 Case Study Area

2.1 Praia da Vitória harbour and bay area

Terceira is an island in the Azores archipelago, located in the North Atlantic Ocean, approximately 1,500 km from the west coast of Portugal. It covers an area of 400.6 km², and Praia da Vitória, located on the eastern coast of Terceira Island, is becoming increasingly vulnerable to coastal hazards intensified by climate change (Fortes *et al.*, 2020). The harbour and its surrounding infrastructure are crucial to the region's economy; however, their susceptibility to wave overtopping and other coastal hazards poses significant challenges. Figure 2.1 shows a map of the Azores archipelago, including the study area.

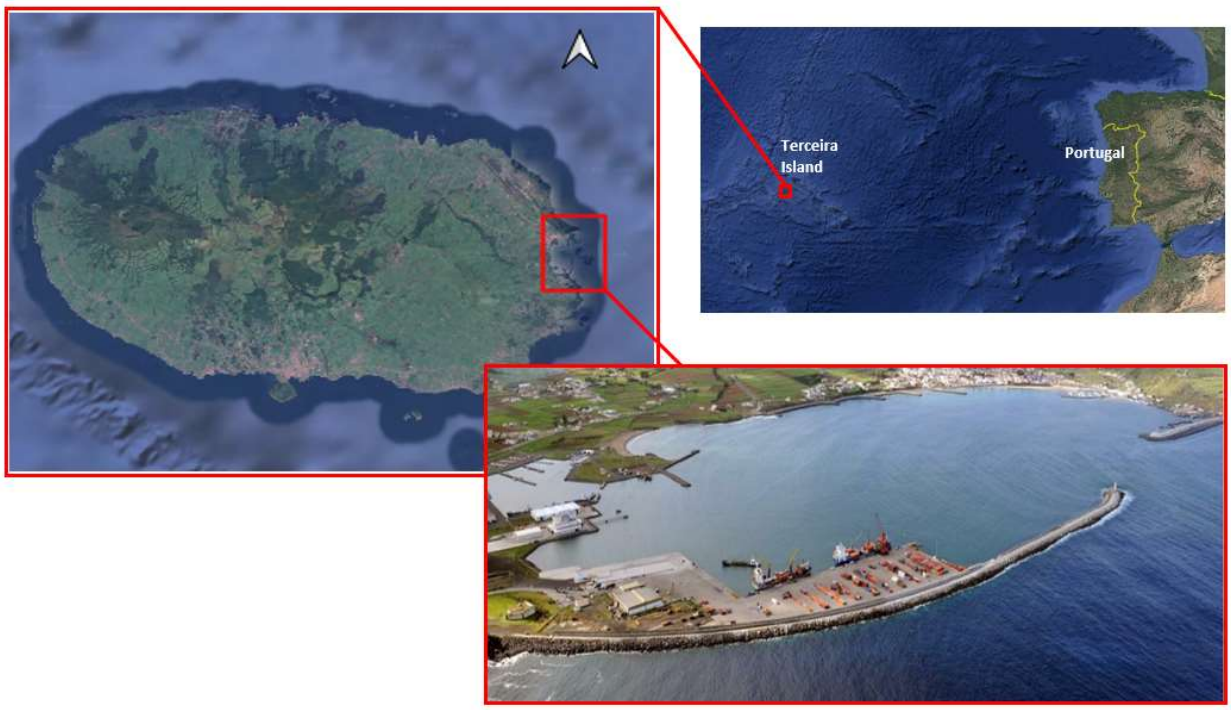

Figure 2.1 -Map of the Azores archipelago, Portugal, created using Google Earth imagery (© Google, 2025)

The bay and the harbour are sheltered by two main breakwaters: the north breakwater and the south breakwater. The bay also has a series of groynes and a frontal defence wall (Figure 2.2).

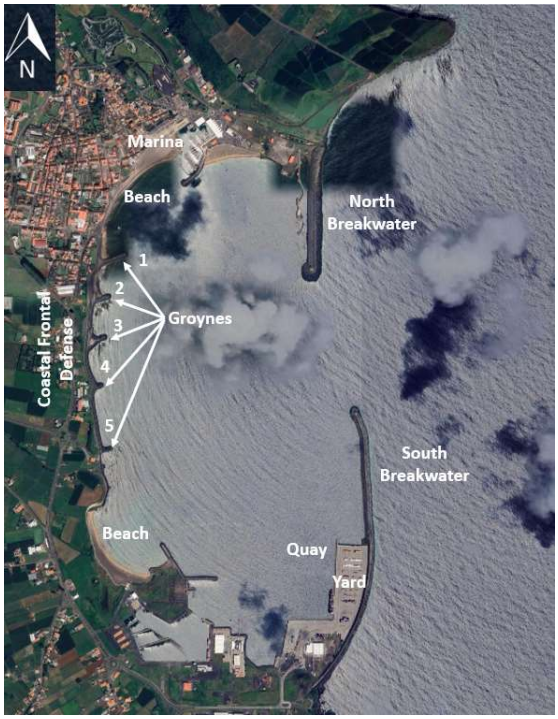

Figure 2.2- Coastal and port structures in Praia da Vitória, created using Google Earth imagery (© Google, 2025).

The south breakwater is approximately 1,300 m long and provides shelter for the commercial port, the fishing harbour, the cement terminal, the "Graciosenses" maritime transport sector, and the passenger quay. In the commercial port, there are three quays (Figure 2.3): Quay 7, Quay 10, and Quay 12. Quay 10 and Quay 12 are dedicated to commercial ships, while Quay 7 is designated for inter-island passenger traffic. Quay 7 features 150 m of dock with a depth of approximately 7 m, accommodating ships up to 120 m in length. Quay 10 offers 200 m of dock and a depth of about 10 m, suitable for vessels up to 150 m. Quay 12, the largest, has 350 m of dock space and a depth of 12 m, handling ships up to 270 m. It is equipped with two cranes; Gottwald, which is 45 m high with a load capacity of 100 tons, and Grove 5180, which stands at 60 m with a capacity of 180 tons. The maximum capacity of Quay 12 is 3,200 containers.

Figure 2.3- Quay wall arrangement of commercial harbour (left), and aerial view of container yard and south breakwater(right) in Praia da Vitoria.

2.2 Wave and wind regimes

To characterise the wave conditions at Praia da Vitória harbour and bay, wave characteristics at point A were analysed. The data, available from 1989 to 2024, was obtained from the database of the HIDRALERTA system. In this system, the ERA5 hindcast data, collected at points N, S, E, and W (Figure 2.4), is the fifth-generation ECMWF (maintained by the European Centre for Medium-Range Weather Forecasts) reanalysis for global climate and weather. The data were available at a 6-hour frequency with a spatial resolution of 80 km from January 1, 1979, and at a 1-hour frequency with a spatial resolution of 30 km from January 1, 2008. Then, a 3-nested-grid setup of the SWAN model, built into the HIDRALERTA system, propagated the wave spectral parameters from deep water to the foreshore of Praia da Vitória Port.

In the HIDRALERTA system, to validate the numerical results, wave data collected at the wave buoy (point B), located 830 m deep, were compared with the numerical results from the SWAN simulations. The wave regime at Praia da Vitória harbour and bay was derived from SWAN data at point A. In the HIDRALERTA system, this data is used as forcing conditions for the DREAMS model. In this study as well, forcing conditions were obtained from point A. The distribution of significant wave height (Hs) across different directions is illustrated in the polar plot in Figure 2.5. The most frequent wave direction observed was from the north (N), followed closely by the northeast (NE). The highest Hs ranged between 5.5 m and 6 m, although these occurrences

represented less than 1% of the total events. Despite their low occurrence percentage, these events represent significant weather impacts on the region during the observation period.

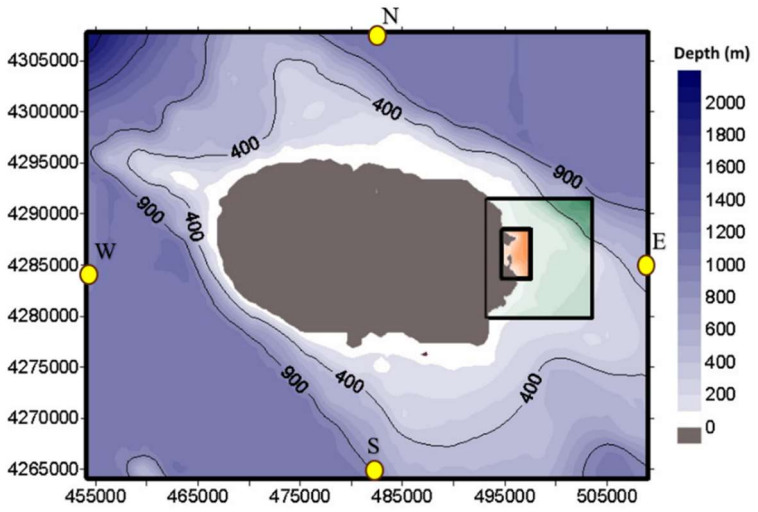

Figure 2.4- ERA5 hindcast data (ECMWF) collection points (N, S, E, W) and SWAN's 3-nested grids (built into the HIDRALERTA system).

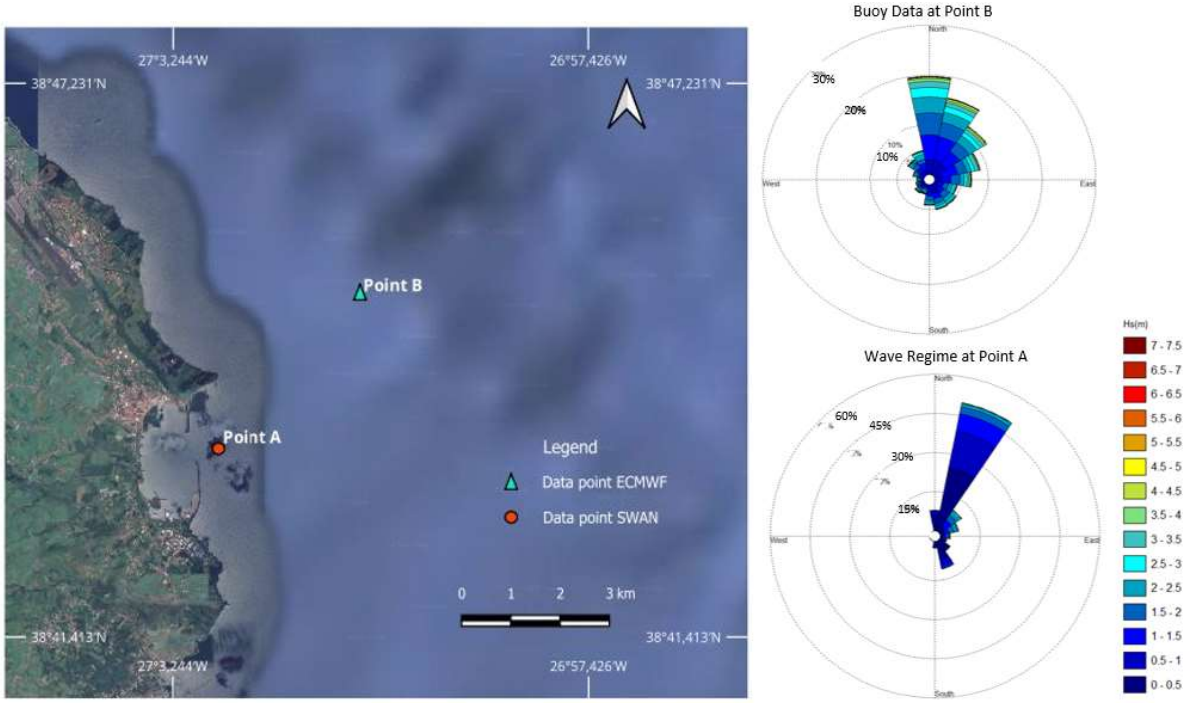

Figure 2.5- Wave regimes at points A and B based on data from 1989 to 2024. Top right: data from wave buoy records at point B . Bottom right: data from SWAN built-in model in the HIDRALERTA system at point A. Created using QGIS 3.36 and Google Earth imagery (© Google, 2025)

Analysing the wave regime at point A, based on the SWAN model data from 1989 to 2024 (Figure 2.5), it can be seen that the most dominant wave direction was north-north-east (NNE). The most frequent Hs fell within the ranges of 0 to 0.5 m, 0.5 m to 1 m, and 1 m to 1.5 m. The occurrence percentages for these ranges were approximately 21%, 11%, and 5%, respectively. Additionally, Hs of 1.5 m to 2 m were observed with an occurrence percentage of about 2%. While Hs between 2 m and 3 m were noted, the occurrence percentage was minimal, being less than 1%.

To better understand how these conditions vary throughout the year, the analysis was extended to observe the monthly and seasonal variation of wave data from 1989 to 2024.

The maximum wave height during the winter season was greater than 4 m for most of the time (Figure 2.6 (a)). This indicates that wave conditions in the Praia da Vitória coastal area are significantly impacted during the winter. A wave height of 6.2 m was recorded in March 2004, while a height of 6.83 m was observed in February 2005. Additionally, wave heights between 5 m and 6 m were recorded in only four years: 1993, 2001, 2007, and 2008. Throughout the year, the average monthly maximum period remained relatively stable at around 10 s, showing no significant fluctuations. A similar trend can be observed in the direction of wave heights, resulting in an incident angle of approximately 60 degrees. This consistency in wave period and direction highlights the complex dynamics of wave behaviour in this coastal region.

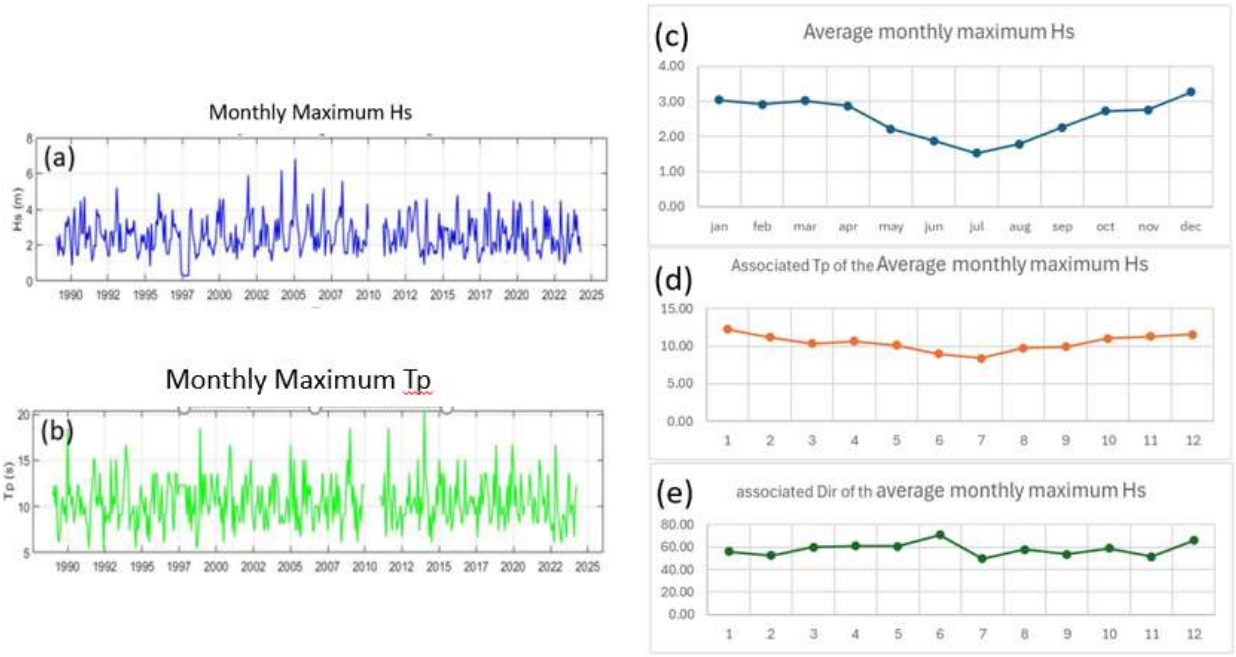

Figure 2.6- Monthly average analysis of wave parameters (1990-2025),(a) monthly maximum H_s, (b) monthly maximum T_p, (c) average maximum H_s, (d) associated T_p of the average maximum H_s, and (e) associated direction of the average maximum H_s, based on data from 1989 to 2024 at point A from SWAN built-in model in the HIDRALERTA system.

2.3 Past overtopping events and consequences

Praia da Vitória Harbour has faced significant challenges due to wave overtopping over the years. On December 21, 2001, the breakwater experienced severe overtopping, leading to significant damage to the structures. High waves coming from the southeast and northeast severely damaged the north and south breakwaters, and caused flooding in the container yard of the commercial harbour (Figure 2.7).

Figure 2.7- Damage to the south and north breakwater after the storm event on 21st December 2001 (*Source:* Poseiro (2019))

Additionally, on February 26th and 27th, 2005, while rehabilitating the damaged breakwaters, another storm hit Praia da Vitória port with a significant wave height of 7.21 m, a mean period of 11.3 s, and waves arriving from the northeast. This event caused severe damage to both breakwaters, resulting in rocks being transported from the breakwater to the container yard. This led to damage to cargo and equipment and endangered the staff of the commercial port (Poseiro, 2019) (Figure 2.8).

Figure 2.8- Damage to the south and north breakwaters, and the container yard in the storm on 26th to 27th February 2005 (*Source:* Poseiro (2019)).

Another storm event reached the Praia da Vitória harbour on January 24th, 2007, with a significant height of 8 m. This caused severe destruction to the south breakwater, overtopping the wave return wall, which had a crest height of +11.2 m (ZH), and flooded the container yard, damaging the cargoes (Figure 2.9).

Figure 2.9-Damage and overtopping of the wave wall on the south breakwater protecting the container yard, leading to flooding of the yard during the storm event on January 24th, 2007 (*Source:* Poseiro (2019)).

On March 14th, 2013, another storm hit the Praia da Vitória harbour. It generated high waves that pushed into the inner part of the harbour basin, causing overtopping of the south breakwater and the frontal defence wall, which protects the coastal road along the shoreline (Figure 2.10).

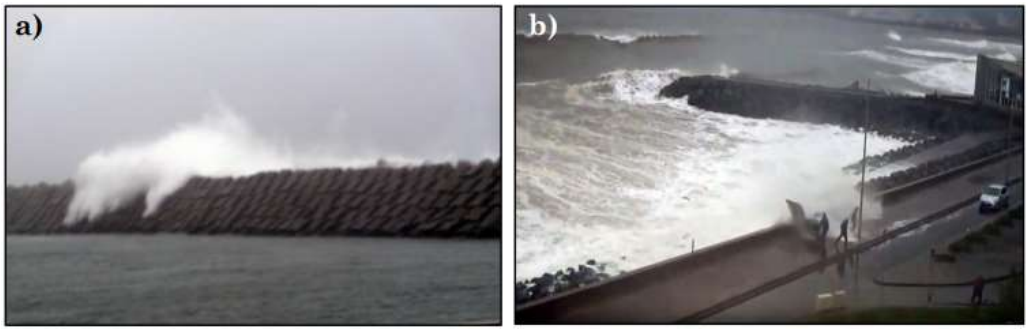

Figure 2.10- Overtopping of the south breakwater (a) and frontal defence wall causing disturbance to the coastal road (b)during hurricane Alex on January 15th, 2016 (*Source*: Poseiro (2019)).

Hurricane Alex impacted Terceira Island on January 15th, 2016, with a maximum wave height of 12.1 m. During the event, the south and north breakwaters were severely overtopped, and according to local reports, small to medium overtopping occurred at the frontal defence wall (Figure 2.10 and Figure 2.11).

Figure 2.11- (e) Overtopping of south breakwater, flooding yard (a,b,c and e), and severe overtopping of the north breakwater (d)(*Source:* Poseiro (2019)).

3 Methodology

This methodology outlines the assessment of overtopping at Praia da Vitória harbour in Terceira, Azores, using a two-dimensional SWASH numerical model simulation.

This methodology consists of two main components: (1) South breakwater's physical model tests replication using a two-dimensional SWASH model, (2) the simulation of a two-dimensional SWASH model for the whole harbour and bay domain. Both studies were conducted using SWASH version 11.01A, released in January 2025, which effectively simulates various phenomena, including wave propagation, wave breaking, wave-structure interaction, wave transmission through structures, wave-induced circulation, and non-linear interactions, especially from foreshore to shallow water.

3.1 Test case 1 - South breakwater's section physical model tests replication

In this study, a physical model test conducted at LNEC in January 2025 for a selected profile along the south breakwater (Figure 3.1) was replicated at prototype scale in SWASH as a two-dimensional model. This physical model was built and tested at a scale of 1:52, in accordance with Froude's similarity law. Two cases that led to overtopping of the profile were selected to evaluate the model's performance, and Table 3.1 presents the parameters for each case.

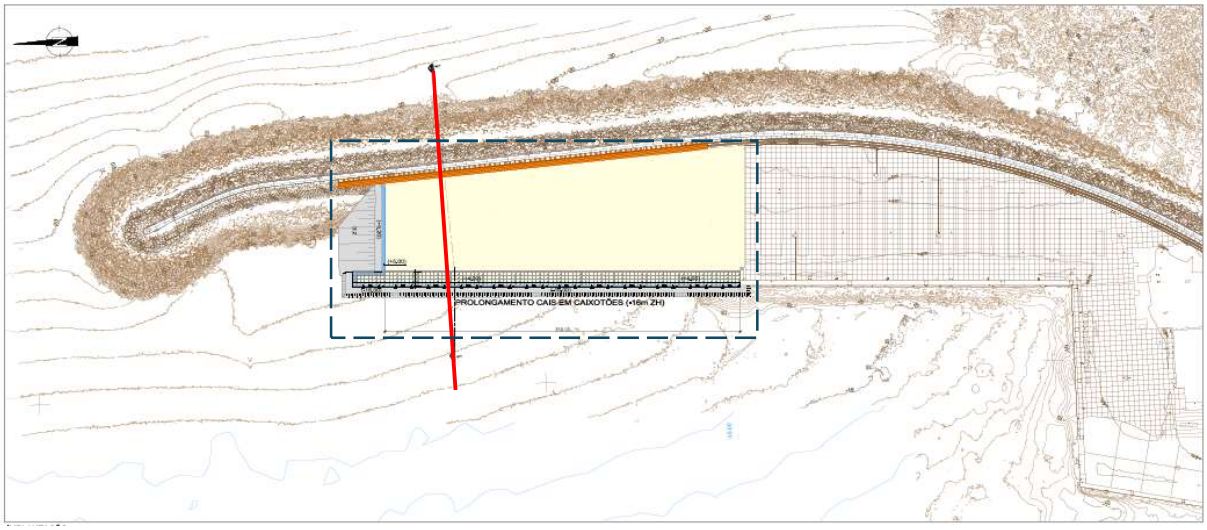

Figure 3.1- Cross-section along the south breakwater chosen for two-dimensional physical model test at the LNEC in January 2025 (*Source:* Lemos *et al*. (2025)).

Table 3.1- Test cases chosen from the physical model test for simulation in the SWASH.

Case	**H_s (m)**	**T_p (s)**	**Simulation time (minutes)**
Test 112	8	18	180
Test 113	9	18	180

Six gauges were deployed in the physical model test (Figure 3.2). Four gauges were dedicated to monitor water surface elevation (S1 to S4), while the others (S5 and S6) were used to collect overtopping data. Our numerical study primarily focuses on the data collected by gauges S1, S2, S3 and S6. All the data from the physical model test were converted to prototype scale and analysed alongside the output from the SWASH model to enable a quantitative comparison of water surface elevation at S1, S2, and S3, as well as cumulative overtopping volume at S6.

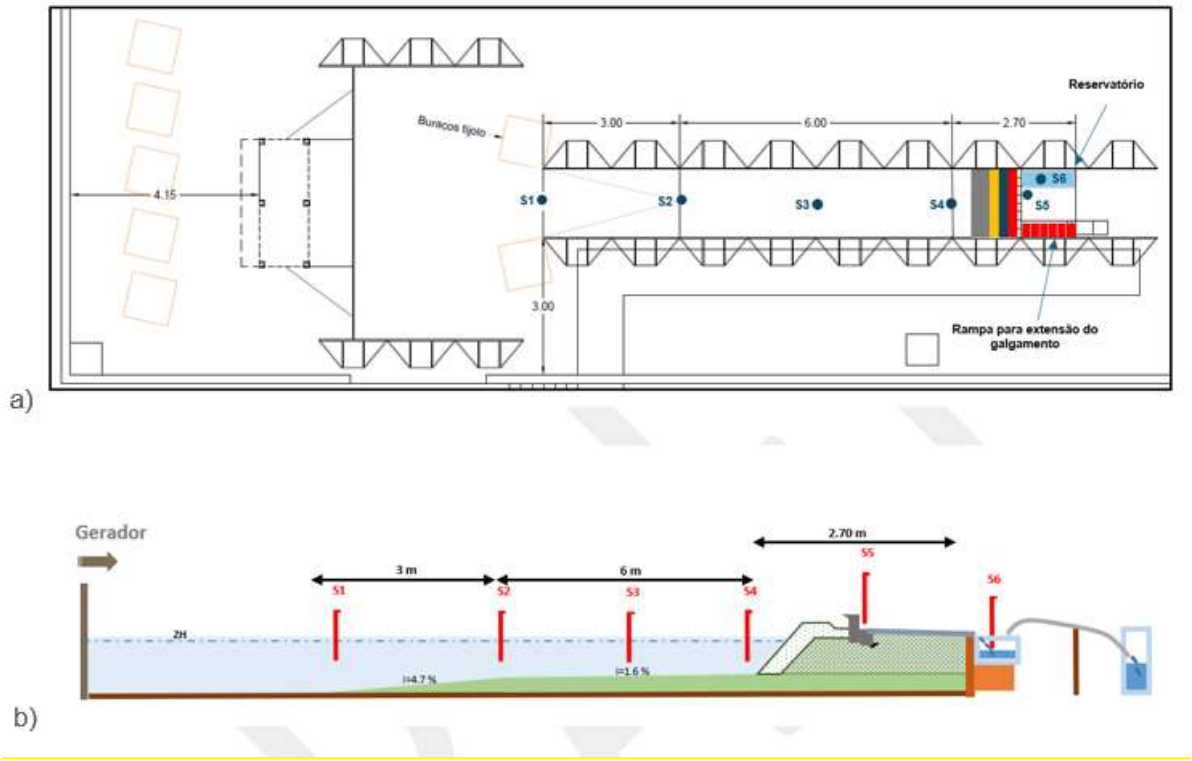

Figure 3.2- (a) Plan view of the physical model setup in model scale with probes S1 to S6, (b) Cross section of the model(*Source:* Lemos *et al*. (2025)).

3.1.1 Numerical model set-up

The physical model setup was replicated in a two-dimensional model at the prototype scale (Figure 3.3 and Figure 3.4) . The horizontal and sloped bottoms, along with the breakwater, were treated as impermeable layers and incorporated bottom roughness to enhance energy dissipation due to roughness and seepage. An unstructured triangular mesh was used as a computational grid. Gauge locations were precisely aligned with those of the physical model to facilitate comparisons with the experimental data. In the numerical model, the recurved wave return wall, as represented in the physical model, required some simplifications and was treated as a vertical wall.

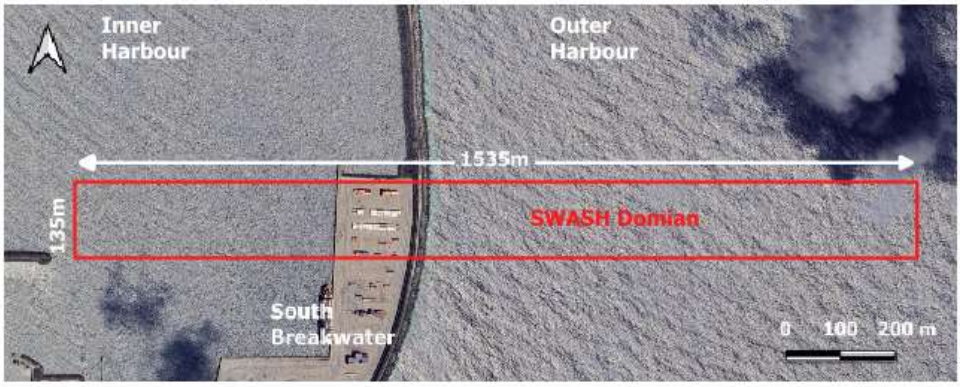

Figure 3.3- SWASH domain of the replication of the physical model at the prototype scale, created using QGIS 3.36 and Google Earth imagery (© Google, 2025)

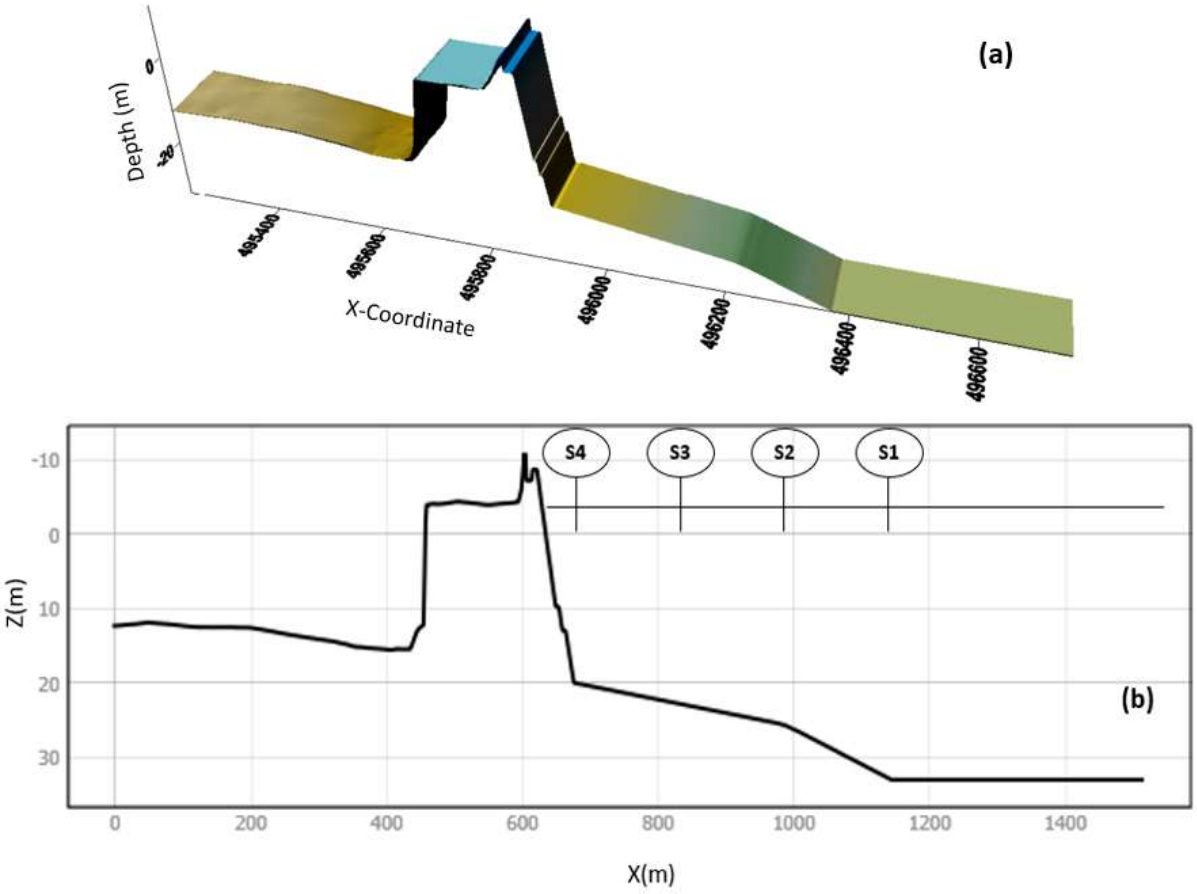

Figure 3.4- (a) 3D bathymetric surface generated using Surfer software, and (b) cross section of the 2D SWASH model.

Bottom roughness of the breakwater and the seabed were input as Manning's coefficients. This was included in the model as a separate file using the INPGRID command. A regular grid with a resolution of one meter was employed. The file was read using the READINP command, which allowed SWASH to extract the bottom roughness for the unstructured computational grid through interpolation. It was important to specify the order in which SWASH should read the values from the file. For this purpose, the [idla] option was available, and option 3 was used for this simulation. This option instructs SWASH to read the file from left to right, starting in the lower-left corner of the file. Each new line in the file should begin on a new line.

The SWASH model can define the time step based on the Courant number and requires establishing both the maximum and minimum Courant values for the computational domain. The model calculated the Courant number for grid points, and if the calculated Courant number exceeded the maximum Courant value, the time step was halved. Conversely, if the calculated Courant number fell below the minimum Courant value, the time step was doubled. The model's convergence improves when the minimum Courant number is set lower than 0.1 instead of the recommended 0.4 in the SWASH manual (Poseiro, 2019). For this simulation, the minimum Courant value was set to 0.1, and the maximum Courant value was set to 0.5. The default initial time step, Δt, was fixed at 0.0125 s.

In the physical model, each case was simulated for 180 minutes.. According to the SWASH user manual 11.01A, to achieve steady-state conditions, it was recommended to add spin-up time to the simulation time. Since this simulation lasted three hours and observed the overtopping event before the spin-up time recommended in the SWASH user manual, no additional time was allocated for spin-up.

3.1.1.1 Domain and bathymetric data assimilation

LiDAR survey, conducted in October 2024 with one-meter spacing for the south breakwater to obtain the elevation of the breakwater and the container yard. In the physical model test, there were two bottom slopes between the toe of the breakwater and the wave maker. In the prototype scale, the water depth at the toe of the structure was 21 m (ZH), and the bottom slope started at 1.6%

until the depth reached 25 m (ZH). At that point, a 4.7% slope began and continued until the depth reached 33 m (ZH). The wave maker was positioned at a depth of 33 m (ZH). The total distance between the toe of the breakwater and the wave maker was 468 m.

However, in the SWAH model simulation, more space was allocated by increasing the length to 840 m between the toe of the structure and the wave maker, while maintaining the same bottom level. This allows the numerical wave space to develop and then propagate towards the structure fully. As the bottom level remained unchanged, the domain extension has a flat bottom, which does not affect wave characteristics; this adjustment does not differ from the conditions in the physical model test. Additionally, a distance of 480 m was allocated from the container yard to the opposite boundary of the wave maker to facilitate the exit of waves from the domain.

Bathymetry was defined as positive downwards and negative upwards from the ZH reference. The bathymetry data was input into the model as a separate file using the INPGRID command. A regular grid with a resolution of one meter was utilised. The file was read using the READINP command, which allowed SWASH to extract the bottom level for the unstructured computational grid through interpolation. To specify the order in which SWASH should read the values from the file, the [idla] option was available, and option 3 was used for this simulation.

3.1.1.2 Computational mesh generation

The aim of using an unstructured triangular grid for this study was to enhance flexibility in representing complex coastal geometries and to permit localised mesh refinement in areas with strong wave dynamics. Unlike structured grids, unstructured grids can easily accommodate complicated geometries and provide variable grid resolution without the constraints typically associated with structured grids (Zijlema, 2020). Therefore, the GMalha unstructured triangular grid generator (Pinheiro *et al.*, 2008), developed at LNEC, was used to create the unstructured grid for this simulation.

The primary parameters for mesh generation included the minimum number of points per wavelength and the wave parameter, defined as the wave period at the wave maker. The refinement of the mesh at each location was determined based on the calculated wavelength at that point, taking into account the water depth. After the refinement process, the mesh is optimized to insure

optimal valence of nodes (optimal value is 6) and minimize the bandwidth of the mesh (maximum node index difference in each neighbouring element). This optimization process is key to ensure mesh quality and thus minimize CPU times and model stability. The main output files generated were the triangle element file and the node file, which served as input for the SWASH simulation. All nodes of the triangles were named in a counter-clockwise manner, and the nodes located on the boundaries were identified separately using a boundary marker. In this simulation, nodes on the south, east, north, and west boundaries were marked as 1, 2, 3, and 4, respectively, while nodes within the domain were marked as 0. These boundary markers were used to impose boundary conditions during the simulation.

3.1.1.3 Boundary conditions

A weak boundary condition was applied at the wave input boundary using the JONSWAP wave spectrum with $\gamma = 3.3$. A Sommerfeld radiation condition was implemented at the end of the numerical domain to facilitate the exit of waves from the domain (Zijlema *et al.*, 2011). All other boundaries were treated as closed boundaries.

3.1.1.4 Numerical methods

In the SWASH numerical model, frequency dispersion can be considered by increasing the number of vertical layers in the model. An accurate estimate of the vertical gradient of non-hydrostatic pressure components was achieved using compact schemes, while enhancing the resolution at the bottom and near the free surface through computational grid lines that follow the bathymetry of the seabed.

The dimensionless depth coefficient, *kd* (where *k* represents the wave number and *d* represents the water depth), determines the number of layers required to accurately assess frequency dispersion (SWASH user manual 11.01A). According to the SWASH user manual, a higher *kd* requires more layers. For primary waves, if *kd* was less than or equal to 2.9, one layer was sufficient. If *kd* was less than or equal to 7.7, at least two layers were necessary. In this study, for both test cases, *kd*

was less than 0.5, and a single layer was used, resulting in a 1% error in the phase velocity of both standing and progressive waves.

Since numerical results depend on the implemented numerical schemes, Suzuki *et al.* (2012) recommend using combinations such as CORRDEP + FIRST, UPWIND + FIRST, and UPWIND + MUSCL. The CORRDEP scheme determines the discretisation of water depths at points where the model calculates velocity. In this simulation, a first-order CORRDEP scheme was used. Additionally, an UPWIND first-order scheme was employed, which discretises the governing equations to estimate the value of a quantity at a point by using the value at the neighbouring grid point in the direction from which the flow originates.

In this study, a one-layer model was developed incorporating the activation of the non-hydrostatic BOX scheme. Additionally, the CORRDEP + FIRST and UPWIND + FIRST schemes were utilized, with MUSCL being the default option for CORRDEP.

3.1.2 Model calibration

A potential approach to investigating overtopping over a breakwater using the SWASH model involves defining the breakwater as a permeable structure and assigning porosity based on the material's properties. However, previous studies have shown that this is a challenging task due to difficulties in simulating energy dissipation and flow resistance within the porous layers of the structure (Pés, V.M., 2013; Salas Pérez, 2014).

In this dissertation, the effects of friction and rugosity of the breakwater were incorporated into the model through a Manning's coefficient, which represents the comprehensive energy dissipation due to roughness and seepage. Since the literature did not provide a friction value for breakwaters with a tetrapod armour layer, part of this dissertation involved calibrating the model using various Manning's coefficients to achieve overtopping discharges that matched those observed in physical model tests in prototype scale.

Before validating the overtopping discharge, data at gauges S1, S2, and S3 were used to analyse the free surface elevations. The collected data was analysed wave by wave, employing the zero

upward-crossing method and spectral-domain analysis, using the classical Fast Fourier Transform (FFT) technique.

Zero upward-crossing method was used to obtain, wave height parameters, including H_{mean}, $H_{1/3}$, $H_{1/10}$ and H_{max}, as well as wave period parameters such as $T_{H1/3}$, and T_{max} . The Fast Fourier Transform (FFT) method provided the significant wave height ($H_{m0)}$ and associated peak period ($T_{p)}$. These parameters were scaled to prototype using Froude scaling laws. For the length scale, $N_L = L_P/L_M$; for the time scale, $N_T = \sqrt{N_L}$; and for the volume scale, $N_V = N_L^3$.For a detailed description of these parameters, refer to the List of notation.

3.1.2.1 Test 112

In the physical model test, simulations were conducted for four peak wave periods: 12 s, 16 s, 18 s, and 20 s. For each wave period, five different significant wave heights: 7 m,8 m,9 m,10 m, and 11 m were considered.

During Test 112, the simulation for a peak wave period of 18 s and a significant wave height of 8 m was examined. However, it was observed that the wave maker did not generate the exact wave parameters specified in the table that were input into it. Consequently, calibration of the significant wave height and peak wave period was performed using data available from gauges S1, S2 and S3.

Since the literature does not provide a friction value for breakwaters with a tetrapod armour layer, and to obtain an initial friction coefficient for the outer slope of the south breakwater to start the simulation, the equation by Le Roux (2003), which calculates the friction factor for coastal structures, was employed. This equation determines the friction factor for various coastal structures based on two variables: the equivalent diameter of the particles (D) and the wave period (T). During this calculation, the weight of each tetrapod armour unit, which was 300 kN, and a wave period of 18s were considered, resulting in a friction coefficient of 0.04 $s/m^{1/3}$ for the outer slope of the breakwater.

Bottom friction for the seabed was considered as 0.019 s/m$^{1/3}$. To identify the combination of nominal significant wave heights (Hs) and peak wave periods (T_p) that produced wave parameters at gauge S1, S2, and S3 similar to those observed in the physical model test, several combinations varying Hs and T_p were simulated in the SWASH model, assuming a friction coefficient of 0.04 s/m$^{1/3}$. Once the combination that yielded the minimum average Root Square Percentage Error of wave parameters (RSPE^{WP}) as explained in equation (6), at gauges closest to the physical model test data, the nominal combination of Hs and T_p was determined for further SWASH simulations.

$$\mathrm{RSPE}^{WP} = \left(\left(\frac{H_{s,G1,NM}}{H_{s,G1,PM}} \right)^2 + \left(\frac{T_{p,G1,NM}}{T_{p,G1,PM}} \right)^2 \right)^{0.5} \quad (6)$$

Where $H_{s,G1,NM}$, $T_{p,G1,NM}$ are the significant wave height, and peak wave period computed at wave gauge 1 in the numerical model and $H_{s,G1,PM}$, $T_{p,G1,NM}$ are the significant wave height, and peak wave period measured at wave gauge 1 in the physical model.

After determining the nominal wave parameters, additional simulations were conducted with friction coefficients varying from 0.04 s/m$^{1/3}$ to 0.15 s/m$^{1/3}$ for the outer slope of the breakwater (Table 3.2), while maintaining Manning's coefficient unchanged in other areas. The purpose of this additional simulation was to obtain a Manning's coefficient for the outer slope of the breakwater that produces the closest cumulative overtopping volume after 10000s with the physical model test. The simulation time for each case was 180 minutes, including spin-up time. For each simulation, cumulative overtopping volumes were compared with the results from the physical model test at prototype scale. For this purpose, the parameter Root Square Percentage Error of volume (RSPE^{V}) was defined as follows;

$$\mathrm{RSPE}^{V} = [\,((V_{NM} - V_{pM})/V_{pM})^2\,]^{0.5} \quad (7)$$

Where, V_{NM} is predicted cumulative overtopping volume by SWASH simulation, and V_{PM} is measured cumulative overtopping volume by physical model test.

Table 3.2- Chosen nominal Hs and T_p and Manning's coefficients of the outer slope of the south breakwater for SWASH simulation- Test 112

Simulation	Manning's coefficient ($s/m^{1/3}$)	H_s (m)	T_p (s)
T112_01		8.1	18.0
T112_02		7.2	17.0
T112_03	0.04	7.0	16.0
T112_04		6.8	15.8
T112_05		6.6	15.6
T112_04_m1	0.05	6.8	15.8
T112_04_m2	0.06	6.8	15.8
T112_04_m3	0.07	6.8	15.8
T112_04_m4	0.08	6.8	15.8
T112_04_m5	0.09	6.8	15.8
T112_04_m6	0.10	6.8	15.8
T112_04_m7	0.11	6.8	15.8
T112_04_m8	0.12	6.8	15.8
T112_04_m9	0.13	6.8	15.8
T112_04_m10	0.14	6.8	15.8

3.1.2.2 Test 113

Test 113 was performed with a peak wave period of 18 s and a significant wave height of 9 m in the physical model test. The Manning's coefficient, obtained from calculations in Section 3.1.2.1, was 0.04 $s/m^{1/3}$ for the outer slope of the breakwater, which was adopted as the initial friction value. Bottom friction for the seabed was considered to be 0.019 $s/m^{1/3}$. Several combinations varying Hs and T_p were simulated in the SWASH model (Table 3.3), and the same procedure described in Test 112 was followed to calibrate Manning's coefficient of the outer slope of the south breakwater.

Table 3.3 - Chosen nominal -Chosen nominal H_s and T_p, and Manning's coefficients of the outer slope of the south breakwater for SWASH simulation- Test 113.

Simulation	Manning's Coef. ($s/m^{1/3}$)	H_s(m)	T_p(s)
T113_01		9.0	18.0
T113_02		9.0	17.5
T113_03	0.04	9.0	17.0
T113_04		8.5	19.0
T113_05		8.0	19.0
T113_03_m1	0.05	9.0	17.0
T113_03_m2	0.06	9.0	17.0
T113_03_m3	0.07	9.0	17.0
T113_03_m4	0.08	9.0	17.0
T113_03_m5	0.09	9.0	17.0
T113_03_m6	0.10	9.0	17.0
T113_03_m7	0.11	9.0	17.0
T113_03_m8	0.12	9.0	17.0
T113_03_m9	0.13	9.0	17.0
T113_03_m10	0.14	9.0	17.0
T113_03_m11	0.15	9.0	17.0

3.1.3 Sensitivity analysis

A sensitivity analysis was conducted for the physical model replication test of the south breakwater described in Section 3.1. The purpose of this analysis was to evaluate the differences in SWASH model output of cumulative overtopping discharge and computational time across various grid resolutions and seeding numbers at the wave maker.

The grid resolution of the unstructured grid was primarily determined by the minimum number of points per wavelength, the wave parameter defined as the wave period (in seconds) at the wave maker, and the maximum refining depth (in meters). In this study, five different configurations were tested, with minimum points per wavelength of 15, 18, 21, and 27, while keeping the wave period at 18s and the maximum refining depth at 1 m constant for all cases. The original unstructured grid was designed based on 12 points per wavelength, while the peak wave period at the boundary was set at 18s. For each quality of mesh, total number of nodes and bandwidth of the mesh were considered during sensitivity analysis.

The quality of the mesh was assessed by evaluating the node valences of the mesh. A node valence is the number of elements connected to this node. Optimal node valence is six, i.e., when a node is connected to six elements, it is said to be optimal. Non-optimal node valence is defined when a node is connected to more or less than six elements, i.e. five or seven. The mesh quality can be calculated as a percentage value by taking the ratio of total number of nodes with non-optimal valence to total number of elements of the mesh, which reflects the overall quality of the mesh.

Another measure of mesh quality is its bandwidth. A mesh's bandwidth is an important index that influences the computational efficiency of the simulation. Each node in the mesh is connected to a set of neighbouring nodes, and the node indexes of neighbouring nodes can be close or differ greatly, depending on the way the nodes are numbered when the mesh is created. The bandwidth is defined as the maximum difference in node indexes of neighbouring nodes. If the node indexes are scattered around the whole mesh, the matrices will be sparse, i.e. the bandwidth will be very high, which will increase the CPU times and memory requirements. On the contrary, if the bandwidth is small, it means the matrices are concentrated along the main diagonal, and the numerical procedure is more efficient.. This is why some numerical mesh generators have an algorithm to renumber the nodes after the final refined mesh is achieved. This renumbering procedure tries to find the best node numbering in order to minimise the mesh's bandwidth.

Regarding the seeding number sensitivity analysis, an infinite number of wave trains can be generated using the same wave spectrum by varying the seed number, which determines the sequence of waves in the wave train approaching a structure, so that each seeding number gives origin to a unique time series of waves.. Furthermore, Williams *et al.* (2014) investigated the impact of seed number on overtopping discharge and found that it significantly influences discharge at the boundary. In the SWASH model, users can specify the seed number at the boundary. These simulations were typically conducted using a default seed number known as 12345678 (SWASH user manual 11.01 A). For sensitivity analysis, two random additional seed numbers were selected: 21436587 and 87654321.

3.2 Test case 2 - The whole harbour and bay domain

3.2.1 Numerical model set-up

A two-dimensional simulation was conducted for the computational domain over a period of three hours. Initially, the EXPLICIT method was used to determine the time step, which was automatically calculated based on the minimum and maximum Courant values. However, it was observed that the model became unstable when the EXPLICIT method was employed. Consequently, the IMPLICIT method was used with the Crank-Nicolson scheme.

In light of the results from previous SWASH simulations of the physical model and following the recommendations of the SWASH user manual 11.01A, a single layer was applied in this model using non-hydrostatic mode with the BOX scheme. The horizontal and sloped bottoms, along with the breakwater, were treated as impermeable layers and incorporated energy dissipation due to roughness and seepage.

3.2.1.1 Bathymetric data assimilation

In this study, for the definition of the bathymetry to be used in the simulation with the SWASH model, multiple sources of bathymetric data were utilised to ensure an accurate representation of the nearshore area, harbour, and bay. A high-resolution LiDAR survey was conducted in October 2024 around the south breakwater for the proposed expansion project of the multi-purpose pier at the port of Praia da Vitória, providing detailed topographic information at a one-meter resolution (Lemos et al., 2025) (Figure 3.5).

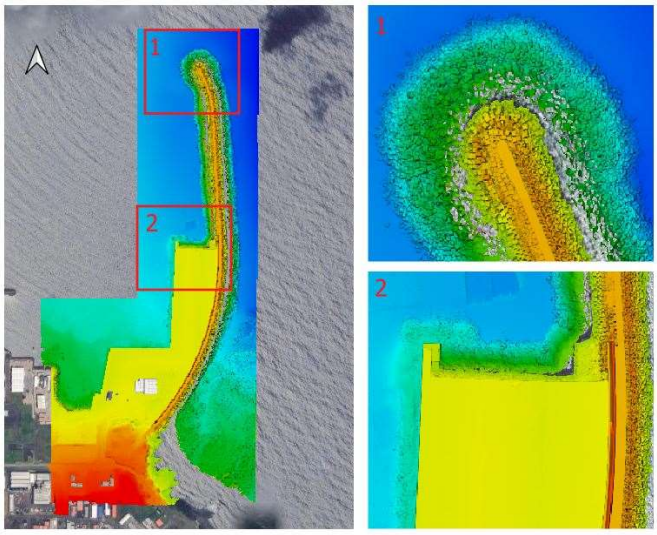

Figure 3.5- LiDAR survey of October 2024, around the south breakwater (Source: Lemos et al. (2025))

Additionally, a bathymetric survey conducted in 2017 supplied crucial depth data for the inner port area. This data was only accessible for the harbour basin and some areas in front of the south breakwater (Figure 3.6).

Figure 3.6- Bathymetric survey in 2017 covering the harbour basin and an area in front of the south breakwater (*Source: LNEC*)

For offshore deep-water conditions, bathymetric data were obtained from the bathymetry used in the SWAN simulations for the Praia da Vitória harbour in the HIDRALERTA system. This data was available at a resolution of 25m (Figure 3.7).

However, no LiDAR data were accessible for the north breakwater, the coastal frontal defence, or the groynes system. Likewise, the elevations of the above coastal structures were sourced from archived design drawings provided by the LNEC. Figure 3.8 shows the layout of the frontal defence wall and groynes.

The layout of the north breakwater, with chainage, is shown in Figure 3.9. Twelve cross sections were available, including details of width and levels at the crown, side slopes, berm width, size of amour stones, and their thickness. Elevations for the inner land area of the computational domain were obtained from the Space Shuttle Radar Topography Mission (SRTM), which provides a digital elevation map with a 30-meter resolution.

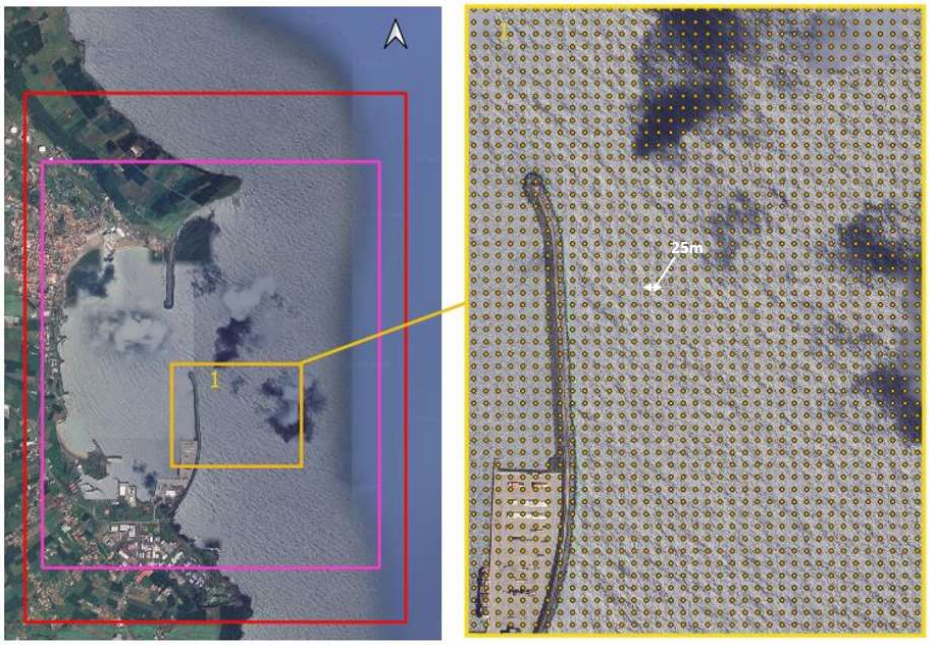

Figure 3.7- Bathymetric data used in the SWAN module (HIDRALERTA system) with 25m resolution, SWAN domain in red and study area in pink, created using Google Earth imagery (© Google, 2025) .

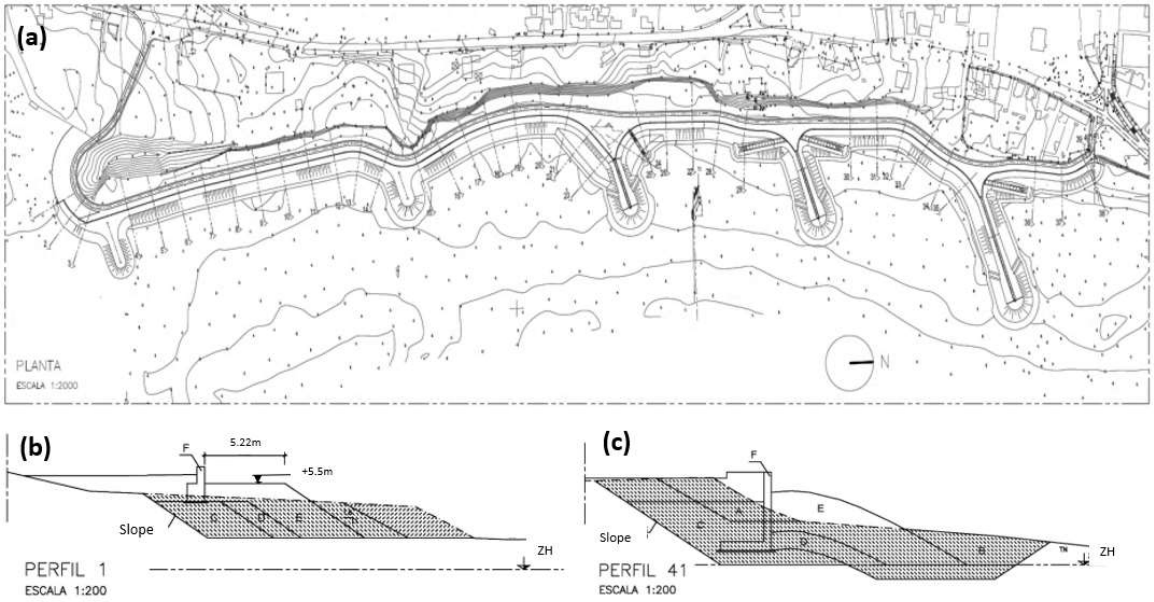

Figure 3.8- (a) Layout of frontal coastal defence, (b) Cross section-1, and (c) Cross section- 41(*Source:* Poseiro (2019)).

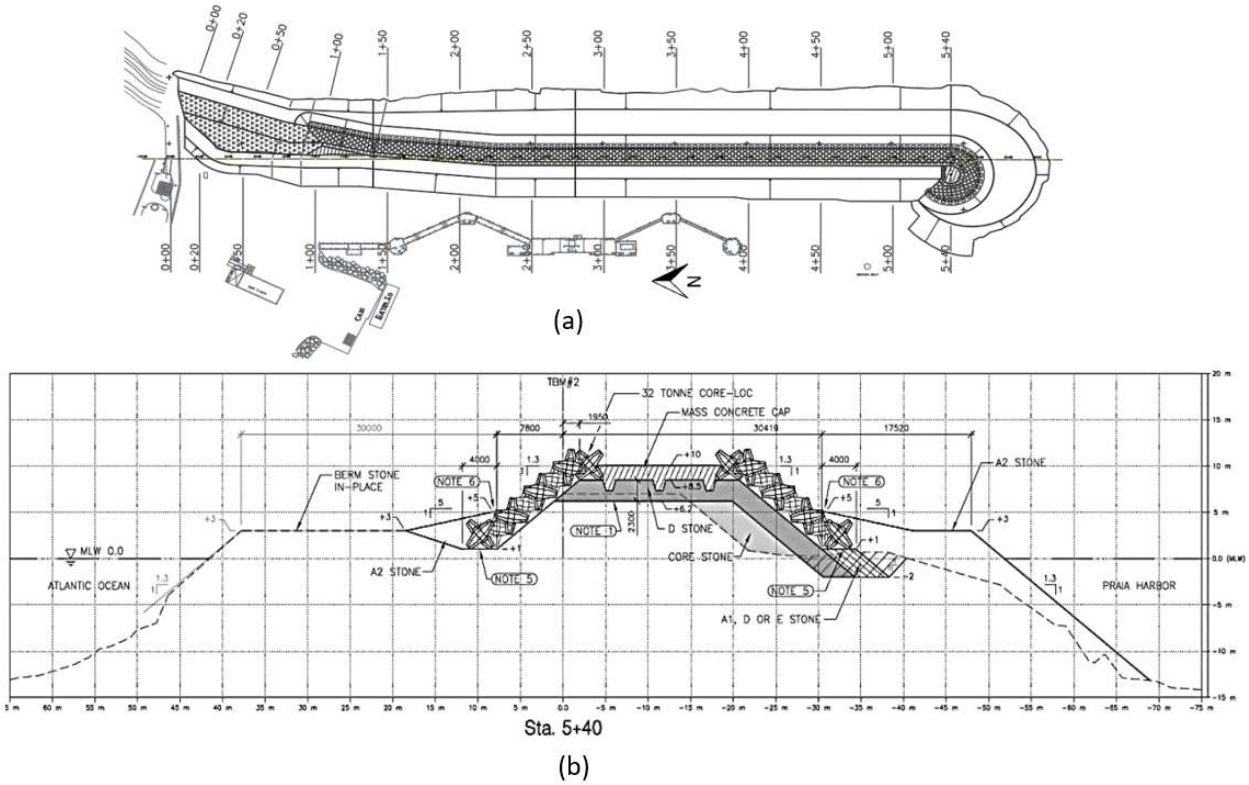

Figure 3.9- (a) Layout of the north breakwater with chainage, (b) details of cross section at chainage 5+40 (*Source*: Poseiro (2019))

Combining these datasets posed a significant challenge in developing a suitable bathymetry model. This becomes even more important when the study area includes complex coastal structures. For the south breakwater, the LiDAR survey from October 2024, was integrated with the bathymetry survey from 2017.

For the northern breakwater, the 2017 survey data were used. As illustrated in Figure 3.10, the bathymetry data varied in resolution around the breakwater. To create a smoother surface, elevation levels were extracted at each cross-section of the northern breakwater by digitising the design drawings using AutoCAD software and they were merged with the 2017 survey data. Figure 3.11 displays the final cross-sections along the northern breakwater.

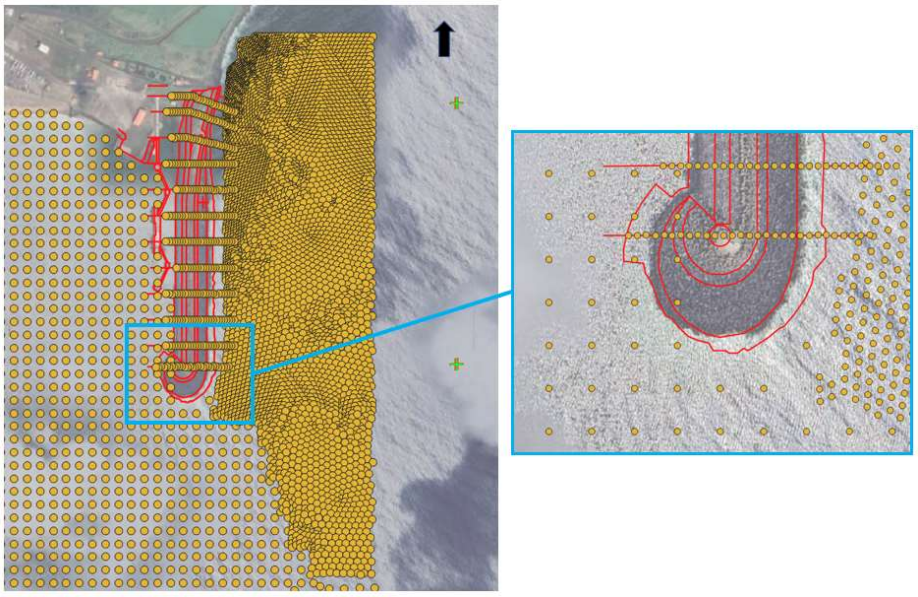

Figure 3.10- Different resolutions of the bathymetry survey in 2017 around the north breakwater.

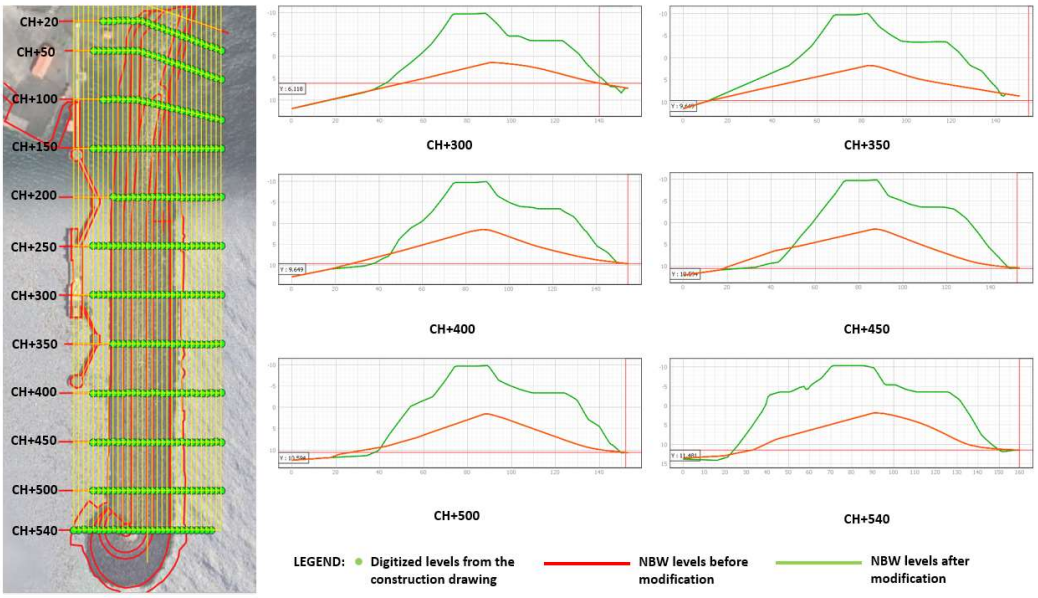

Figure 3.11- Definition of the north breakwater based on the design drawings available in the LNEC.

In the inner bay, it was crucial to generate bathymetry data free from sudden discontinuities, as spikes in the bathymetry can destabilise the simulation. Due to the absence of data for the groyen series and the frontal defence wall, the same methodology used for the northern breakwater, elevations were extracted from the design drawings. However, significant discrepancies were noted between the toe of the groynes and the 2017 bathymetry survey. To address this, adjustments were made to eliminate sharp discontinuities in the nearshore bathymetry, and Figure 3.12 shows the final cross-section at the groyne series. By combining the above-processed bathymetric data, the final bathymetry of the Praia da Vitória harbour and bay area was obtained (Figure 3.13).

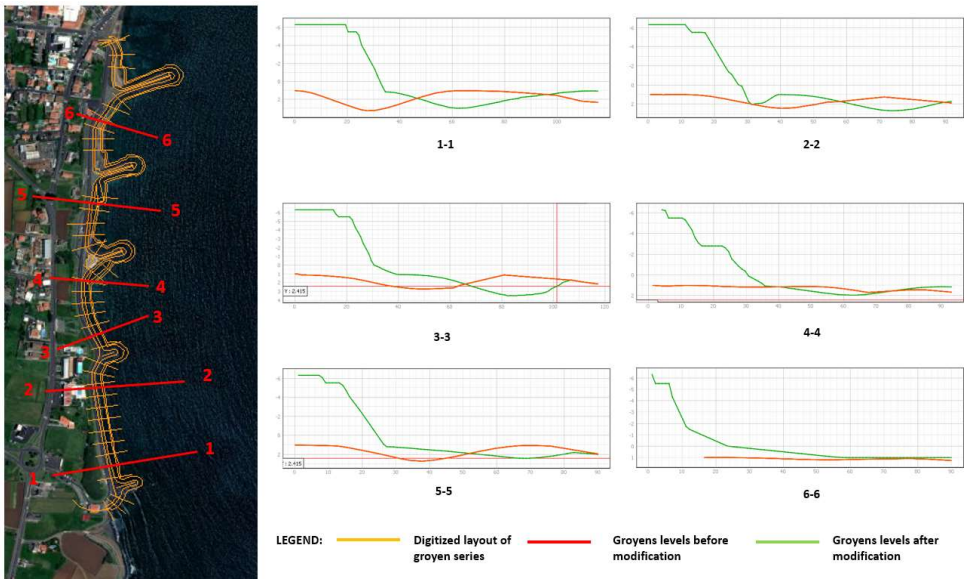

Figure 3.12- Definition of groyens based on design drawings available in the LNEC.

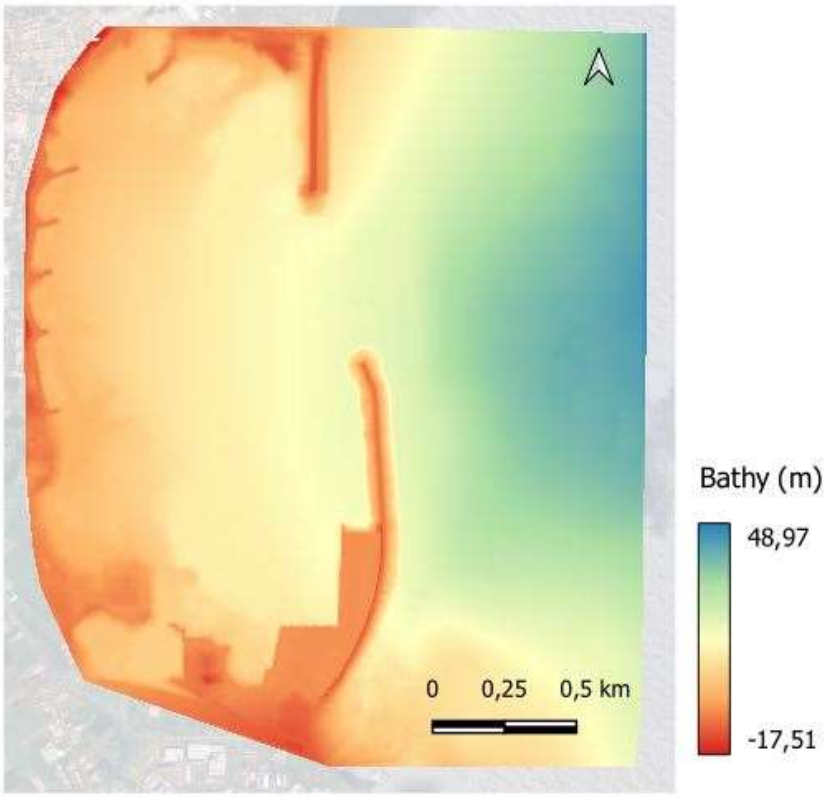

Figure 3.13- Final topo-bathymetry of Praia da Vitória harbour and bay area.

3.2.1.2 Bathymetry and friction grids

Bathymetry data for the computational domain were input into the SWASH model as a separate file. In this model, bathymetry was defined as positive downwards and negative upwards from the ZH reference. The bathymetric data were input into the model using the same procedure outlined in Section 3.1.1.1. Specific elevations of the computational domain can be ignored during computation by identifying them with an exception value under the READINP command. In this domain, the maximum elevation of the coastal structures was +11.2m (ZH), which represents the crest of the wave return wall on the south breakwater. Inside the land, the maximum elevation was +98.0m (ZH). To save computation time and resources, -999 was assigned to all elevations greater than +20m (ZH), and it was considered as the exception value during the simulation.

For the outer slope of the south breakwater, the calibrated Manning's friction coefficient in Section 3.1.2 was used. However, laboratory and field data were not available to calibrate the friction coefficient for the north breakwater and the series of groynes with a frontal defence wall. Therefore, Manning's coefficient for the north breakwater was considered similar to that of the south breakwater. For Manning's coefficient of the groyne series, the equation provided by Leroux (2003) was used. Having done the calculation based on the properties of the rock fill, the friction coefficient for the groyen series was 0.22 $s/m^{1/3}$. Additionally, a friction coefficient of 0.050 $s/m^{1/3}$ was used for the inner land area. Bottom friction for the seabed was considered to be 0.019 $s/m^{1/3}$. Following a similar procedure used for the bathymetry data, all friction values were input into the SWASH model as Manning's coefficients. For this, a regular grid with one-meter resolution was employed, and the SWASH model extracted the friction value for the unstructured computational grid through interpolation.

3.2.1.3 Computational mesh generation

The simulation utilised an unstructured grid, following the same procedure outlined in section 3.1.1.2. According to the SWASH user manual 11.01A, unstructured meshes only allow incident wave directions perpendicular to the open boundary. Therefore, computational meshes were created considering the incident wave direction of each scenario. Based on the incident wave direction, five computational domains were identified (Figure 3.14).

For each event, an unstructured grid was generated using the GMalha unstructured triangular grid generator, developed at the LNEC (Pinheiro *et al.*, 2008). The primary output files generated were the triangle element file and the node file, which served as input for the SWASH simulation. Table 3.4 presents the characteristics of the mesh, including the number of nodes, the number of elements, the average number of nodes per wavelength, the mesh quality, and the bandwidth of each generated mesh

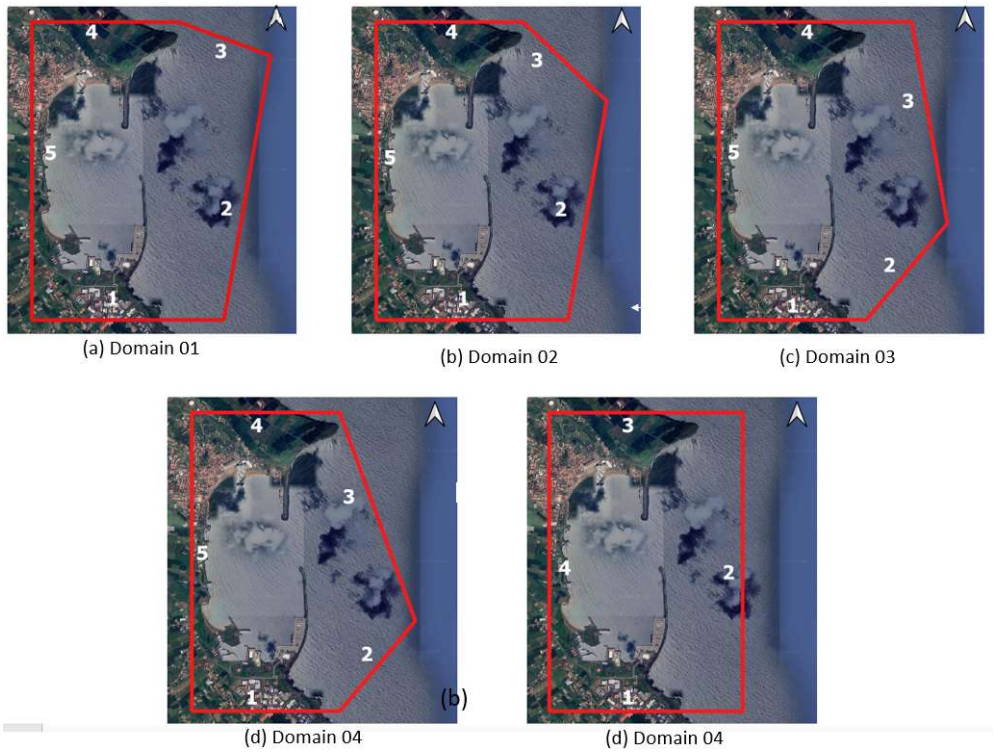

Figure 3.14- Five computational domains chosen based on the incident wave angle of each event.

Table 3.4- Characteristics of generated mesh for SWASH domains.

Domain	Total nodes	Total elements	Mesh quality (SWASH) (%)	Band width
Domian1	84462	168128	92.0	386
Domain2	83781	166780	92.0	375
Domain3	70896	141005	92.0	354
Domain4	84116	167456	93.1	399
Domain5	83578	166357	71.3	382

3.2.1.4 Boundary conditions

The boundary index was used to define the wave-generating boundary, and the relevant boundary index for each scenario is mentioned in Table 3.5. All nodes of the boundary were labelled in a counter-clockwise manner, and the nodes located on the boundaries were identified separately using a boundary marker (1 to 5).

Table 3.5- Details of domains of each scenario and wave maker boundary.

Scenarios	Incident wave angle (^{0})	Domain	Wave maker boundary (1-5)
MF1	20	Domain 01	3
MF2	20	Domain 01	3
MF3	50	Domain 02	3
MF4	80	Domain 03	3
ST1	70	Domain 04	3
ST2	70	Domain 04	3
ST3	80	Domain 03	3
ST4	90	Domain 05	2
ST5	100	Domain 01	2
ST6	130	Domain 03	2

Time series of irregular waves for each scenario were imposed as boundary conditions at the wave maker boundary. To generate time series for irregular waves, the significant wave height and the peak period were utilised as key parameters. The process began with the application of the JONSWAP spectrum, which is commonly used to characterise sea state conditions typical of coastal and harbour environments. Here, γ was set at 3.3, and a time series was generated for one hour and replicated to create a 3-hour time series. To allow waves to exit the numerical domain, a Sommerfeld radiation condition was applied at the boundary located in the water. The remaining boundaries were treated as closed boundaries.

3.2.1.5 Numerical methods

As mentioned in section 3.1.1.4, the dimensionless depth coefficient *kd* (where *k* represents the wave number and *d* represents the depth) was calculated at the toe of the south breakwater to determine the number of vertical layers. In this simulation, *kd* values for each scenario were calculated, and the maximum value was 1.2. According to the SWASH user manual 11.01A, for primary waves, if *kd* was less than or equal to 2.9, one layer was sufficient. Therefore, one layer was selected for the simulation. Additionally, the non-hydrostatic pressure BOX scheme was activated, and CORRDEP + FIRST and UPWIND + FIRST schemes were deployed, with MUSCL being the default option for CORRDEP.

3.2.2 Relevant point locations for wave overtopping assessment

Identifying overtopping points and associated risk zones is crucial for understanding the impact of extreme weather events on coastal and port areas. In the HIDRALERTA system, the Praia da Vitoria harbour area and bay are divided into zones based on the activities that are conducted behind the structures (Pinheiro *et al.*, 2023). These zones were labelled A to I and include the south breakwater, north breakwater, and the set of groynes in the bay, and the frontal defence. In this study, two sets of points were used to extract results from the SWASH model (Figure 3.15). Nine points were selected to measure water levels, ensuring that one point was chosen from each designated zone. Additionally, nine points were positioned on the structures to directly monitor the overtopping associated with the selected water level points.

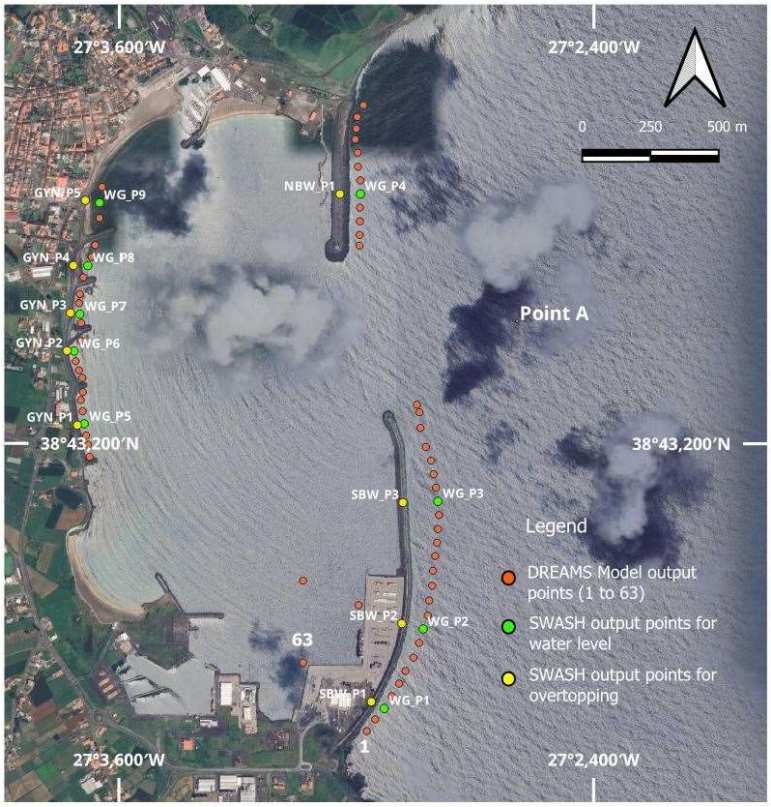

Figure 3.15- Output points of the DREAMS model (in orange dots), SWASH model output points for water level (in green dots), and SWASH output points for overtopping (in yellow dots). Created using QGIS 3.36 and Google Earth imagery (© Google, 2025)

3.2.3 Wave conditions

Two sets of wave conditions were selected from the wave records and regime analysis: most frequent (MF) and extreme events (ST). Different wave height, period, and direction, as well as tide level scenarios, were then selected from the hourly data records. Each scenario corresponds to a specific date and time recorded.

3.2.3.1 Most frequent events

Four scenarios were selected based on the most frequent wave characteristics at point A, which is the output of the built-in SWAN model in the HIDRALERTA system. The events were selected

based on their significant wave height (Hs) and corresponding occurrence percentages. The categories considered were $H_s < 1$ m, 1 m $< H_s <$ 2 m, 2 m $< H_s <$ 3 m, and $H_s >$ 3 m.

Each event was determined by selecting a time instant when the desired wave conditions occurred simultaneously with a predicted medium or high tide level at the site. Details of the maximum wave heights, periods, water levels, and the mean incident wave angle for the scenarios are presented in Table 3.6. The values are derived from estimates provided by the XTIDE, and SWAN models. After the filtering process of all the records of the year 2024, a specific date and time were selected, and the significant wave height, peak wave period and tide level were extracted to simulate in the SWASH model.

Table 3.6- Wave parameter: significant wave height (H_s), wave peak period (T_p), incident wave angle (in degrees north) of the most frequent events from the record of the HIDRALERTA system for year 2024, and selected for SWASH two-dimensional simulation.

Scenario	Event	Instant	Date	Time (hr)	Tide level (m)	Hs (m)	T_p (s)	Direction (^{0}N)
MF1	Most Frequent	Medium Tide(MSL)	1/4/2024	8	1.09	0.95	12.33	20.0
MF2	Most Frequent H_s>1m	High Tide	15/1/2024	17	1.56	1.29	9.10	18.8
MF3	Most Frequent H_s>2m	High Tide	14/1/2024	3	1.69	2.94	11.14	49.4
MF4	Most Frequent H_s>3m	High Tide	13/1/2024	4	1.82	3.45	11.14	84.0

3.2.3.2 Past extreme events

To select 6 cases of extreme events from the data series (from 1979 to 2024), all the storms were extracted from the series, using the Peak Over Threshold (POT) method. A threshold value of 4 meters was set for the peak wave height. If the wave height before and after 3 hours from the time of the peak wave height exceeded 3 meters, it was classified as a storm event in the Praia da Vitória coastal region. After this filtering, a total of 37 storms were identified (Figure 3.16).

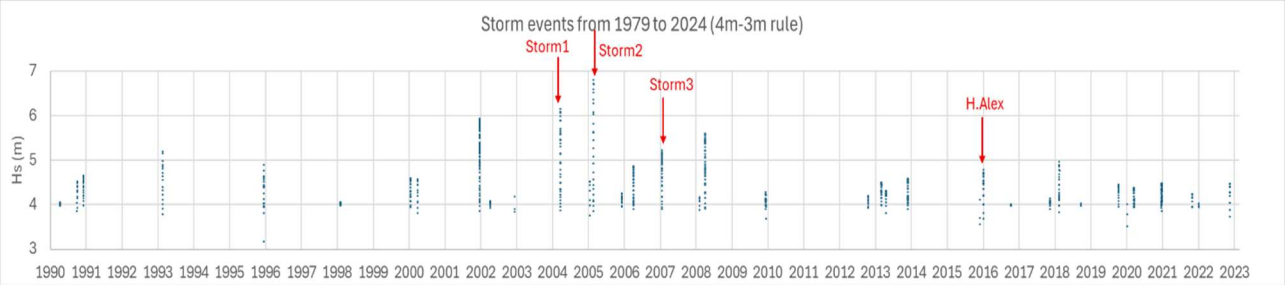

Figure 3.16- Significant wave heights (H_s) of recorded storm events (1989 – 2024), indicating the selected storm events after the analysis.

From these 37 storms, three were selected, including Hurricane Alex. Hurricane Alex was added because it was the most severe storm ever to hit the Azores archipelago. However, due to the storm path and wave incidence, Praia da Vitória port was not the most severely hit of the archipelago.

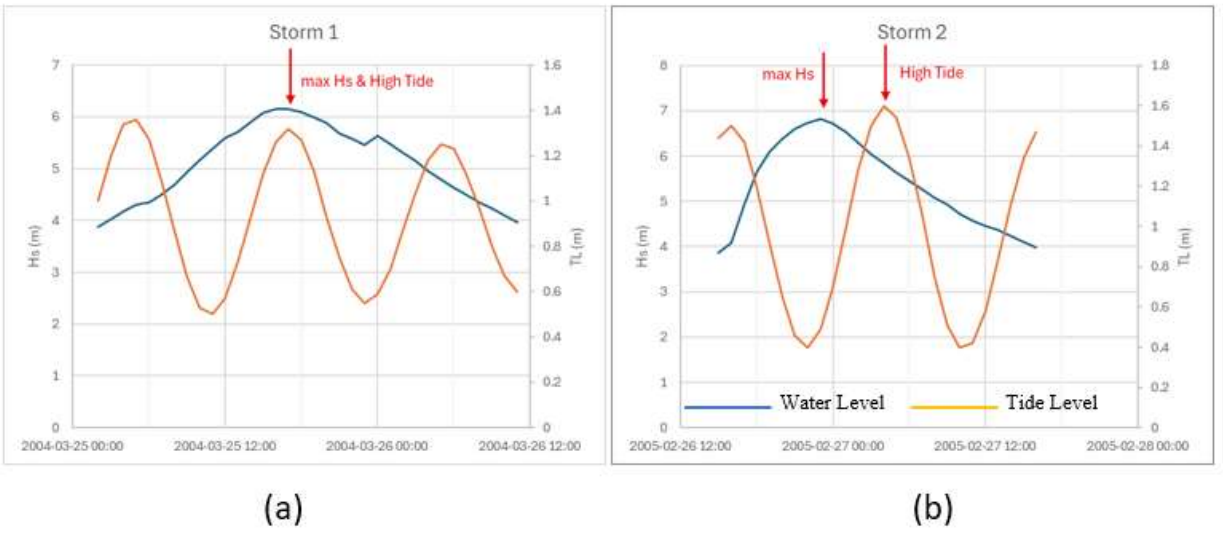

Figure 3.17- Comparison of wave height and tide level during storm 1 (a) and storm 2 (b).

Storm 2 and Hurricane Alex have the particularity of not coinciding with the maximum recorded wave height and the maximum tide level, while for storms 1 and 3, these coincide (Figure 3.17). A total of six storm scenarios were devised for simulation in SWASH (Table 3.7). This table displays the maximum wave heights, periods, water levels, and the mean incident wave angle for each storm scenario. The values are based on predictions provided by the XTIDE, SWAN, and DREAMS models within the HIDRALERTA system.

Table 3.7- Wave parameters, tide level, date, and time of selected storm event to simulate in SWASH model

Scenario	Event	Instant	Date	Time (hr)	Tide level (m)	Hs (m)	T_p (s)	Direction (^{0})
ST1	Storm 1	Max H_s High Tide	25/3/2004	17	1.32	6.15	12.33	67.0
ST2	Storm 2	Max H_s	26/2/2005	23	0.49	6.82	12.33	73.1
ST3		High Tide	27/2/2005	3	1.5	6.04	12.33	77.8
ST4	Storm 3	High Tide	24/1/2007	18	1.47	4.94	10.07	91.4
ST5	Hurricane Alex	Max H_s	15/1/2016	13	0.53	4.79	10.07	95.4
ST6		High Tide	15/1/2016	19	1.49	4.50	11.14	130.3

3.2.4 Model comparison

The primary objective of the two-dimensional SWASH simulation for the entire Praia da Vitória harbour and bay was to assess the capabilities of the SWASH model to perform simulations over a larger domain with complex coastal structures and bathymetry, while collecting data on overtopping discharge and water levels at specific output locations. The wave module of the HIDRALERTA system was driven by 72-hour wave and wind forecasts retrieved daily. This system estimates the average overtopping discharge (in litres per second per metre width) for a 3-hour window using the NN_OVERTOPPING2 neural network based on the wave outputs from the DREAMS model.

The overtopping discharges obtained from the SWASH simulations at corresponding output points were then compared with the results generated by the NN_OVERTOPPING2 (50 % quantile) and images captured during storm events. Additionally, predicted significant wave heights from DREAMS simulations were compared with the SWASH predictions for the most frequent and extreme weather conditions.

4 Results and Discussion

4.1 Test case 1 - South breakwater's section physical model tests replication

4.1.1 Model calibration

4.1.1.1 Test 112

In Test 112, free surface elevation of the SWASH simulation was compared with the physical model test for the first five simulations outlined in Table 3.2 of Section 3.1.2.1, where Manning's coefficient remained constant at 0.04 s/m$^{1/3}$. Table 4.1 to Table 4.5 present the Root Square Percentage Error for the wave parameters (RSPE^{WP}) of the physical model tests, and SWASH simulations at the wave gauge locations.

Table 4.1-RSPE^{WP} between the physical model and SWASH simulation T112_01.

Probe	Physical Model				SWASH Model				RSPE^{WP} (%)				Avg.
	$H_{1/3}$ *(m)*	$T_{1/3}$ *(s)*	H_{mo} *(m)*	T_p *(s)*	$H_{1/3}$ *(m)*	$T_{1/3}$ *(s)*	H_{mo} *(m)*	T_p *(s)*	$H_{1/3}$	$T_{1/3}$	H_{mo}	T_p	(%)
S1	8.36	16.82	7.97	17.45	9.06	19.39	8.98	19.75	8.4	15.3	12.6	13.2	12.4
S2	8.19	17.25	7.85	17.45	8.94	19.99	8.80	19.75	9.1	15.9	12.1	13.2	12.6
S3	7.21	16.09	6.98	17.45	8.82	20.15	8.51	19.75	22.4	25.2	21.9	13.2	20.7
												Avg.	**15.2**

Table 4.2- RSPE^{WP} between the physical model and SWASH simulation T112_02.

Probe	Physical Model				SWASH Model				RSPE^{WP} (%)				Avg.
	$H_{1/3}$ *(m)*	$T_{1/3}$ *(s)*	H_{mo} *(m)*	T_p *(s)*	$H_{1/3}$ *(m)*	$T_{1/3}$ *(s)*	H_{mo} *(m)*	T_p *(s)*	$H_{1/3}$	$T_{1/3}$	H_{mo} *)*	T_p	(%)
S1	8.36	16.82	7.97	17.45	8.54	19.73	8.25	16.39	2.2	17.3	3.6	6.1	7.3
S2	8.19	17.25	7.85	17.45	8.49	19.56	8.10	15.53	3.7	13.4	3.2	11.0	7.8
S3	7.21	16.09	6.98	17.45	7.67	19.60	7.33	19.38	6.4	21.8	5.0	11.1	11.1
												Avg.	**8.7**

Table 4.3- $RSPE^{WP}$ between the physical model and SWASH simulation T112_03.

Probe	Physical Model				SWASH Model				$RSPE^{WP}$ (%)				Avg.
	$H_{1/3}$ *(m)*	$T_{1/3}$ *(s)*	H_{mo} *(m)*	T_p *(s)*	$H_{1/3}$ *(m)*	$T_{1/3}$ *(s)*	H_{mo} *(m)*	T_p *(s)*	$H_{1/3}$	$T_{1/3}$	H_{mo}	T_p	(%)
S1	8.36	16.82	7.97	17.45	8.38	17.60	8.36	15.90	0.3	4.6	4.9	8.9	0.3
S2	8.19	17.25	7.85	17.45	8.56	17.96	8.41	15.90	4.6	4.1	7.2	8.9	4.6
S3	7.21	16.09	6.98	17.45	7.28	18.66	7.07	14.59	1.1	15.9	1.2	16.4	1.1
												Avg.	**6.5**

Table 4.4- $RSPE^{WP}$ between the physical model and SWASH simulation T112_04.

Probe	Physical Model				SWASH Model				$RSPE^{WP}$ (%)				Avg.
	$H_{1/3}$ *(m)*	$T_{1/3}$ *(s)*	H_{mo} *(m)*	T_p *(s)*	$H_{1/3}$ *(m)*	$T_{1/3}$ *(s)*	H_{mo} *(m)*	T_p *(s)*	$H_{1/3}$	$T_{1/3}$	H_{mo}	T_p	(%)
S1	8.36	16.82	7.97	17.45	8.30	17.73	8.07	15.99	0.7	5.4	1.3	8.3	3.9
S2	8.19	17.25	7.85	17.45	8.39	17.63	8.27	15.99	2.5	2.2	5.5	8.3	4.6
S3	7.21	16.09	6.98	17.45	7.14	17.12	6.99	14.35	1.0	6.4	0.1	17.7	6.3
												Avg.	**5.0**

Table 4.5-$RSPE^{WP}$ between the physical model and SWASH simulation T112_05.

Probe	Physical Model				SWASH Model				$RSPE^{WP}$ (%)				Avg.
	$H_{1/3}$ *(m)*	$T_{1/3}$ *(s)*	H_{mo} *(m)*	T_p *(s)*	$H_{1/3}$ *(m)*	$T_{1/3}$ *(s)*	H_{mo} *(m)*	T_p *(s)*	$H_{1/3}$	$T_{1/3}$	H_{mo}	T_p	(%)
S1	8.36	16.82	7.97	17.45	7.75	17.54	7.66	16.29	7.3	4.3	3.9	6.6	5.5
S2	8.19	17.25	7.85	17.45	8.09	17.66	7.94	15.35	1.2	2.4	1.2	12.0	4.2
S3	7.21	16.09	6.98	17.45	6.87	17.23	6.73	14.27	4.7	7.1	3.6	18.2	8.4
												Avg.	**6.0**

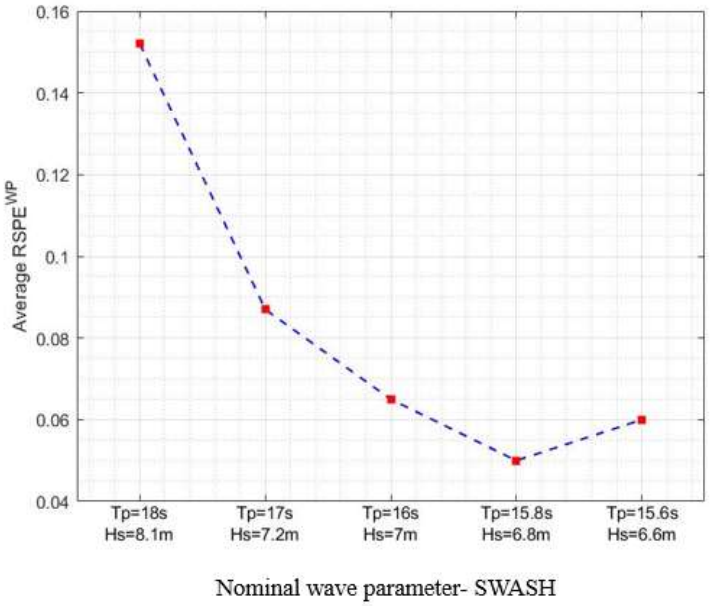

Figure 4.1- $RSPE^{WP}$ (0 to 1 scale) of wave parameters between physical model test and predicted (SWASH) against nominal wave parameters in SWASH simulation – Test 112.

The highest average error was observed across all simulations with the nominal wave parameters Hs of 8.1m and Tp of 18s (Figure 4.1). The most significant error was found at gauge S3, which was closest to the breakwater, except in the simulation T112_03. The lowest average $RSPE^{WP}$ for all three gauges was 5%, which resulted in the simulation T112_04. This indicates the best agreement between the predicted wave characteristics from the two-dimensional SWASH model and the physical model test. This conclusion is further supported by Figure 4.2, which illustrates the comparison of energy spectra between the physical model and the SWASH model at S1, S2, and S3.

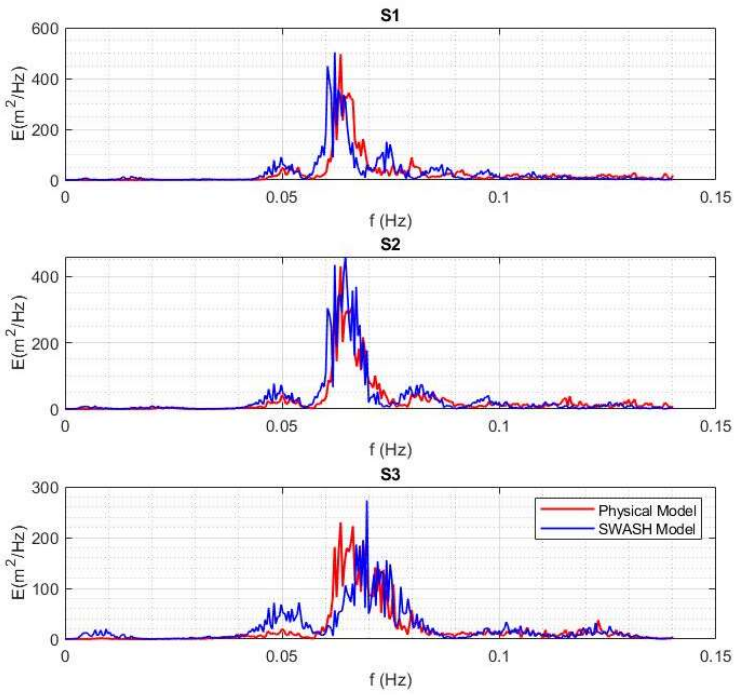

Figure 4.2- Comparison of wave spectra at gauges S1, S2, and S3 with the physical model and SWASH model T112_04.

Predicted SWASH energy spectrum at gauge S2 shows a strong correlation with the physical model test (Figure 4.2). Additionally, the peaks of both spectra align closely at the same frequency. However, gauge S1 and S2 showed a slight shift towards lower frequencies, while gauge S3 showed a minor shift towards higher frequencies compared with the physical model. Despite this frequency shift, the peaks of both spectra at gauge S1 still matched. Both gauges S1 and S2 were located further from the breakwater, while gauge S3 was the closest. The spectrum at gauge S3 shows that the energy in the lower frequency part of the spectrum starts increasing compared with the physical model data.

.

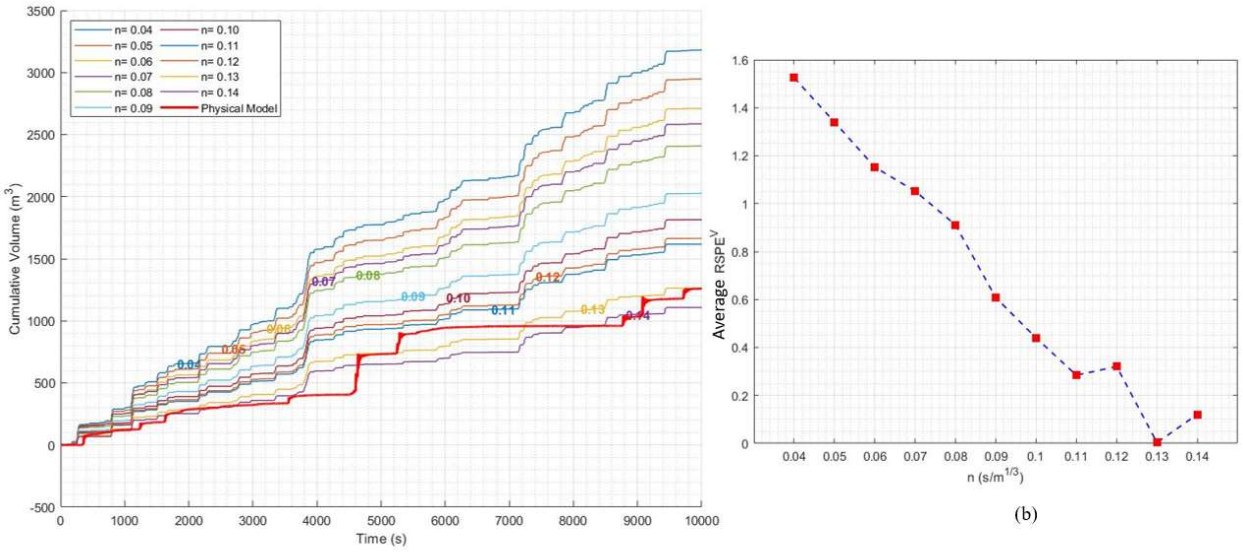

(a) (b)

Figure 4.3-(a).Cumulative volume over time, and (b) $RSPE^V$ (o to 1 scale), across varying Manning's coefficient (n). Hs of 6.8m and Tp of 15.8s are nominal wave parameters in SWASH simulation.

Cumulative overtopping volume decreased from 3181.3 m^3 to 1,108 m^3 when the friction coefficient increased from 0.04 $s/m^{1/3}$ to 0.14 $s/m^{1/3}$ at the outer slope of the south breakwater (Figure 4.3(a)). Additionally, a decreasing trend in the average Root Square Percentage Error ($RSPE^V$) was observed as the friction coefficient increased, as shown in Figure 4.3(b). At a friction coefficient of 0.13 $s/m^{1/3}$, the predicted cumulative overtopping volume reached 1264 m^3, closely matching the measured volume of 1260 m^3 from the physical model test. However, beyond a friction coefficient of 0.13 $s/m^{1/3}$, the $RSPE^V$ began to increase, indicating a divergence from the measured data at higher friction values. Specifically, after 10000s, the predicted cumulative overtopping volume for a friction coefficient of 0.14 $s/m^{1/3}$ was 1108 m^3, reflecting a 12% deviation from the measured data. Despite this deviation at 10000 s, this simulation demonstrates strong predictive capability for cumulative overtopping throughout the entire duration. These results of Test 112 indicate that most probably a suitable Manning's coefficient for the south breakwater was around 0.13 $s/m^{1/3}$.

4.1.1.2 Test 113

In Test 113, the validation of free surface elevation was performed for the first five simulations outlined in Table 3.3 of Section 3.1.2.2. Manning's coefficient of outer slope of south breakwater remained constant at 0.04 $s/m^{1/3}$ for the first five simulations.

Table 4.6- $RSPE^{WP}$ between the physical model and SWASH simulation T113_01

Probe	Physical Model				SWASH Model				$RSPE^{WP}$ (%)				Avg.
	$H_{1/3}$ *(m)*	$T_{1/3}$ *(s)*	H_{mo} *(m)*	T_p *(s)*	$H_{1/3}$ *(m)*	$T_{1/3}$ *(s)*	H_{mo} *(m)*	T_p *(s)*	$H_{1/3}$	$T_{1/3}$	H_{mo}	T_p	(%)
S1	9.80	16.78	9.24	17.68	10.2	19.09	10.1	16.20	3.8	13.8	9.4	8.4	8.8
S2	9.64	16.95	9.10	17.46	10.4	20.13	10.1	16.20	8.3	18.7	10.8	7.2	11.2
S3	8.50	16.27	8.10	17.46	10.2	19.96	9.83	18.98	20.8	22.6	21.3	8.8	18.4
												Avg.	**12.8**

Table 4.7-$RSPE^{WP}$ between the physical model and SWASH simulation T113_02.

Probe	Physical Model				SWASH Model				$RSPE^{WP}$ (%)				Avg.
	$H_{1/3}$ *(m)*	$T_{1/3}$ *(s)*	H_{mo} *(m)*	T_p *(s)*	$H_{1/3}$ *(m)*	$T_{1/3}$ *(s)*	H_{mo} *(m)*	T_p *(s)*	$H_{1/3}$	$T_{1/3}$	H_{mo}	T_p	(%)
S1	9.80	16.78	9.24	17.68	10.3	20.43	9.95	16.09	5.4	21.8	7.7	9.0	11.0
S2	9.64	16.95	9.10	17.46	10.4	21.71	9.82	16.09	7.9	28.0	7.8	7.8	12.9
S3	8.50	16.27	8.10	17.46	10.0	20.56	9.37	21.70	17.8	26.4	15.7	24.3	21.0
												Avg.	**15.0**

Table 4.8- $RSPE^{WP}$ between the physical model and SWASH simulation T113_03.

Probe	Physical Model				SWASH Model				$RSPE^{WP}$ (%)				Avg.
	$H_{1/3}$ *(m)*	$T_{1/3}$ *(s)*	H_{mo} *(m)*	T_p *(s)*	$H_{1/3}$ *(m)*	$T_{1/3}$ *(s)*	H_{mo} *(m)*	T_p *(s)*	$H_{1/3}$	$T_{1/3}$	H_{mo}	T_p	(%)
S1	9.80	16.78	9.24	17.68	10.3	20.32	9.91	16.31	5.4	21.1	7.3	7.8	10.4
S2	9.64	16.95	9.10	17.46	10.3	19.72	9.80	16.31	7.4	16.3	7.7	6.6	9.5
S3	8.50	16.27	8.10	17.46	9.70	20.56	9.10	14.64	14.2	26.3	12.3	16.1	17.2
												Avg.	**12.4**

Table 4.9-RSPE^{WP} between the physical model and SWASH simulation T113_04

Probe	Physical Model				SWASH Model				RSPE^{WP} (%)				Avg.
	$H_{1/3}$ *(m)*	$T_{1/3}$ *(s)*	H_{mo} *(m)*	T_p *(s)*	$H_{1/3}$ *(m)*	$T_{1/3}$ *(s)*	H_{mo} *(m)*	T_p *(s)*	$H_{1/3}$	$T_{1/3}$	H_{mo}	T_p	(%)
S1	9.80	16.78	9.24	17.68	10.36	20.8	9.91	19.76	5.7	23.9	7.3	11.7	12.1
S2	9.64	16.95	9.10	17.46	10.37	20.7	9.85	21.50	7.6	21.9	8.2	23.2	15.2
S3	8.50	16.27	8.10	17.46	10.77	21.5	10.0	21.50	26.7	32.3	24.3	23.2	26.6
												Avg.	**18.0**

Table 4.10- RSPE^{WP} between the physical model and SWASH T113_05.

Probe	Physical Model				SWASH Model				RSPE^{WP} (%)				Avg.
	$H_{1/3}$ *(m)*	$T_{1/3}$ *(s)*	H_{mo} *(m)*	T_p *(s)*	$H_{1/3}$ *(m)*	$T_{1/3}$ *(s)*	H_{mo} *(m)*	T_p *(s)*	$H_{1/3}$	$T_{1/3}$	H_{mo}	T_p	(%)
S1	9.80	16.78	9.24	17.68	9.73	20.5	9.37	19.76	0.7	22.6	1.4	11.7	9.1
S2	9.64	16.95	9.10	17.46	9.75	20.4	9.31	21.50	1.2	20.6	2.3	23.2	11.8
S3	8.50	16.27	8.10	17.46	10.13	21.4	9.54	21.50	19.3	31.7	17.7	23.2	23.0
												Avg.	**14.6**

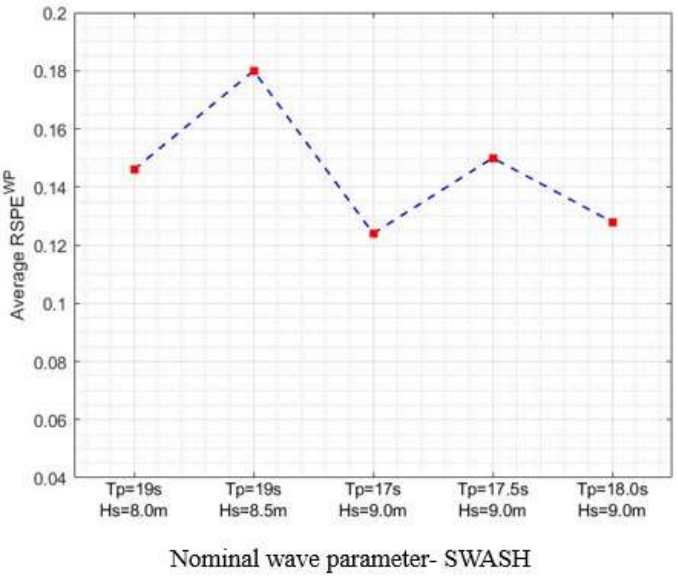

Figure 4.4- Average RSPE^{WP} (0 to 1 scale) of wave parameters between physical model test and predicted against nominal wave parameters in SWASH simulation-Test 113.

The highest average $RSPE^{WP}$ occurred during the simulation with nominal wave parameters with H_s of 8.5 m and T_p of 19.0 s (Figure 4.4). Among individual gauges, the most significant deviation, 26.6% was observed at S3, positioned nearest to the breakwater in simulation T113_04. The lowest average $RSPE^{WP}$ 12.4% was achieved in simulation T113_03, indicating optimal agreement between the two-dimensional SWASH model and physical test data.

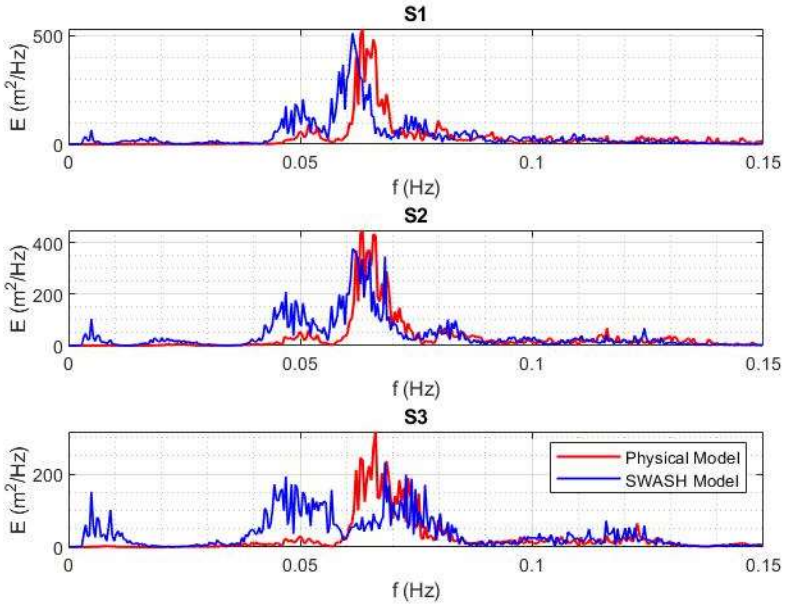

Figure 4.5- Comparison of wave spectrum at gauges S1, S2, and S3 for Test113_03 in the SWASH model.

It was clear across all three gauges that the spectrum energy began shifting toward the low-frequency part of the spectrum (Figure 4.5). This indicates an increase in low-frequency energy compared with the physical model test. To identify Manning's coefficient for the south breakwater, additional simulations were performed to compare the cumulative overtopping volume with the physical model, using various Manning's coefficients at the outer slope of the south breakwater with nominal wave parameters of H_s of 9.0 m and T_p of 17.0 s.

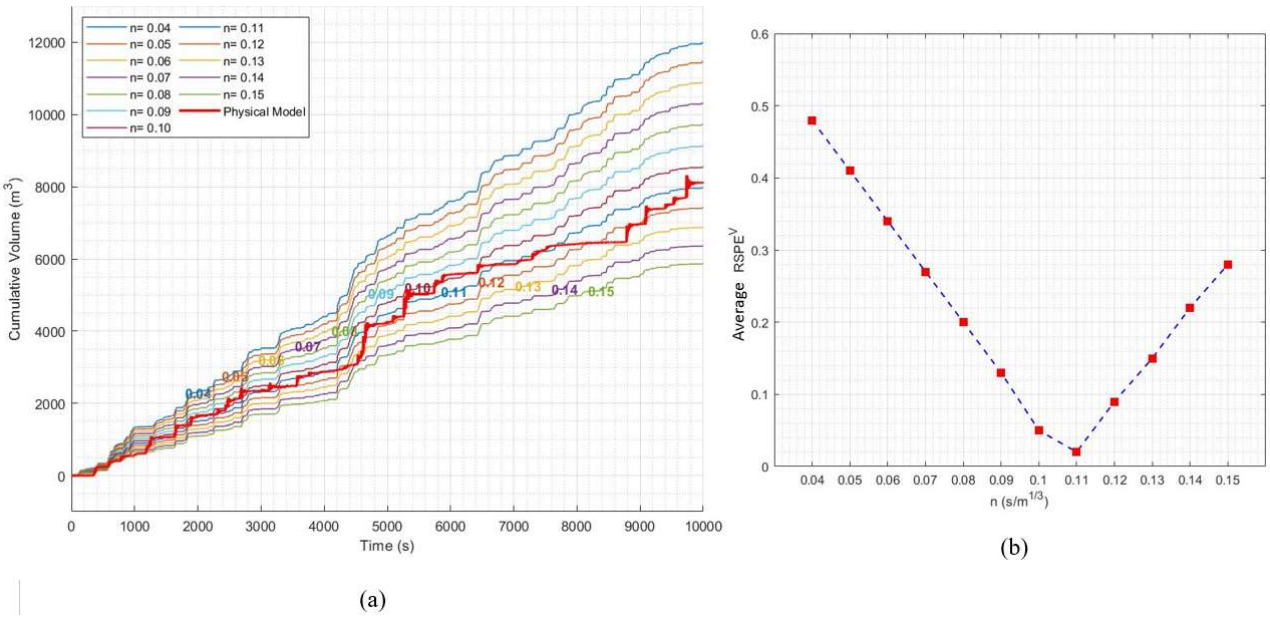

Figure 4.6-(a). Cumulative volume over time and (b) $RSPE^V$ across varying Manning's coefficient (n). H_s of 9.0 m and T_p of 17.0 s are nominal wave parameters in the SWASH simulation.

Cumulative overtopping volume gradually decreases from 11,990 m³ to 5,870.3 m³ when the friction coefficient increases from 0.04 to 0.15 s/m$^{1/3}$ (Figure 4.6(a)). Additionally, Figure 4.6(b) illustrates a downward trend in the average RSPEV as the friction coefficient increases. At a friction coefficient of 0.11 s/m$^{1/3}$, the predicted cumulative overtopping volume reached 7,976 m³, closely matching the measured volume of 8,113.1 m³ from the physical model test. However, beyond a friction coefficient of 0.11 s/m$^{1/3}$, the average RSPEV begins to increase. Despite the deviation of cumulative overtopping volume at 10000 s, simulations with friction coefficients of 0.12 s/m$^{1/3}$ also demonstrated strong predictive capabilities for cumulative overtopping estimation throughout the entire duration. These results indicate that most probably a suitable Manning's coefficient for the south breakwater was around 0.11 s/m$^{1/3}$ according to Test 113.

4.1.2 Sensitivity analysis

4.1.2.1 Meshing resolution and quality

Four different mesh resolutions were examined by varying the input parameter, the number of points per wavelength in the mesh generator, while assuming the wave period remains constant.

Table 4.11- Input/ Output parameters of each unstructured mesh and CPU times.

Mesh	Input Parameter	Mesh output parameters					SWASH CPU time (hours)
	Minimum No. of points per wavelength	Total no. of nodes	Avg. no. of points per wavelength	Minimum no. of points per wavelength	Quality of mesh (%)	Band width	
Mesh1	12	7948	44	18	95.2	53	7.93
Mesh2	15	8162	44	19	96.0	42	22.74
Mesh3	18	8298	44	20	94.6	45	21.63
Mesh4	21	10114	47	23	78.6	78	58.46
Mesh5	27	16723	59	28	97.2	90	52.36

It was observed that the number of points per wavelength as an input parameter did not affect the average number of points per wavelength across the entire domain; this value remained constant from Mesh1 to Mesh3 (Table 4.11). However, it slightly increased when the number of points per wavelength was set to 21 and further increased to 59 when the input parameter was 27. On the other hand, the minimum number of points per wavelength gradually increased as the input parameter increased. In Mesh1, Mesh2 and Mesh3, the mesh quality remained between 94.6% and 96.0%. However, the quality of Mesh4 drastically reduced to 78.6%, and again increased to 97.2% in Mesh5. Additionally, the bandwidth of the matrix is an important factor in determining the computational efficiency. When the input parameter increases from 12 to 18, the bandwidth shows a gradual decrease. However, in Mesh4, the bandwidth starts increasing and continues to increase in Mesh5.

Initially, CPU time starts increasing with the total number of nodes in the domain (Figure 4.7). However, after reaching the highest CPU time of 58.46 hours, it starts to decrease gradually. In this study, the lowest CPU time was found when the bandwidth was 53.

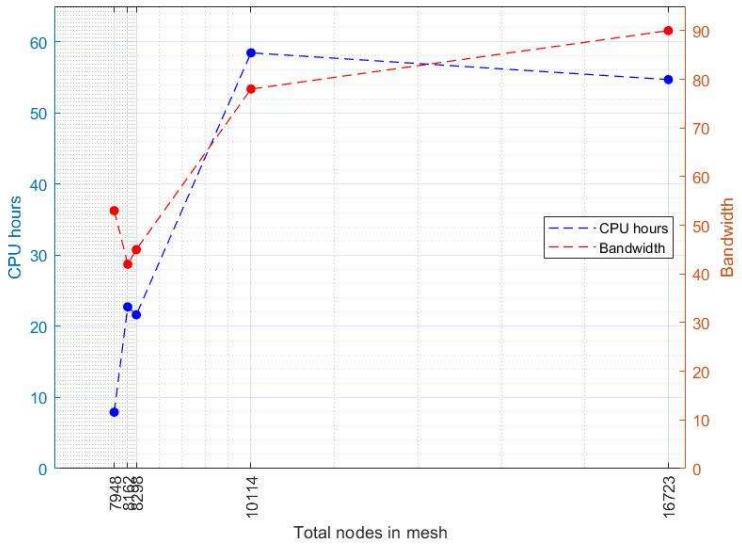

Figure 4.7- (a)Impact of total node count on CPU time and bandwidth across different meshes.

The most significant difference in cumulative overtopping volume was observed after 10000 s, when the mesh quality was 78.6% (Figure 4.8). When the quality of the mesh was 95.2%, the predicted cumulative volume was 1263.9 m^3, closely matching the physical model test results. As the mesh quality further improves, the predicted cumulative overtopping volume begins to deviate from the measured data. Therefore, it was clear that increasing the mesh quality from the optimum value caused the predicted cumulative volume to diverge from the measured data in the physical model test.

A sensitivity analysis on mesh resolution was conducted for Test112_04_m9 to examine how the number of nodes in the simulation domain and the mesh quality influence $RSPE^{WP}$ at gauges S1, S2, S3 and the cumulative overtopping volume after 10000 s. At all three gauges, the maximum $RSPE^{WP}$ was recorded in the mesh with a total number of nodes 10114 and begins to decrease once the number of nodes increases (Figure 4.9).

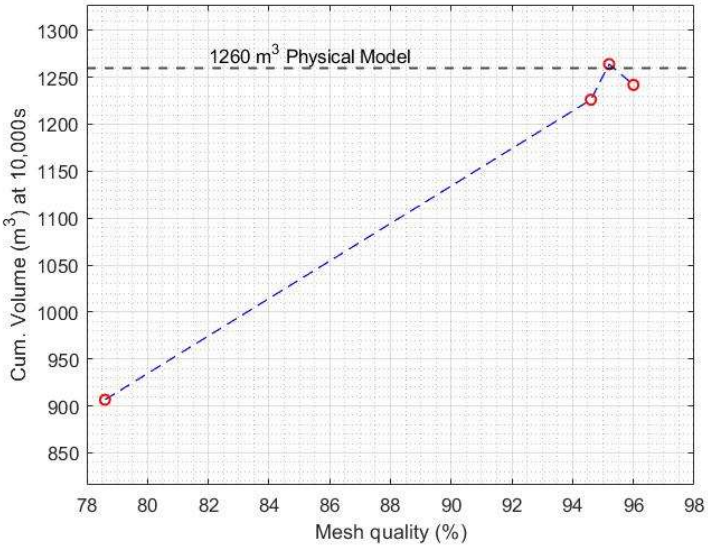

Figure 4.8- Cumulative volume versus mesh quality for T112_04_m9 in SWASH simulation.

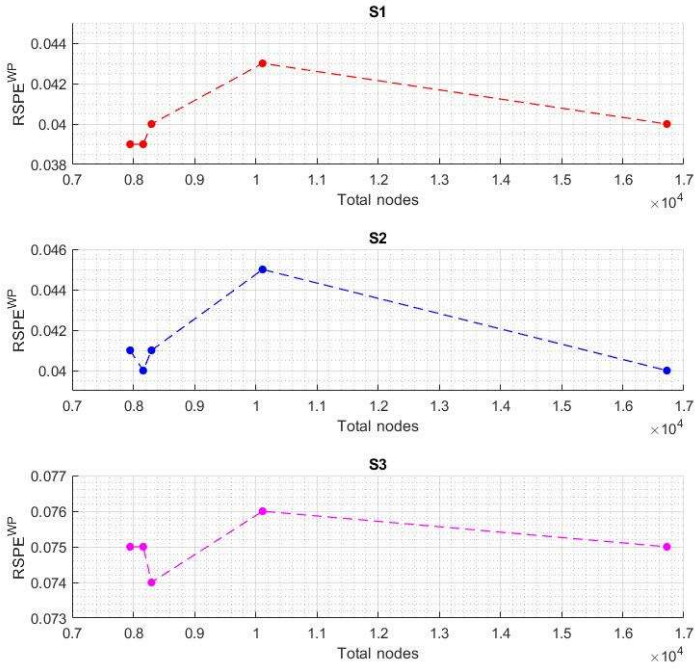

Figure 4.9- Variation of $RSPE^{WP}$ at S1, S2, and S3 in Mesh1 to Mesh5-T112_04_m09.

4.1.2.2 Seeding number

Three different randomly selected seed numbers, 21436587, 87654321, and 12345678, were used for this sensitivity analysis. The seed number 12345678 was the default number in the SWASH model. In this study, the seeding effect on overtopping volume was examined using combinations of nominal wave parameters and Manning's coefficients identified in T112_04_m9 and T113_03_m7, under sections 4.1.1.1 and 4.1.1.2.

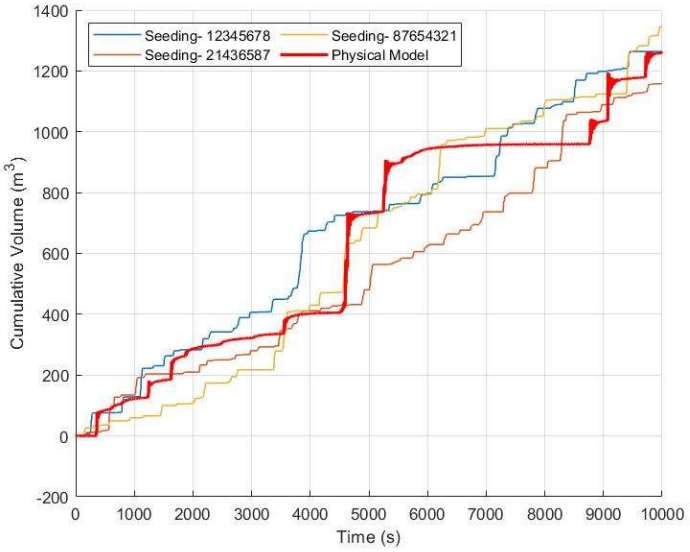

Figure 4.10- Variation of cumulative volume for various seedings - T112_04_m9.

Seeding number 12345678 exhibited the slightest deviation, showing an error of 0.3% (after 10000s) compared to the physical model test (Figure 4.10). It was noted that the maximum individual overtopping volume occurred earlier in this simulation than in the physical model. However, the overall pattern remained consistent throughout the time series. The simulation with seeding number 21436587 shows 8.1% lower cumulative volume prediction after 10000s. On the other hand, the third simulation with seeding number 87654321 yielded the highest cumulative overtopping volume at the end of the simulation, totaling 1345.1 m^3. This resulted in a 6.7% overestimation when compared with the physical model test. In this test, different seeding numbers

resulted in deviations ranging from -8.1% to 6.7%. Overall, all simulations demonstrated a good agreement with the physical model test data.

Seeding number 12345678 exhibited the slightest deviation, with an $RSPE^V$ of 15.2% (after 10000s) compared with the physical model (Figure 4.11). For seeding numbers 21436587 and 87654321, the $RSPE^V$ values were 21.2% and 29.3%, respectively. For the first 3000s, all three simulations exhibited good agreement with one another; however, deviations began to occur as time progressed. For T113_03_m7, different seeding numbers resulted in deviations between -15.2% and -29.3% after 10000s.

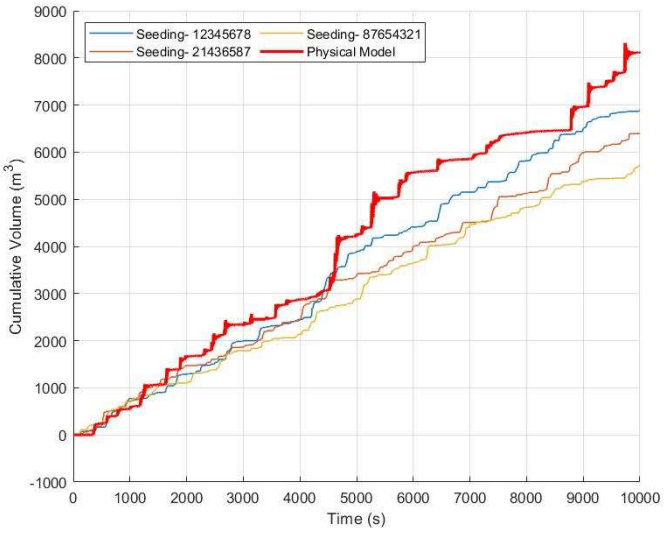

Figure 4.11- Variation of cumulative volume for various seedings - T113_03_m7.

$RSPE^V$ starts to decline across all seeding cases as the simulation time window increases (Figure 4.13). In 112_04_m9, the three seeding values displayed distinct behaviours during the initial phase of the simulation. The maximum deviation was observed after 4000s, reaching 67.6% for seeding: 12345678, and 2.5% and 7% for seeding: 21436587 and 87654321, respectively. This deviation decreased to 0.3% after 10,000s of simulation for seeding: 12345678, while it was 8.1% and 6.8% for seedings: 21436587 and 87654321, respectively.

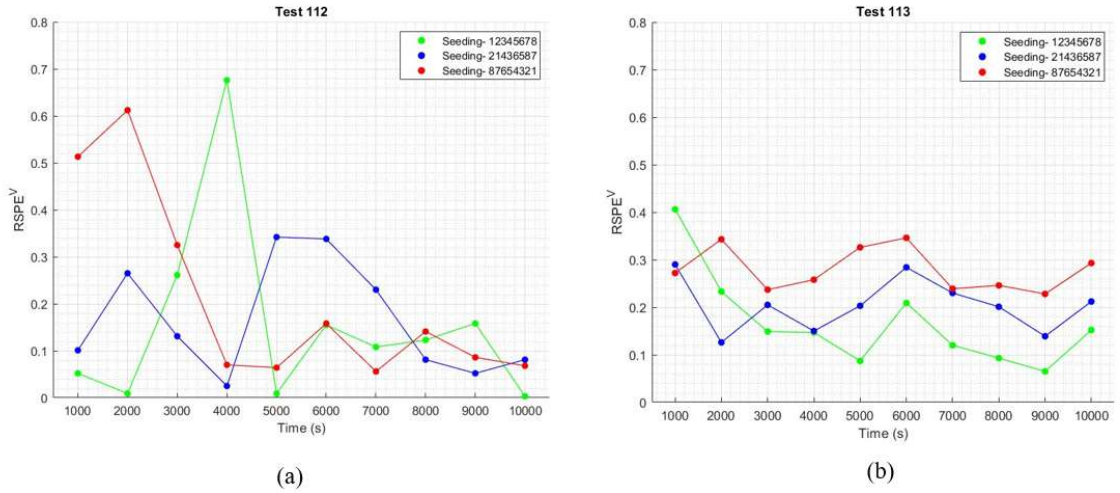

Figure 4.12-Variation of $RSPE^V$ (0 to 1 scale) for different seedings: (a) T112_04_m9, (b) T113_03_m7 .

In T113_03_m7, the highest deviation was 40.6% after 1000 s of simulation for seeding: 12345678, with 29% and 27.2% for seeding: 21436587 and 87654321, respectively (Figure 4.13 (b)). After 10000 s of simulations, these values changed to 15.2%, 21.2%, and 29.3% for seeds 12345678, 21436587, and 87654321, respectively. This indicates that $RSPE^V$ decreases as the simulation time increases. However, fluctuations in $RSPE^V$ were more significant in T112_04_m9 than in T113_03_m7. In Test 113_03_m7, $RSPE^V$ values gradually reduced over time without the initial variability seen in T112_04_m9. Although a peak was observed for seeding: 12345678 in T112_04_m9, this seeding generally showed lower error rates among the three seeding numbers.

4.1.3 Discussion

4.1.3.1 Manning's friction coefficient for the outer slope of the south breakwater

The analysis showed a decrease in overtopping discharge as the Manning's coefficient for the outer slope of the south breakwater increased in both test cases. In Test 112, the optimal friction value was determined to be 0.13 $s/m^{1/3}$, corresponding to a 5% prediction error for the $RSPE^{WP}$ and a 0.3% deviation in the $RSPE^V$ at the end of the simulation. In Test 113, the predicted wave

parameters had a 12.4% deviation, and the cumulative overtopping volume had a 1.7% deviation compared with the physical model test. The correspondence Manning's coefficient was 0.11 $s/m^{1/3}$, which is closer to the value obtained in Test 112. This indicates that, while achieving convergent friction coefficients following the methodology of this study, $RSPE^{WP}$ values deviate by 7.4% from one another. Zhang et al. (2020) observed that Manning's coefficient is sensitive to R_c/H_{m0}, wave steepness (Sop), and T_p. In his study, Manning's coefficient was adjusted between 0.02 $s/m^{1/3}$ and 0.122 $s/m^{1/3}$ to ensure consistency with the overtopping data from physical model tests, for different R_c/H_{m0} values and wave steepness (S_{op}). However, during the replication of the physical model test, Manning's coefficient for the outer slope of the breakwater was calibrated at a tide level of +3.0 m (ZH) for both test cases. Future studies are recommended to include more test cases with varying tide levels to achieve a more accurate determination of Manning's coefficient for the outer slope of the breakwater.

The findings of this dissertation indicate that the SWASH model was capable of predicting wave parameters with considerable accuracy at a specific location. This was supported by the results of a study conducted by Suzuki in 2017, which demonstrated that the SWASH model generally reproduces the wave at a given location. However, it was observed that the $RSPE^{WP}$ of predicted wave parameters is higher for gauges that are closer to the structure.

In both Test 112 and Test 113, low-frequency spectrum energy tends to increase at wave gauge S3, which was closest to the structure. This shift was significant in Test113 than in Test112. In the SWASH simulation, the breakwater was treated as impermeable, and a Manning's coefficient was applied to dissipate energy caused by surface roughness and seepage. When waves approach structures, some of the wave energy is dissipated through breaking and interaction with the structure, while a certain amount of energy is reflected. These reflected waves interact with the incoming waves, potentially resulting in the transfer of energy to lower frequencies and the generation of longer waves. This phenomenon was visible through the formation of a peak in the low-frequency range. The shift of spectrum energy towards the low-frequency range confirms the findings of Suzuki et al. (2012). In the physical model test, the structure was modelled as a porous structure with tetrapod armours on the outer slope. Due to the characteristics of porous media, wave reflection would be lower than in the SWASH simulation. Therefore, this spectrum shift was not so significant in the physical model.

4.1.3.2 Mesh resolution and quality

The sensitivity analysis of the mesh resolution revealed that careful selection of the computational grid was crucial, as it significantly impacts the overtopping discharge in simulations. Increasing the number of points per wavelength was one option to improve mesh quality; however, this study shows that mesh quality did not always increase proportionately with the number of points. After reaching an optimum point, mesh quality begins to decrease with further increases in the number of points per wavelength. There was no significant difference in cumulative overtopping when the quality of mesh was 94.6% to 96.0%. However, a significant decline in overtopping volume was observed when the mesh quality decreased. This observation aligns with Suzuki et al. (2014), who demonstrated that, for a regular computational grid, the resolution of the computational grid impacts overtopping discharge. The findings in this thesis indicate that Suzuki *et al*. (2014) conclusions also apply to unstructured computational grids.

Furthermore, this study's predictions of wave parameters such as $H_{1/3}$, $T_{1/3}$, H_{mo}, and T_p using SWASH were only deviated 5% (T112_04) and 12.4% (T113_03) from the physical model data. This confirmed the conclusions of Suzuki et al. (2014) and Suzuki *et al*. (2017) regarding SWASH's capability to accurately predict wave parameters such as significant wave height, peak wave period, and time series of free surface elevation. However, Suzuki *et al*., 2014), observed that there was no significant influence of the grid resolution of the structured grid on wave transformation. In contrast to their findings, this study found that the wave transformation was influenced by the resolution of the unstructured grid.

4.1.3.3 Seeding number

SWASH overtopping predictions were significantly influenced by the time series in the offshore boundary. This study illustrates that overtopping discharge was highly sensitive to the sequence of individual waves, which can affect the overtopping volumes, even if the energy spectrum has the same shape and magnitudes. This finding was further supported by the research of McCabe *et al*. (2012) and Williams *et al*. (2014). Additionally, it was observed that the sensitivity was more

pronounced during shorter simulation times, with differences diminishing as the duration increased. This highlights the importance of selecting an appropriate simulation length to accurately capture the mean overtopping behaviour over time. Furthermore, the study shows that as the simulation time lengthens, the influence of seeding effects decreases. However, additional simulations with varying wave parameters and a broader range of random seedings are needed to validate this conclusion more robustly.

4.2 Test case 2 - The whole harbour and bay domain

4.2.1 Wave propagation and transformation

For the simulation of the whole harbour and bay domain, the National Distributed Computing Infrastructure (INCD) cluster was utilised. The INCD provides high-performance computing services to researchers in Portugal. All the runs were aimed to run for a total simulation of 3h (10800s). For various reasons, the runs stopped before reaching this mark. One of the reasons was the INCD's simulation time constraint, which allows for continuous model runs up to a maximum duration of 4 days. Therefore, simulations requiring more than 4 days of running time were automatically stopped by the system. In other cases, the model becomes unstable after some time, and SWASH terminates it. A detailed summary of the simulation parameters for the events simulated in the SWASH model is given in Table 4.12.

.

Table 4.12- Simulation time and computational efficiency of SWASH model runs.

Scenario	Date and time	Total simulation time achieved(s)	Run stop reason	CPU hours
MF1	2024-04-01 08:00	4,153	Cluster time limit	96
MF2	2024-01-15 17:00	3,538	Cluster time limit	96
MF3	2024-01-14 03:00	3002	Unstable	-
MF4	2024-01-13 04:00	475	Unstable	-
ST1	2004-03-25 17:00	4038	Cluster time limit	96
ST2	2005-02-26 23:00	None	Unknown	-
ST3	2005-02-27 03:00	1213	Unstable	-
ST4	2007-01-24 18:00	1549	Unstable	-
ST5	2016-01-15 13:00	4,254	Cluster time limit	96
ST6	2016-01-15 19:00	1807	Unstable	-

For each event, the Fast Fourier Transform (FFT) method was used to determine the energy spectrum of the wave signal and obtain significant wave height and peak period. It should be noted that event MF4 was disregarded due to its short simulation time. Sample spectra and water level observations from the monitoring points (P 03, P 09, and P 18) located in front of the south breakwater during the MF1 simulation are illustrated in Figure 4.13.

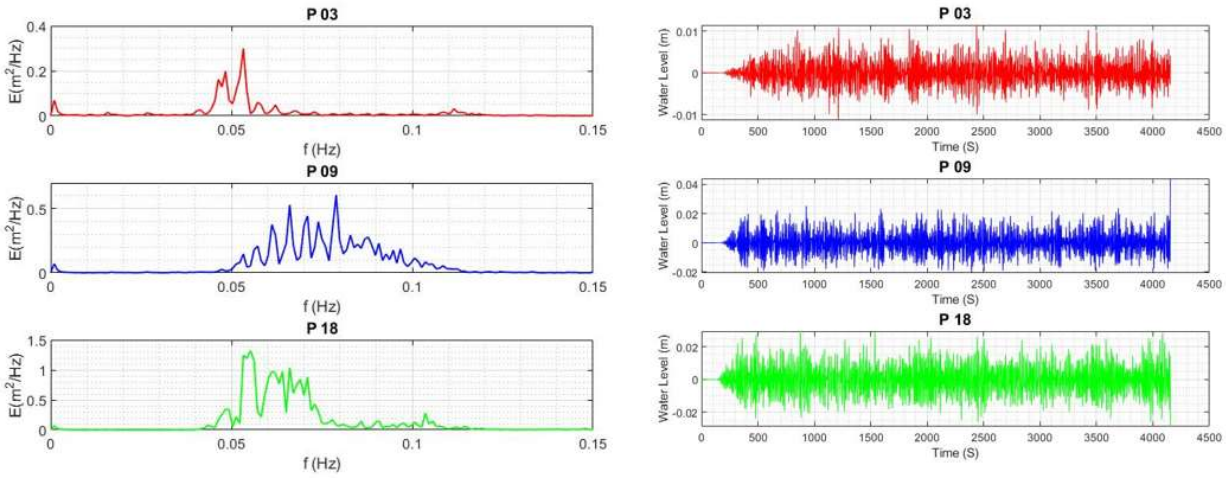

Figure 4.13- Energy spectrum (left) and observed water level (right) at observation points: P 03, P 09, and P 18 in front of south breakwater- event MF1.

To compare significant wave height predictions of DREAMS and SWASH models, statistical parameters such as relative difference, and Root Mean Square Error (RMSE) were calculated as illustrated in Table 4.13 to Table 4.14 for each event.

Table 4.13- Comparison of significant wave height prediction of DREAMS and SWASH model for event MF1.

MF1 Event							
Point location		DREAMS H_s (m)	SWASH H_s (m)	Abs. diff. H_s (m)	Relative diff. (%)	RSME (m)	RSME (m) Avg.
South Breakwater	P 03	0.73	0.15	0.58	130.8	0.44	0.34
	P 09	0.83	0.41	0.42	67.6		
	P 18	0.32	0.57	0.25	56.4		
North Breakwater	P 30	0.18	0.48	0.29	88.3	0.29	
Bay Waterfront	P 41	0.01	0.40	0.39	190.0	0.28	
	P 48	0.01	0.28	0.26	182.6		
	P 51	0.04	0.25	0.21	142.8		
	P 55	0.02	0.31	0.29	177.0		
	P 59	0.05	0.24	0.20	135.7		

Table 4.14- Comparison of significant wave height prediction of DREAMS and SWASH model for event MF2.

MF2 Event							
Point location		DREAMS H_s (m)	SWASH H_s (m)	Abs. diff. H_s (m)	Relative diff. (%)	RSME (m)	RSME (m) Avg.
South Breakwater	P 03	0.58	0.19	0.39	100.7	0.34	0.32
	P 09	0.92	0.53	0.40	54.9		
	P 18	0.68	0.51	0.18	30.1		
North Breakwater	P 30	0.22	0.59	0.37	90.7	0.37	
Bay Waterfront	P 41	0.03	0.32	0.30	170.7	0.22	
	P 48	0.04	0.18	0.14	129.2		
	P 51	0.05	0.33	0.28	143.6		
	P 55	0.05	0.23	0.18	129.2		
	P 59	0.04	0.22	0.18	137.7		

Table 4.15- Comparison of significant wave height prediction of DREAMS and SWASH model for event MF3

MF3 Event							
Point location		DREAMS Hs(m)	SWASH HS(m)	Abs. diff. Hs (m)	Relative diff. (%)	RSME (m)	RSME (m)
South Breakwater	P 03	3.21	0.25	2.96	170.9	3.05	1.90
	P 09	4.10	0.83	3.27	132.9		
	P 18	4.34	1.43	2.91	101.0		
North Breakwater	P 30	1.01	2.11	1.10	70.6	1.10	
Bay Waterfront	P 41	0.41	0.83	0.42	67.1	0.52	
	P 48	0.42	0.76	0.34	57.5		
	P 51	0.37	0.63	0.26	52.4		
	P 55	0.26	1.13	0.86	123.9		
	P 59	0.25	0.74	0.49	98.1		

Table 4.16 - Comparison of significant wave height prediction of DREAMS and SWASH model for event ST1.

ST1 Event							
Point location		DREAMS H_s (m)	SWASH H_s (m)	Abs. diff. H_s (m)	Relative diff. (%)	RSME (m)	RSME (m) Avg.
South Breakwater	P 03	6.71	1.67	5.04	120.2	3.95	2.37
	P 09	7.80	4.03	3.77	63.8		
	P 18	8.22	5.52	2.69	39.2		
North Breakwater	P 30	2.68	3.77	1.09	33.7	1.09	
Bay Waterfront	P 41	1.17	0.91	0.26	24.9	0.20	
	P 48	0.78	0.72	0.06	7.9		
	P 51	0.78	0.84	0.06	7.9		
	P 55	0.78	1.13	0.35	36.4		
	P 59	0.51	0.59	0.08	15.3		

Table 4.17- Comparison of significant wave height prediction of DREAMS and SWASH model for event ST3.

ST3 Event							
Point location		DREAMS H_s (m)	SWASH H_s (m)	Abs. diff. H_s (m)	Relative diff. (%)	RSME (m)	RSME (m) Avg.
South Breakwater	P 03	5.84	1.07	4.77	138.0	4.0	2.37
	P 09	7.80	2.80	5.00	94.4		
	P 18	6.13	5.59	0.55	9.3		
North Breakwater	P 30	3.19	3.93	0.74	20.8	0.74	
Bay Waterfront	P 41	1.17	1.17	0.00	0.0	0.46	
	P 48	0.78	1.16	0.38	38.9		
	P 51	0.78	1.16	0.38	39.6		
	P 55	0.78	1.61	0.83	69.3		
	P 59	0.51	0.83	0.32	48.4		

Table 4.18- Comparison of significant wave height prediction of DREAMS and SWASH model for event ST4.

ST4 Event							
Point location		DREAMS H_s (m)	SWASH H_s (m)	Abs. diff. H_s (m)	Relative diff. (%)	RSME (m)	RSME (m) Avg.
South Breakwater	P 03	5.84	2.14	3.70	92.7	3.24	1.88
	P 09	7.80	4.04	3.76	63.6		
	P 18	6.13	4.23	1.90	36.6		
North Breakwater	P 30	3.19	3.25	0.05	1.6	0.05	
Bay Waterfront	P 41	1.17	0.88	0.29	28.0	0.39	
	P 48	0.78	1.08	0.30	32.3		
	P 51	0.78	1.15	0.37	38.5		
	P 55	0.78	1.35	0.57	53.7		
	P 59	0.51	0.83	0.32	48.1		

Table 4.19- Comparison of significant wave height prediction of DREAMS and SWASH model for event ST5.

ST5 Event							
Point location		DREAMS H_s (m)	SWASH H_s (m)	Abs. diff. H_s (m)	Relative diff. (%)	RSME (m)	RSME (m) Avg.
South Breakwater	P 03	5.49	1.86	3.63	98.9	2.22	2.35
	P 09	3.98	3.64	0.33	8.8		
	P 18	4.51	3.31	1.21	30.9		
North Breakwater	P 30	5.81	2.41	3.40	82.7	3.4	
Bay Waterfront	P 41	1.17	0.54	0.63	73.5	0.32	
	P 48	0.78	0.48	0.30	48.1		
	P 51	0.78	0.71	0.07	8.8		
	P 55	0.78	0.93	0.15	17.8		
	P 59	0.51	0.46	0.04	9.0		

Table 4.20- Comparison of significant wave height prediction of DREAMS and SWASH model for event ST6.

ST6 Event							
Point location		DREAMS H_s (m)	SWASH H_s (m)	Abs. diff. H_s (m)	Relative diff. (%)	RSME (m)	RSME (m) Avg.
South Breakwater	P 03	5.02	1.80	3.22	94.3	2.11	3.49
	P 09	1.87	3.36	1.49	57.0		
	P 18	2.75	3.65	0.91	28.3		
North Breakwater	P 30	6.63	0.97	5.66	148.7	5.66	
Bay Waterfront	P 41	0.51	0.50	0.01	1.5	0.30	
	P 48	0.78	0.57	0.21	31.7		
	P 51	0.78	0.73	0.05	6.0		
	P 55	0.78	1.35	0.57	53.7		
	P 59	0.51	0.79	0.28	43.1		

In event MF1 (Table 4.13), the highest relative difference of 130.8% was observed at point 03, located in front of the south breakwater. Overall, DREAMS tend to overestimate wave heights compared to SWASH, with an RMSE of 0.44 m at points near the breakwater. In contrast, at the location in front of the north breakwater, the SWASH model shows a greater estimate compared to DREAMS, with a difference of 0.37m. Although the RMSE at points in front of the bay waterfront was measured at 0.28 m, points 41 and 48 exhibited relative differences of 190% and 182.6%, respectively. In general, SWASH also overestimates wave heights, particularly in areas near the bay waterfront. Considering all observation points during the MF1 event, the overall RMSE was 0.34 m.

Furthermore, in MF1and MF2, the average RMSE for all points was 0.34m and 0.32m, respectively. However, in the MF3 event, the average RMSE is significantly higher than in MF1 and MF2, at 1.9m. Additionally, the Hs of the MF3 event, at 2.94m, is larger than in MF1 and MF2, which are 0.95m and 1.29m, respectively, and there is no significant difference in Tp among the three events. This indicates that when the Hs increases, the DREAMS model tends to overestimate wave heights more than the SWASH model.

In the ST1 event (Table 4.16), there is a significant absolute difference of 5.04m at point 03 (south breakwater), indicating considerable divergence between the two models. The resulting RMSE for all points in front of the south breakwater is 3.95m, with the DREAMS model overestimating compared to the SWASH model. At point 30, the two models exhibit an RMSE of 1.09 m, demonstrating good agreement at points 48 and 51, with a relative difference of 7.9%.

The ST3 event (Table 4.17) also exhibits notable discrepancies, particularly at point 03, where the absolute difference is 4.77 m. However, at point P18, both models show good agreement, with a relative difference of 9.3%, even during extreme events. The predictions perfectly match at point 41. Similar to the ST1 event, ST3 shows an RMSE of 4m for points in front of the south breakwater. Overall, the RMSE for all points in both the ST1 and ST3 events is the same, recorded at 2.37m.

The ST4 event (Table 4.18) demonstrates improved model alignment, with lower discrepancies at locations such as point 30 (north breakwater), where the relative difference is only 1.6% and the RMSE is 0.05m. This event also shows the lowest RMSE, at 1.88m, compared to all other extreme events.

In ST5 (Table 4.19), similar trends were observed, with point 03 showing a high relative difference of 98.9%. However, two models performed well at points 51 and 59, resulting in relative differences of 8.8% and 9.0%, respectively. In the ST6 event, the highest discrepancy was noted at point 30 (north breakwater), where the absolute difference was 5.66m, leading to a relative difference of 148.7%. This indicates a significant failure of both models in this region. In contrast, the models performed well at points 41 and 51, with relative differences of 1.5% and 6%, respectively.

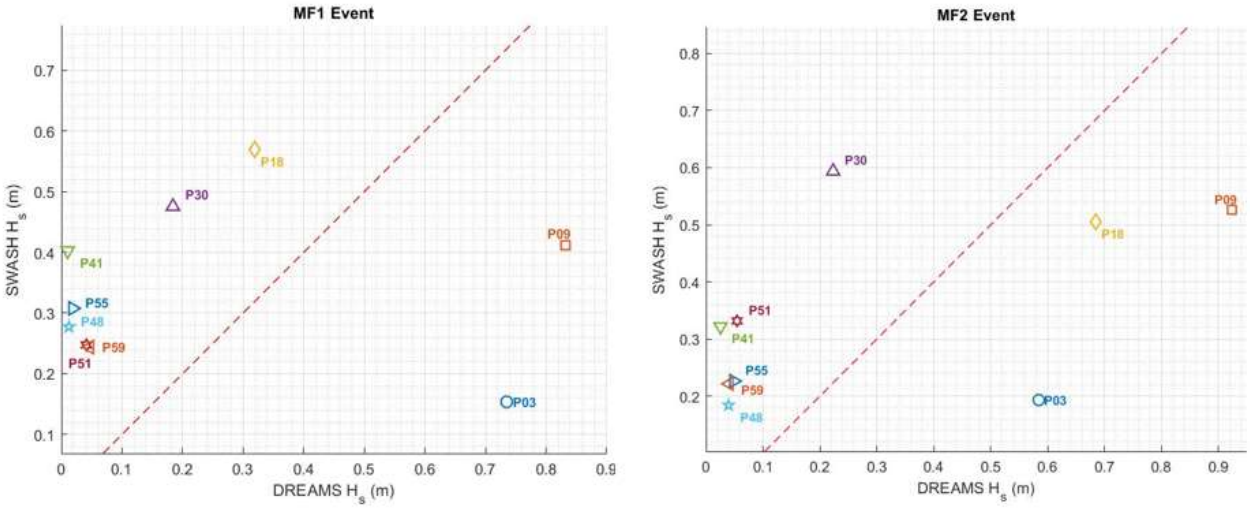

Figure 4.14- Comparison of Hs prediction of DREAMS and SWASH models for MF1 (left) and MF2(right) events.

Since the Root-Mean-Square Error (RMSE) alone does not account for potential outliers or extreme discrepancies, separate scatterplots were generated for each event (Figure 4.14, and Figure 4.15). For both events MF1 and MF2, the SWASH model overestimated the wave height compared to the DREAMS model at points located in front of the bay waterfront. However, at points 03 and 09, the predictions made by the DREAMS model were significantly higher than those of the SWASH model. Additionally, at point 30, the SWASH model also overpredicted the wave height.

During storm events, both models show good agreement when predicting wave height less than 1m at points along the bay waterfront (Figure 4.15). However, in the ST6 event, all points in front of the south breakwater and north breakwater showed that DREAMS predictions were significantly higher than those of SWASH. Except for point 09, DREAMS overestimated the wave height for points 03, 18, and 30 during the ST6 event. The comparison of wave height prediction between the two models across all events is shown in Figure 4.16.

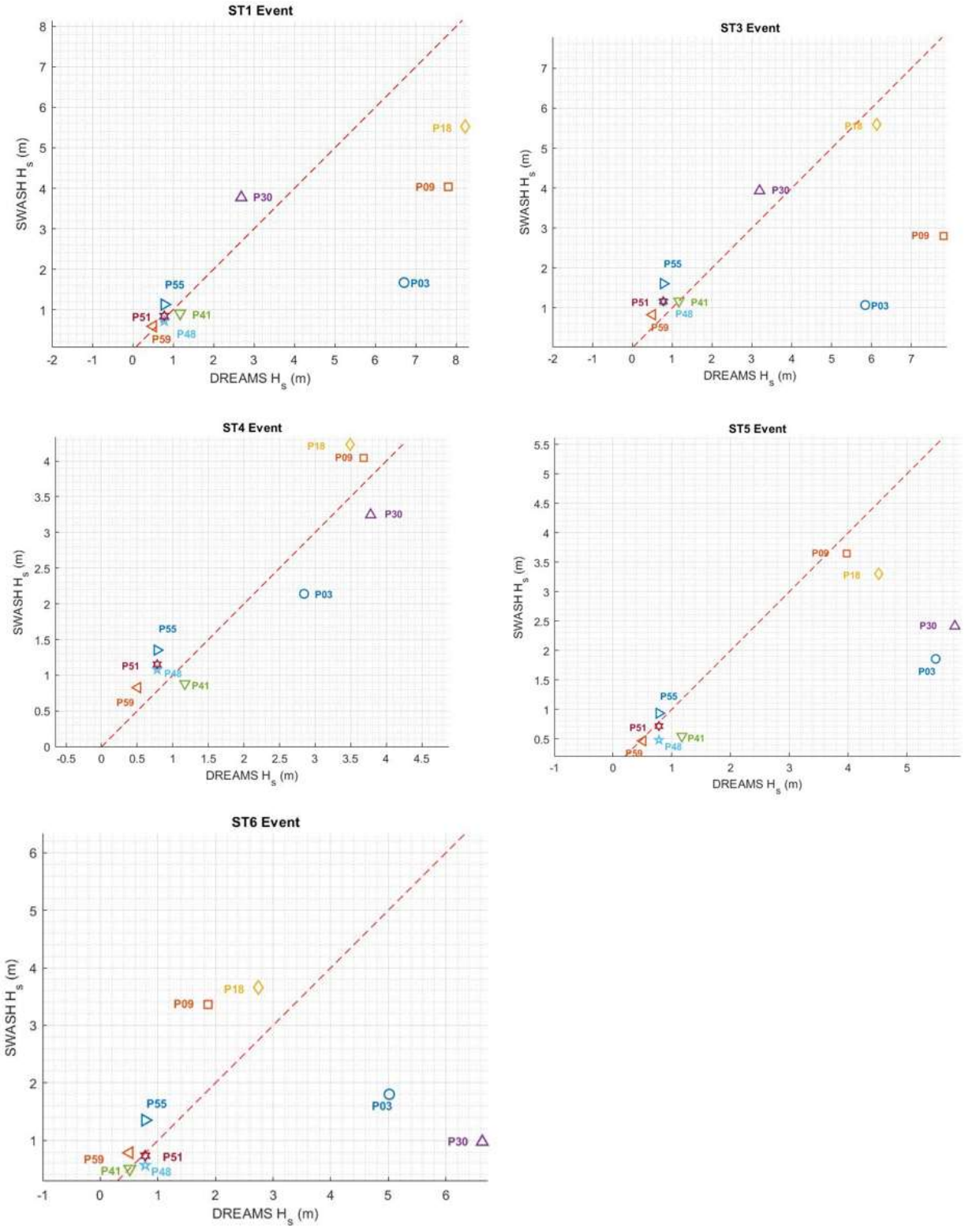

Figure 4.15- Comparison of Hs prediction of DREAMS and SWASH models for extreme events ST1, ST3, ST4, ST5, and ST6 events.

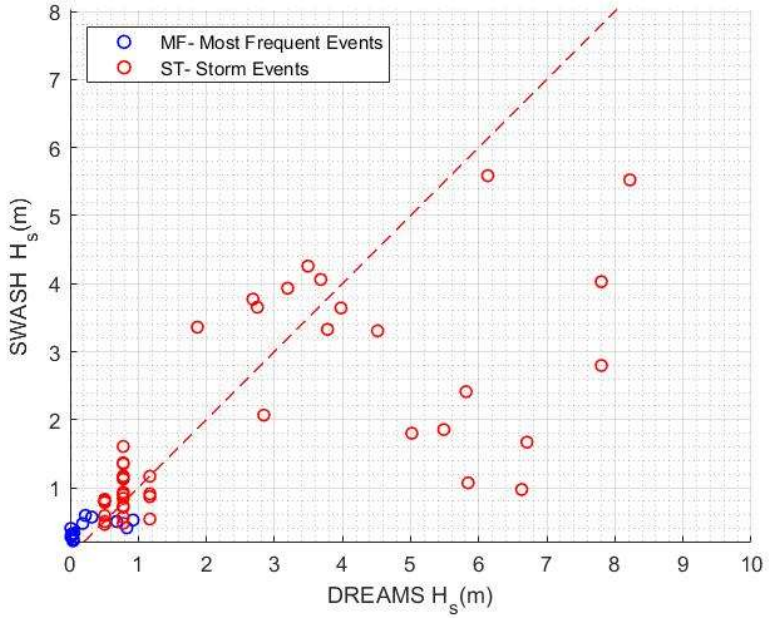

Figure 4.16-Comparison of SWASH and DREAMS predictions for significant wave height (H_s) across most frequent (blue dots) and storm events (red dots).

It was worth noting that, in the DREAMS model, the final wave height (H_s) was determined by selecting the minimum value between the model's predicted wave height and a value calculated using a fixed breaker parameter (0.78 times the water depth). This ensures that the wave height does not exceed the physical limit defined by the breaker condition.

Snapshots of the sea state after 1000 seconds of simulation are presented for both the most frequent events and extreme events in Figure 4.17 and Figure 4.18.

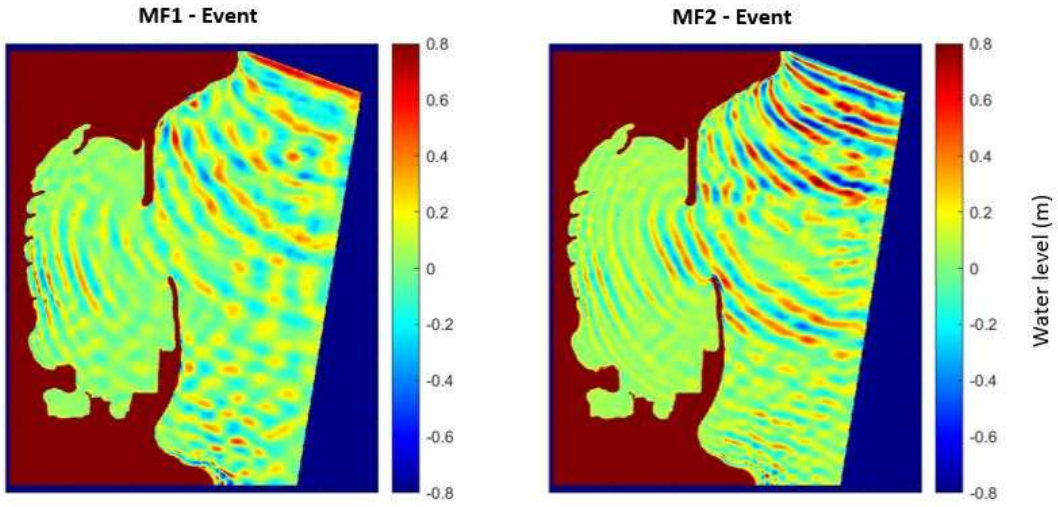

Figure 4.17- Snapshot of simulation domain (Water levels) at 1000 seconds for MF1, and MF2 events.

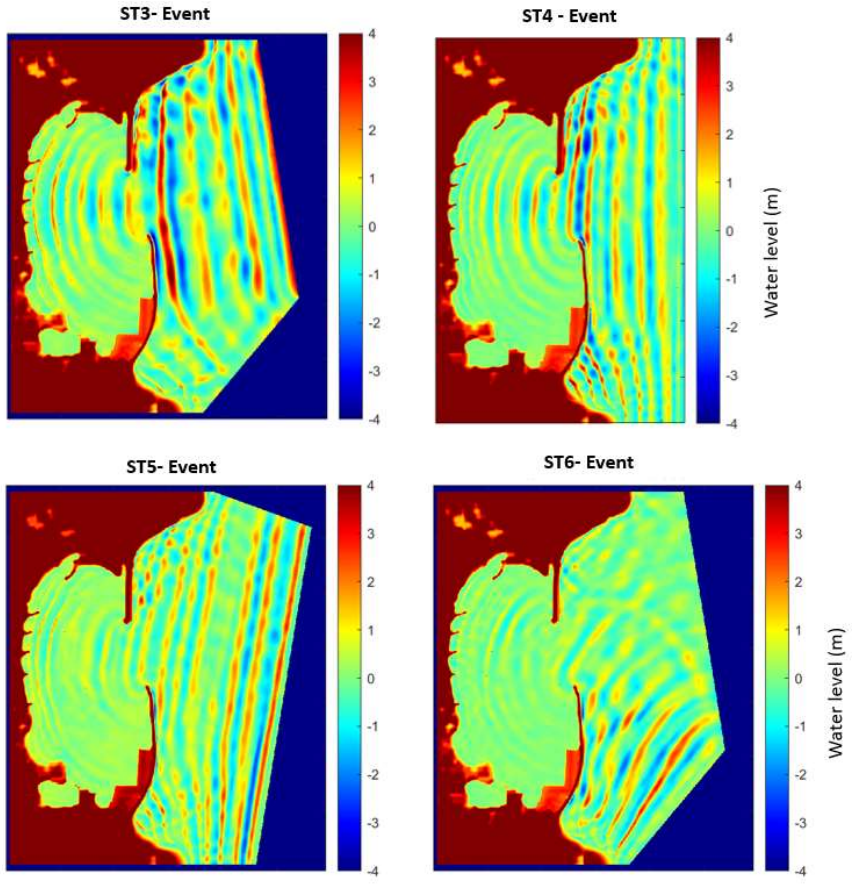

Figure 4.18- Snapshot of simulation domain (Water levels) at 1000 seconds for ST1, ST3, ST4, ST5, and ST6 events.

4.2.2 Wave overtopping

Overtopping discharges at each location were calculated based on the output of SWASH simulations and compared with those predicted by the NN_OVERTOPPING2 model (Table 4.20). To calculate the overtopping discharge at each observation point, the cumulative overtopping at each location was computed and converted into discharge using the simulation time. Plots showing the instantaneous overtopping rate and cumulative overtopping volume over simulation time for selected events are presented in Figure 4.19- to Figure 4.23. For plots of all simulated events, please refer to Annexe A.

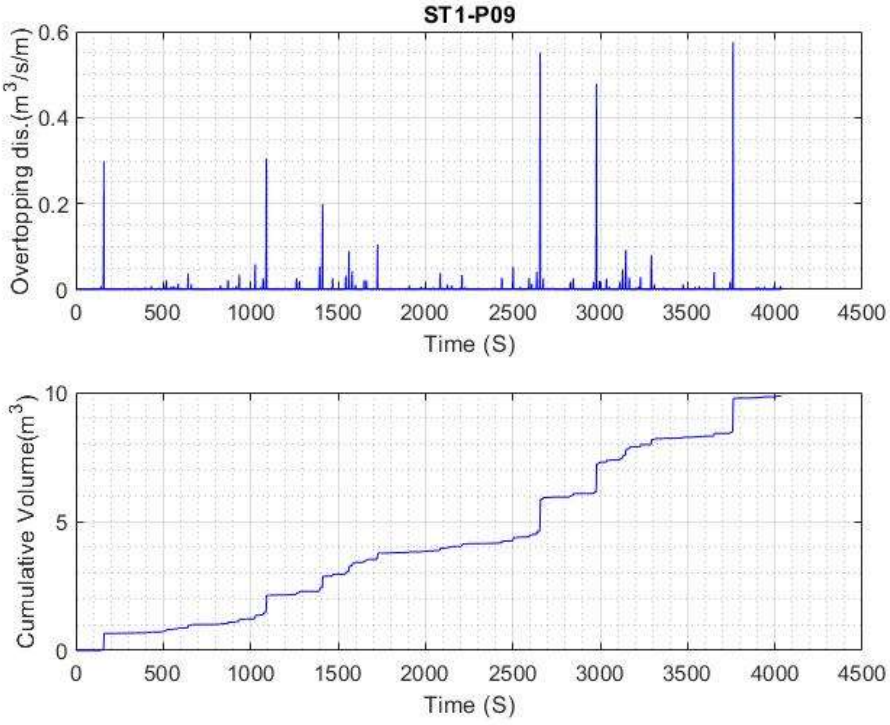

Figure 4.19- Overtopping instantaneous rate (Top) and cumulative overtopping (Bottom) for ST1 event at Point 09 (south breakwater).

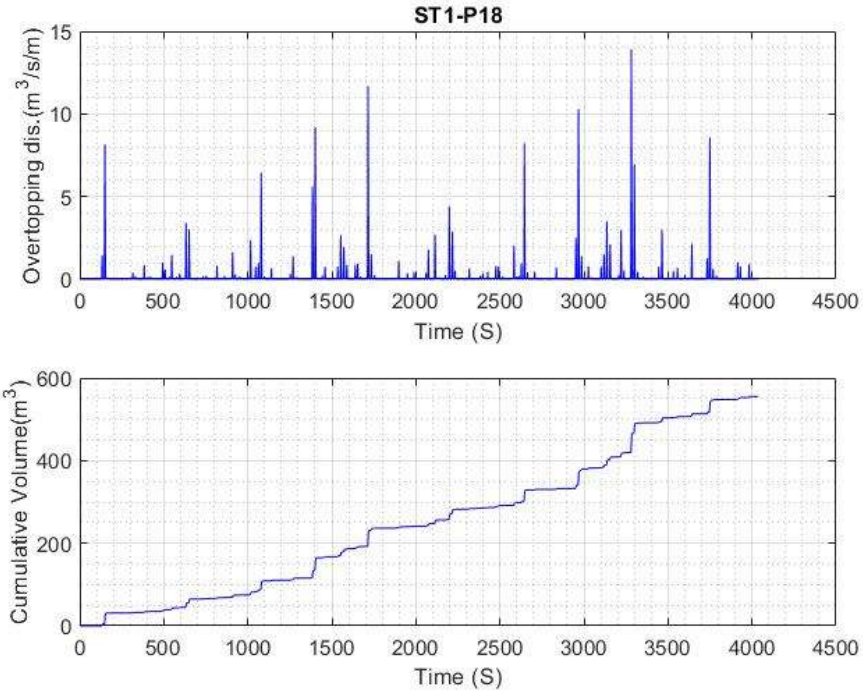

Figure 4.20- Overtopping instantaneous rate (Top) and cumulative overtopping (Bottom) for ST1 event at Point 18 (south breakwater).

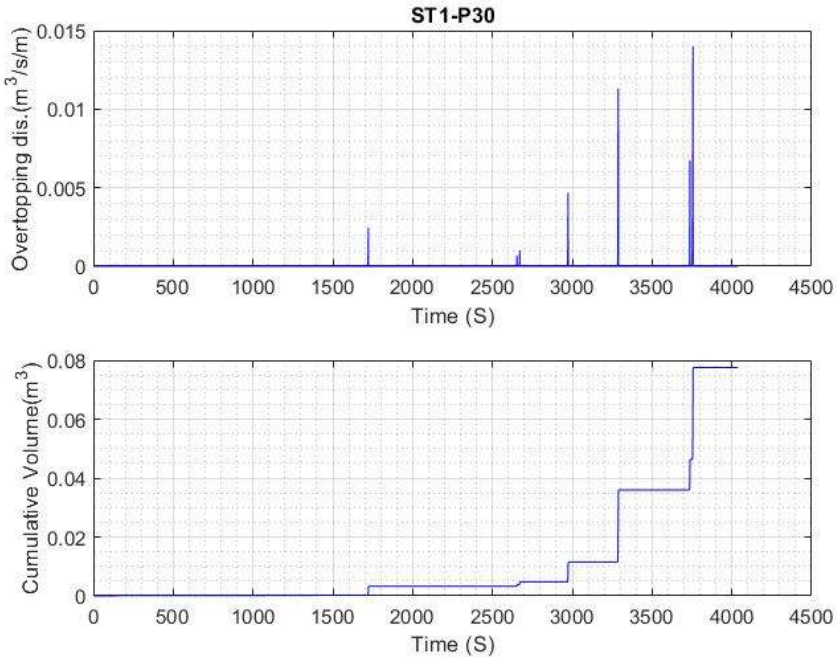

Figure 4.21-Overtopping instantaneous rate (Top) and cumulative overtopping (Bottom) for ST1 event at Point 30 (north breakwater).

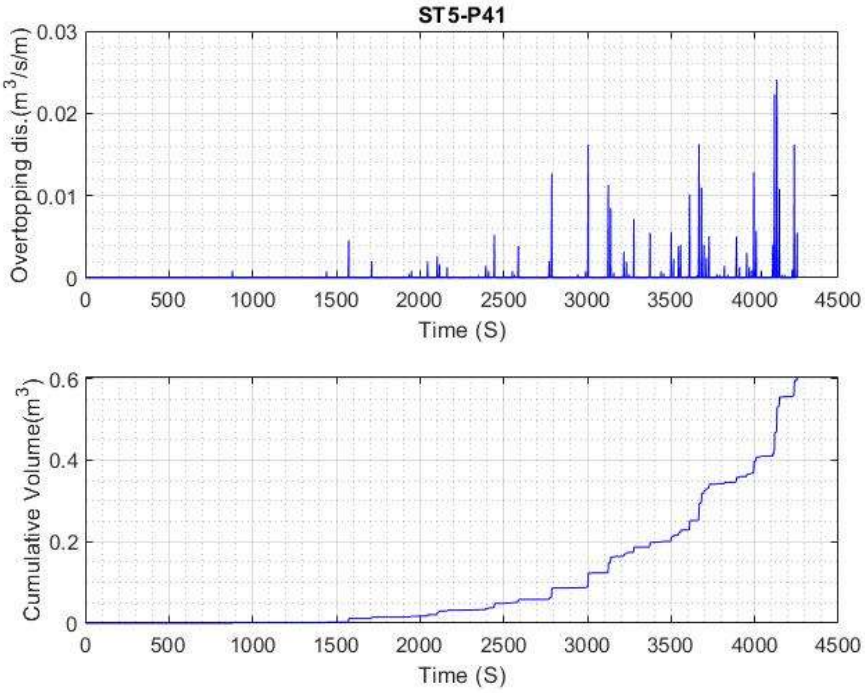

Figure 4.22- Overtopping instantaneous rate (Top) and cumulative overtopping (Bottom) for ST5 event at Point 41 (groyne series).

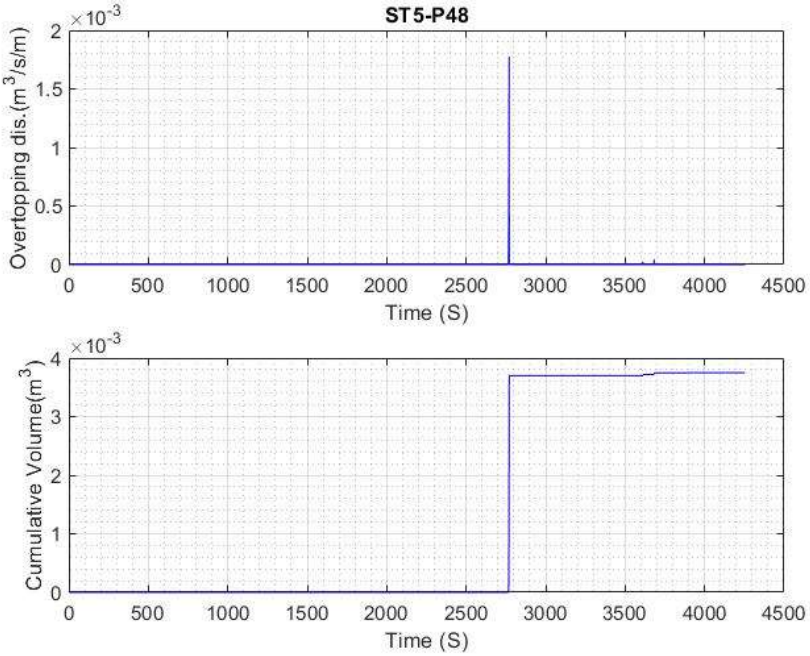

Figure 4.23- Overtopping instantaneous rate (Top) and cumulative overtopping (Bottom) for ST5 event at Point 48 (groyne series).

Table 4.21- Comparison of overtopping flow predictions between NN_OVERTOPPING2 (NN2) and SWASH (S) models at various locations for events.

Event	Location	NN_VERTOPPING2 (NN2) Prediction (l/s/m)	SWASH Prediction (l/s/m)	SWASH-NN2 (l/s/m)
MF1	P 41	0	0.01	0.01
	P 51	0	0.85	0.85
MF2	P 41	0	1	1.00
	P 51	0	2	2.00
MF3	P48	0	0.05	0.05
	P51	0	0.05	0.05
ST1	P 03	0.78	0.02	-0.76
	P 09	3.48	2.44	-1.04
	P 18	66.80	138	70.76
	P 30	0.00	0.02	0.02
	P 41	0.45	17.87	17.42
	P 48	0.41	3.32	2.91
	P 51	0.20	1.81	1.61
	P 55	0.13	0.52	0.39
	P 59	0.01	0.001	-0.01
ST3	P 18	118.00	124.20	6.20
	P 41	0.37	0.09	-0.28
	P 55	0.10	0.010	-0.09
ST4	P 09	0.01	0.01	0.00
	P 18	2.96	16.54	13.59
ST5	P 03	0.04	0.00	-0.04
	P 09	0.01	0.00	-0.01
	P 18	0.80	0.20	-0.60
	P 41	0.18	0.14	-0.04
	P 51	0.03	1.90	1.87
ST6	P 18	0.51	2.42	1.91

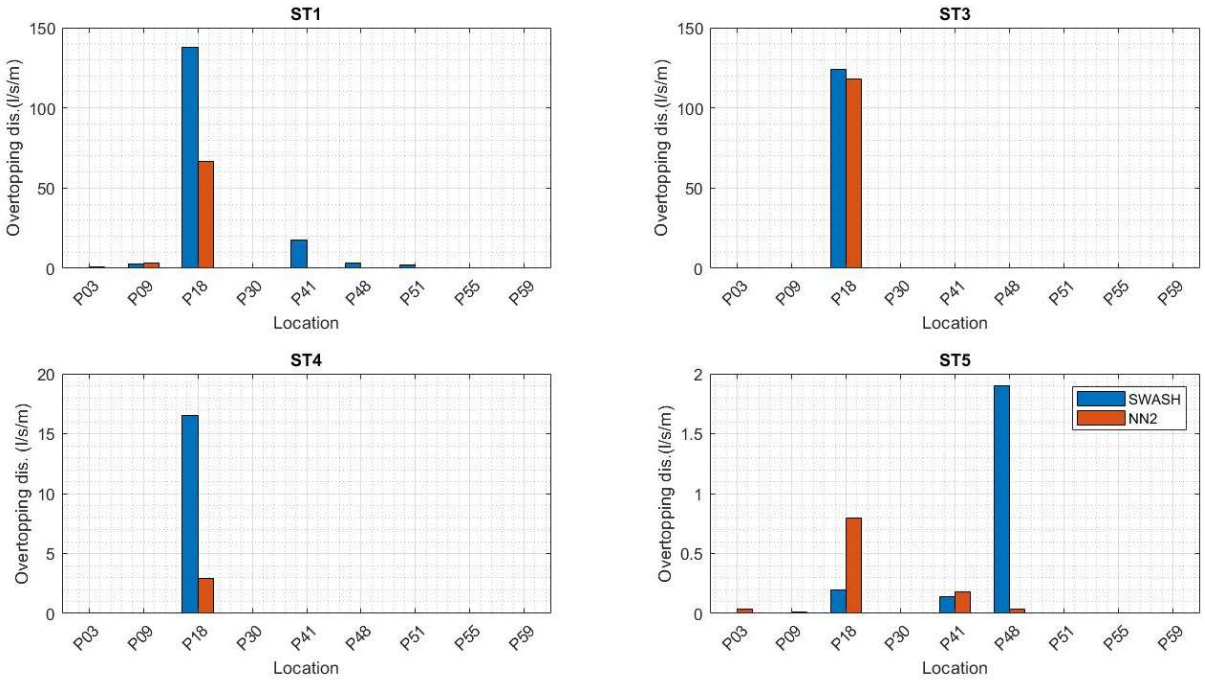

Figure 4.24- Comparison of NN_OVERTOPPING2 (NN2) predictions and SWASH simulation result for storm events at each location.

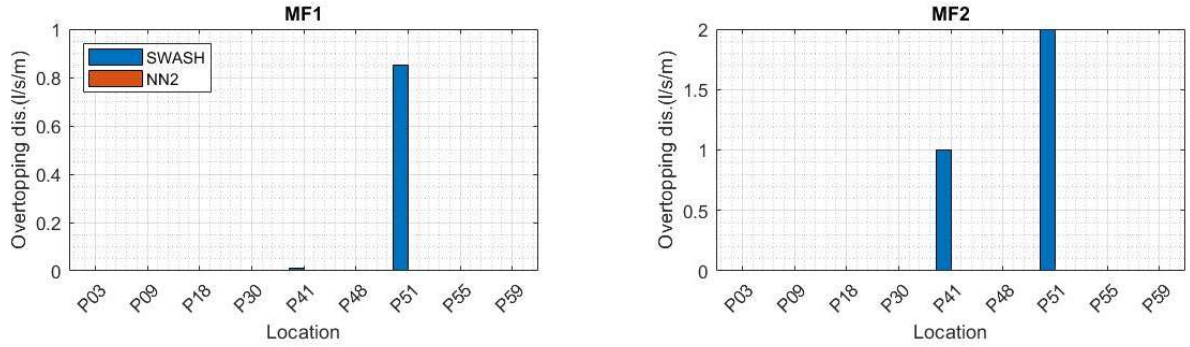

Figure 4.25- Comparison of NN_OVERTOPPING2 (NN2) predictions and SWASH simulation result for the most frequent event at each location

During event ST1, the NN_OVERTOPPING2 model predicted overtopping over the wave return wall on the south breakwater, at points 03 and 09 (Table 4.20). The SWASH model also predicted overtopping at point 09, with discharge values that were closely aligned with those of NN_OVERTOPPING2 (Figure 4.26). However, at point 18, the SWASH model overpredicted the

overtopping discharge compared to NN_OVERTOPPING2. At points located on the frontal defence wall, the SWASH model indicated overtopping discharge, while the NN_OVERTOPPING2 model did not show any overtopping.

During the event ST3 (Figure 4.24), the overtopping predictions from the SWASH and NN_OVERTOPPING2 models closely align, with values of 124.2 l/s/m and 118.0 l/s/m, respectively. These volumes are significantly higher than the overtopping discharges, as shown in Figure 2.8 in section 2.3, which illustrates the damage to the north and south breakwaters during the event. The overtopping waves almost completely displaced the armour layer at the head of the north breakwater. Additionally, rocks were drawn into the yard protected by the wave return wall crest level at +11.2m (ZH). However, neither the SWASH nor the NN_OVERTOPPING2 models predicted overtopping over the wave return wall. During the ST1 event, overtopping was observed over the wave return wall in the SWASH model. This event was successfully simulated for 4038 s until the cluster time limit was reached. Conversely, during the ST3, the simulation achieved a duration of 1213 s. The overtopping observation for the ST3 event might change if the simulation is extended further.

In the event of ST4 (Figure 4.24), the NN_OVERTOPPING2 and SWASH models only predict overtopping at point 18, which was in front of the south breakwater. However, Figure 2.9 in section 2.3 shows the prediction of overtopping. Similar to the ST3 event, the ST4 simulation lasted 1549 s and was unstable. Therefore, the simulation time is not sufficient to draw a conclusion regarding the performance of SWASH in predicting overtopping.

During Hurricane Alex, which was event ST5 (Figure 4.24), NN_OVERTOPPING2 predicted overtopping at points 03, 09, 18, 41, and 48, while the SWASH model predicted overtopping only at points 18, 41, and 48. The SWASH prediction was significantly higher than NN_OVERTOPPING2 at point 48, which was an observation point on the frontal defence wall. This was confirmed by Figure 2.10 in section 2.3, which shows severe overtopping over the frontal defence wall during Hurricane Alex. Therefore, the SWASH model shows promising predictions at point 48. Furthermore, severe overtopping was observed over the south breakwater closer to point 18. However, SWASH underpredicts the overtopping discharge at point 18 compared to the NN_OVERTOPPING2 model.

During the most frequent event simulations, the NN_OVERTOPPING2 model did not predict any overtopping events at points 03, 09, and 18, while the SWASH model provided similar predictions (Table 4.23). However, at the observation points along the series and the frontal defence wall, the SWASH model predicts overtopping discharge at points 41 and 51, whereas the NN_OVERTOPPING2 model shows no overtopping. There were no images of overtopping events for the most frequent events to validate the model results.

Moreover, to compare the predictability of the overtopping occurrence between the SWASH and NN_OVERTOPPING2 models, a qualitative comparison was conducted by checking whether overtopping occurred at each point during each event (Table 4.24).

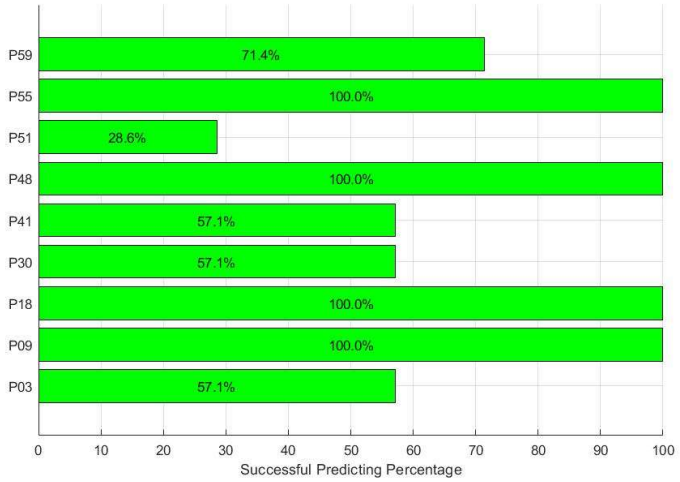

Figure 4.27- Successful prediction percentage of NN_OVERTOPPING2(NN2) and SWASH model.

At points 09, 18, 48, and 55, predictions of overtopping or non-overtopping by the two models align perfectly with each other (Figure 4.26). Except at point 52, which shows 28.6% of success, at all other points, predicting percentages reached more than 57%. However, in this study, only Manning's coefficient for the south breakwater was calibrated, and the SWASH model shows promising results that calibrating Manning's coefficient can lead to more accurate predictions.

Table 4.22- Comparison of overtopping predictions between NN_OVERTOPPING2 (NN2) neural network and SWASH (S) numerical model at various locations.

Event	H_s* (m)	T_p* (s)	Tide (m)	Instances of Overtopping																	
				P03		P09		P18		P30		P41		P48		P51		P55		P59	
				NN2	S	NN2	S	NN2	S	NN2	S	NN2	S	NN2	S	NN2	S	NN2	S	NN2	S
MF1	0.95	12.33	1.09	x	x	x	x	x	x	x	x	x	✓	x	x	x	✓	x	x	x	x
MF2	1.29	9.10	1.56	x	x	x	x	x	x	x	x	x	✓	x	x	x	✓	x	x	x	x
MF3	2.94	11.14	1.69	✓	x	✓	x	✓	x	x	x	x	x	x	✓	x	✓	x	x	x	x
ST1	6.15	12.33	1.32	✓	✓	✓	✓	✓	✓	x	✓	✓	✓	✓	✓	✓	✓	✓	✓	✓	✓
ST3	6.04	12.33	1.5	x	x	x	x	✓	✓	x	x	✓	✓	x	x	x	x	✓	✓	✓	x
ST4	4.94	10.07	1.47	✓	x	✓	✓	✓	✓	x	x	✓	x	x	x	✓	x	x	x	✓	x
ST5	4.79	10.07	0.53	✓	x	x	x	✓	✓	✓	x	x	x	x	x	✓	x	x	x	x	x
ST6	4.5	11.14	1.49	✓	x	x	x	✓	✓	✓	x	x	x	x	x	✓	x	x	x	x	x

Note: * H_s and T_p are nominal wave parameters used for SWASH simulation

X- Overtopping not observed, ✓ - Overtopping observed

4.2.3 Discussion

4.2.3.1 Significant wave heights prediction

At the nearshore observation points, SWASH tends to overestimate the significant wave height compared to the predictions of the DREAMS model. DREAMS is based on linear wave theory and represents monochromatic incident waves characterised by a single frequency and direction. This approach limits its ability to account for nonlinear wave interactions and depth-induced wave breaking, particularly in shallower regions where waves steepen and break more noticeably. Additionally, wave reflection at the boundaries is treated differently in each model. DREAMS use a reflection coefficient provided by the user as a percentage of the incident wave height that is reflected into the numerical domain. In contrast, SWASH handles wave reflection naturally as the waves interact with the bottom and the coastline. On the other hand, at the observation points in front of the south and north breakwaters, the DREAMS model often overestimates wave heights compared to the SWASH simulation. This occurs because DREAMS use a post-calculations fixed breaker parameter of 0.78 (the ratio of wave height to depth) to calculate wave breaking. Here, the model assumes that waves will continue to propagate and grow as they approach the shore, even in shallow depths where breaking occurs, which leads to higher predicted wave heights than the SWASH model. However, to test the accuracy of the SWASH prediction, the model must be validated with field data.

4.2.3.2 Overtopping discharges

One of the main objectives of this thesis was to test the capabilities of the SWASH model in simulating overtopping at prototype scale, covering the entire harbour and bay areas with complex coastal structures and bathymetry. To assess this, nine events were simulated, including six extreme events and four of the most frequent events. Out of these nine simulations, the SWASH model successfully produced overtopping in eight events. However, one event proved unstable immediately after launching. When comparing the SWASH model outputs with the predictions of NN_OVERTOPPING2 and observed images during storm events, the results showed a good agreement. Some discrepancies were observed in the overtopping volumes at the groyne series and the north breakwater, where the Manning's coefficient had not been calibrated. This highlights that

by calibrating Manning's coefficient in these structures, the SWASH model can provide reliable predictions for overtopping in such areas.

Simulation time is crucial for accurately analysing overtopping behaviour during specific events, as it directly affects the detection of overtopping occurrences. In this study, a one-hour time series was generated and then replicated to create a three-hour time series using the JOSWAP spectrum, which served as a boundary condition at the wave-making boundary. However, during simulations ST3, ST4, and ST6, the simulation times lasted only 1213 s, 1549 s, and 1807 s, respectively. These durations are shorter than a complete cycle of the spectrum.

Although there is evidence of images overtopping the wave return wall during storm events ST3 and ST4 (Figure 2.8 and Figure 2.9), the SWASH model did not predict overtopping over the return wall. This limited simulation time may not have allowed enough opportunity for larger waves to develop, particularly if they are part of a longer wave train or occur later in the event cycle. This was confirmed by the results of the ST1 event, which produced overtopping over the return wall, lasting 4038 s.

During the most frequent events, MF1 and MF2, which have relatively low significant wave heights of 0.95 m and 1.29 m, the SWASH model produced overtopping at the observation points on the frontal defence wall inside the bay. However, the NN_OVERTOPPING model did not predict any overtopping. In this study, only Manning's coefficient of the southern breakwater was calibrated, while Manning's coefficient for the groynes was based on the Le Roux (2003) equation. Therefore, at this stage, it is difficult to evaluate the sensitivity of the SWASH model to minor variations in wave height and water level, which may be crucial for accurately predicting overtopping in scenarios involving small waves.

4.2.3.3 Numerical simulation

In the context of replicating a physical model test, an explicit method was initially used for the entire domain simulation, with a minimum Courant number of 0.1 and a maximum Courant number of 0.5. However, shortly after launching, the simulations became unstable. This instability may have been caused by the Courant-Friedrichs-Lewy (CFL) condition, which governs the

maximum allowable time step; the time step must be sufficiently small to prevent instability. If the time step is significantly large, the simulation can become unstable and "blow up."

In contrast, with a semi-implicit method, the time step can be larger without causing instability (Backhaus, 1983). According to the SWASH user manual (version 11.01A), the default time integration method is set to a semi-implicit approach. Consequently, after implementing the semi-implicit method with the Crank-Nicolson scheme, simulations MF1, MF2, ST1, and ST5 became stable. However, some simulations experienced instability shortly after launching, while others became unstable after running for some time.

Results showed that the stability of the simulation is sensitive to increases in significant wave height and decreases in tide level. When comparing the performance of simulations ST1 and ST2, both of which had the same peak wave period of 12.33 s, shared the same domain, and had the same incident wave direction, it was observed that the ST2 simulation became unstable shortly after launch. In contrast, the ST1 simulation successfully ran until it was terminated due to the cluster time limit.

For the ST2 simulation, the significant wave height was 6.82 m, which is 0.67 m larger than that of ST1. Additionally, the tide level for ST2 was 0.49 m, which was 0.83 m lower than ST1. This instability in ST2 could be attributed to the increased wave steepness as the waves approached the nearshore, leading to wave breaking, wave reflections, and heightened turbulence near the bottom, all of which can contribute to numerical instability. Additionally, the increment in wave height induces greater non-linearity in wave propagation, which further exacerbates instability in the simulation.

In a 2014 study, Suzuki observed instability during the simulation of a two-dimensional SWASH model for an impermeable dike, which was intended to predict overtopping discharge. However, in the current study, SWASH successfully simulated both normal and extreme events at the prototype scale of Praia da Vitória harbour. The model demonstrated its ability to predict wave parameters at specific locations and estimate overtopping discharge with acceptable accuracy, even in an environment characterized by complex coastal structures and varying bathymetry. Despite the challenges posed by such a dynamic environment, SWASH maintained model stability and provided reliable results, making it a valuable tool for simulating overtopping in coastal areas.

5 Conclusions

5.1 Main conclusions

This study aimed to investigate if SWASH is suited to replace the existing models in the HIDRALERTA EWS and to implement a two-dimensional SWASH numerical set-up for the Praia da Vitória full-scale harbour and bay areas.

SWASH numerical model was successfully implemented both in a 2D flume (1515m by 135m) of a cross-section of the south's Breakwater and in 2D domain (3350m by 2300m, approximately 8.5km^2) containing the entirety of the port and bay area.

The calibration of the Manning coefficient for the two-dimensional SWASH model was performed using physical model tests of a cross-section of the south breakwater. The Manning coefficient is responsible for wave energy dissipation in the numerical model, especially in very shallow waters, such as in the vicinities of the coastal structures on the boundaries. This coefficient's calibration was performed for the area of the outer slope of the south breakwater. The remaining numerical domain was set with the default Manning coefficient. Results showed that the model's performance in estimating overtopping is highly sensitive to the calibration of Manning's coefficient for the outer slope of the breakwater. Once Manning's coefficient was calibrated correctly, the model was able to produce accurate results with low computational effort. Based on the physical model test replication, two Manning coefficients were obtained for two test cases, with the values being closely matched.

The simulations of the entirety of the port and bay area where compared with the results obtained with the HIDRALERTA methodology (DREAMS model for wave propagation and NN_ovwertopping2 for wave overtopping predictions). The comparison process included wave spectral parameters at several point locations near the defence structures of the port and bay area, as well as mean instantaneous wave overtopping discharges over those same structures. A total of nine test case scenarios were simulated, covering selected past storm events and most frequent wave conditions based on the wave regime.

Several considerations can be drawn from the results:

1. The SWASH model demonstrated its ability to simulate wave propagation across the entire harbour and bay area, from the foreshore to shallow waters, as well as modelling overtopping processes over complex coastal structures and bathymetric domains.
2. The model's performance in estimating both wave propagation in nearshore shallow waters and wave overtopping is highly sensitive to the method by which the wave energy is transformed and/or dissipated when interacting with the bottom and structures' slopes. In this case, demonstrated by several tests varying Manning coefficient;
3. The model's performance in estimating mean overtopping discharge strongly depends on the quality of the bathymetric data. This is particularly significant when dealing with complex coastal structures and bathymetry. In most observation points, the mean overtopping discharges predicted by the SWASH model were of the same order of magnitude as those predicted by the NN_OVERTOPPING2 model. However, in certain locations, SWASH underpredicted the overtopping discharge.
4. The seeding number of the boundary-imposed wave time series affected the wave sequence and therefore the overtopping volumes accumulation. However, given enough simulation time the average overtopping discharge converges to a value.
5. Selecting an appropriate simulation time is crucial, as the influence of the wave height time series (different seeding numbers for the same wave energy spectrum) at the boundary on mean overtopping discharges diminishes with the length of the simulation.
6. Unstructured meshes allowed the simulation of a large domain within a reasonable time frame by taking advantage of the non-uniform mesh resolution based on the water depths and corresponding wavelengths and a powerful mesh renumbering algorithm to minimize mesh's bandwidth.
7. The quality of the mesh significantly influences the computational time required for simulations and also the outputs of the model, namely wave propagation and wave overtopping and..
8. Special attention should be given to defining input parameters to meet stability requirements. The study found that when the explicit time integration method was used,

the model became unstable, while the semi-implicit method produced more stable computations.

9. Parallel processing is available only for structured grids in SWASH's current version. The computational efficiency of the simulations could potentially be improved by incorporating parallel processing for unstructured meshes.

5.2 Challenges and future work

In this dissertation, the first approach was to replicate a physical model test at prototype scale using the two-dimensional SWASH model and calibrate it with two test cases that led to overtopping, in order to obtain the most suited Manning's coefficient for the outer slope of the south breakwater. While the two test cases enabled the calculation of Manning's coefficient, which aligned with the measured overtopping discharge from the physical model test, certain limitations were observed during the study. Both selected test cases had similar tide levels. To obtain a more reliable Manning's coefficient, it is recommended to simulate additional test cases with varying tide levels, allowing for an investigation of the correlation between Manning coefficient and water depth.

During the sensitivity analysis of the replication of physical model test in two-dimensional SWASH model, it was observed that the computational time (CPU hours) for simulations was significantly influenced by the refinement of the unstructured mesh. When simulating the entire harbour and bay, the computational cost was too high to achieve the desired 3-hour simulation time due to constraints in the computational infrastructure (INCD) simulation time. It is recommended to aim for an average number of nodes per wavelength of around 45 to optimise CPU hours for this type of domain simulation. The results showed that higher values of average nodes per wavelength did not produce more accurate results, while significantly increasing CPU times.

For future simulations of the harbour and bay with SWASH, results should be validated with real-world data. In this study, the wave propagation capabilities of SWASH were compared with DREAMS numerical model data, and overtopping capabilities were compared with NN_OVERTOPPING predictions, witness observations accounts and images, which were available during and after the storm events. While these comparisons were sufficient to understand

the behaviour and limitations of the SWASH model in simulating complex coastal structures and bathymetry, to determine whether the overtopping estimations from SWASH are reliable enough to be used in an early warning forecast system, further validation with in-situ measured data, video imagery, or other sources is necessary.

References

Altomare, C., Suzuki, T., Chen, X., Verwaest, T., & Kortenhaus, A. (2016). Wave overtopping of sea dikes with very shallow foreshores. *Coastal Engineering*, *116*, 236–257. https://doi.org/10.1016/j.coastaleng.2016.07.002

Backhaus, J. O. (1983). A semi-implicit scheme for the numerical solution of the shallow water equations for application to shelf sea modelling. *Continental Shelf Research*, *2(4), 243–254*. https://doi.org/10.1016/0278-4343(83)90020-6

Bates, P. D., & De Roo, A. P. J. (2000). A simple raster-based model for flood inundation simulation. *Journal of Hydrology*, *236*(1–2), 54–77. https://doi.org/10.1016/S0022-1694(00)00278-X

Besley, P. (1999). *Overtopping of seawalls – Design and assessment manual*. Environment Agency.

Booij, N., Ris, R. C., & Holthuijsen, L. H. (1999). A third-generation wave model for coastal regions: 1. Model description and validation. *Journal of Geophysical Research: Oceans*, *104*(C4), 7649–7666. https://doi.org/10.1029/98JC02622

Coeveld, E. M., Van Gent, M. R. A., & Pozueta, B. (2005). *Neural network: Manual NN_OVERTOPPING2 (CLASH WP8)*. Reharbour BV.

De Waal, J. P., & Van Der Meer, J. W. (1992). Wave run-up and overtopping at coastal structures. *Roceedings of the 23rd International Conference on Coastal Engineering (ICCE)*.

European Environment Agency. (2015). *State of Europe's seas (EEA Report No. 2/2015)*. https://www.eea.europa.eu/publications/state-of-europes-seas

EurOtop. (2007). *European Manual for the Assessment of Wave Overtopping. Eds. Pullen, T., Allsop, N.W.H., Bruce, T., Kortenhaus, A., Schüttrumpf, H. & van der Meer, J.W.* https://www.overtopping-manual.com

EurOtop. (2016). *Manual on wave overtopping of sea defences and related structures. An overtopping manual largely based on European research, but for worldwide application. Van der Meer, J.W., Allsop, N.W.H., Bruce, T., De Rouck, J., Kortenhaus, A., Pullen, T., Schüttrumpf, H., Troch, P. & Zanuttigh, B.* https://www.overtopping-manual.com

EurOtop. (2018). *Manual on wave overtopping of sea defences and related structures. An overtopping manual largely based on European research, but for worldwide application. Van der Meer, J.W., Allsop, N.W.H., Bruce, T., De Rouck, J., Kortenhaus, A., Pullen, T., Schüttrumpf, H., Troch, P. & Zanuttigh, B.* EurOtop. www.overtopping-manual.com

Flater, D. (2024). *Xtide* [Computer software]. https://flaterco.com/xtide

Fortes, C. (2002). *Nonlinear wave transformations in harbors: A finite element analysis* [PhD thesis]. IST (Instituto Superior Técnico), Mechanical Engineering.

Fortes, C. J. E. M., Reis, M. T., Pinheiro, L., Poseiro, P., Serrazina, V., Mendonça, A., Smithers, N., Santos, M. I., Barateiro, J., Azevedo, E. B., Salvador, M., & Reis, F. V. (2020). The HIDRALERTA system: Application to the ports of Madalena do Pico and S. Roque do Pico, Azores. *Aquatic Ecosystem Health & Management*, *23*(4), 398–406. https://doi.org/10.1080/14634988.2020.1807295

Goda, Y. (1985). *Random seas and design of maritime structures*. University of Tokyo Press.

Gomez-Gesteira, M., Rogers, B. D., Crespo, A. J. C., Dalrymple, R. A., Narayanaswamy, M., & Dominguez, J. M. (2012). SPHysics – development of a free-surface fluid solver – Part 1: Theory and formulations. *Computers & Geosciences*, *48*, 289–299. https://doi.org/10.1016/j.cageo.2012.02.029

Hedges, T. S., & Reis, M. T. (2004). Accounting for random wave run-up in overtopping predictions. *Proceedings of the Institution of Civil Engineers - Maritime Engineering*, *157*(3), 113–122. https://doi.org/10.1680/maen.2004.157.3.113

Herbert, D. M. (1993). *Wave overtopping of vertical walls* (No. SR 316). Ministry of Agriculture, Fisheries and Food 1993.

Hsu, T., & Liu, P. L. -F. (2004). Toward modeling turbulent suspension of sand in the nearshore. *Journal of Geophysical Research: Oceans*, *109*(C6), 2003JC002240. https://doi.org/10.1029/2003JC002240

Hu, K., Mingham, C. G., & Causon, D. M. (2000). Numerical simulation of wave overtopping of coastal structures using the non-linear shallow water equations. *Coastal Engineering*, *41*(4), 433–465. https://doi.org/10.1016/S0378-3839(00)00040-5

Lamb, R., Crossley, M., & Waller, S. (2009). A fast two-dimensional floodplain inundation model. *Proceedings of the Institution of Civil Engineers - Water Management*, *162*(6), 363–370. https://doi.org/10.1680/wama.2009.162.6.363

Lara, J. L., Ruju, A., & Losada, I. J. (2011). Reynolds averaged Navier–Stokes modelling of long waves induced by a transient wave group on a beach. *Proceedings of the Royal Society A: Mathematical, Physical and Engineering Sciences*, *467*(2129), 1215–1242. https://doi.org/10.1098/rspa.2010.0331

Lashley, C. H., Van Der Meer, J., Bricker, J. D., Altomare, C., Suzuki, T., & Hirayama, K. (2021). Formulating Wave Overtopping at Vertical and Sloping Structures with Shallow Foreshores Using Deep-Water Wave Characteristics. *Journal of Waterway, Port, Coastal, and Ocean Engineering*, *147*(6), 04021036. https://doi.org/10.1061/(ASCE)WW.1943-5460.0000675

Le Roux, J. P. (2003). Wave friction factor as related to the Shields parameter for steady currents. *Sedimentary Geology*, *155*(1–2), 37–43. https://doi.org/10.1016/S0037-0738(02)00157-4

Lemos, R., Silva, L. G., Fortes, C. J., & Martinez, C. (2025). *AMPLIAÇÃO DO CAIS MULTIUSOS DO PORTO DA PRAIA DA VITÓRIA (ILHA TERCEIRA – AÇORES) Ensaios de estabilidade e galgamentos em modelo físico bidimensional*. DEPARTAMENTO DE HIDRÁULICA E AMBIENTE, The Laboratório Nacional de Engenharia Civil, Portugal.

Losada, I. J., Lara, J. L., Guanche, R., & Gonzalez-Ondina, J. M. (2008). Numerical analysis of wave overtopping of rubble mound breakwaters. *Coastal Engineering*, *55*(1), 47–62. https://doi.org/10.1016/j.coastaleng.2007.06.003

Madsen, P. A., & Sørensen, O. R. (1992). A new form of the Boussinesq equations with improved linear dispersion characteristics. Part 2. A slowly-varying bathymetry. *Coastal Engineering*, *18*(3–4), 183–204. https://doi.org/10.1016/0378-3839(92)90019-Q

Manz, A., Zózimo, A. C., & Garzon, J. L. (2022). Application of SWASH to Compute Wave Overtopping in Ericeira Harbour for Operational Purposes. *Journal of Marine Science and Engineering*, *10*(12), 1881. https://doi.org/10.3390/jmse10121881

Mase, H., Tamada, T., Yasuda, T., Hedges, T. S., & Reis, M. T. (2013). Wave Runup and Overtopping at Seawalls Built on Land and in Very Shallow Water. *Journal of Waterway, Port, Coastal, and Ocean Engineering*, *139*(5), 346–357. https://doi.org/10.1061/(ASCE)WW.1943-5460.0000199

Mase, H., Tamada, T., Yasuda, T., Karunarathna, H., & Reeve, D. E. (2015). Analysis of Climate Change Effects on Seawall Reliability. *Coastal Engineering Journal*, *57*(3), 1550010-1-1550010–1550018. https://doi.org/10.1142/S0578563415500102

McCabe, M. V., Stansby, P. K., & Apsley, D. D. (2012). Random wave runup and overtopping a steep sea wall: Shallow-water and Boussinesq modelling with generalised breaking and wall impact algorithms validated against laboratory and field measurements. *Coast. Eng. 74, 33–49 (2013)*. http://dx.doi.org/10.1016/j.coastaleng.2012.11.010

Neumann, B., Vafeidis, A. T., Zimmermann, J., & Nicholls, R. J. (2015). Future Coastal Population Growth and Exposure to Sea-Level Rise and Coastal Flooding—A Global Assessment. *PLoS ONE 10(3): E0118571*. https://doi.org/DOI:10.1371/journal.pone.0118571

Owen, M. W. (1980). *Design of seawalls allowing for wave overtopping* [Technical Report]. Hydraulics Research Station (HRS).

Papadimitriou, A. G., Metallinos, A. S., Chondros, M. K., & Tsoukala, V. K. (2024). A Novel Input Schematization Method for Coastal Flooding Early Warning Systems Incorporating Climate Change Impacts. *Climate 2024, 12, 178.* https://doi.org/10.3390/ cli12110178

Pés, V.M., E. (2013). *Applicability and Limitations of the SWASH model to predict Wave Overtopping*.

Pillai, K., Etemad-Shahidi, A., & Lemckert, C. (2016). Wave overtopping at berm breakwaters: Review and sensitivity analysis of prediction models. *Coastal Engineering, 120, 1–21*. https://doi.org/10.1016/j.coastaleng.2016.11.003

Pinheiro, L., Fortes, C., Reis, M. T., Santos, J., & Soares, C. G. (2020). RISK FORECAST SYSTEM FOR MOORED SHIPS. *Coastal Engineering Proceedings*, *36v*, 37. https://doi.org/10.9753/icce.v36v.management.37

Pinheiro, L. V., Fortes, C. J. E. M., Santos, J. A., Fernandes, J. L. M., & Walkley, M. (2011). *Finite element model for wave propagation near shore based on extended Boussinesq equations*. *6*(3), 174–191.

Pinheiro, L. V., Fortes, C. J., & Fernandes, L. (2008). *Gerador de malhas de elementos finitos para a simula¸ca˜o nume´rica de propaga¸c˜ao de ondas mari´timas*. *Vol. 24, 4, 369-391 (2008)*.

Pinheiro, L. V., Zózimo, A. C., & Fortes, C. J. E. M. (2023). New developments in the Praia da Vitória Coastal Bay and Harbor Early Warning System. *Coastal and Offshore Science and Engineering*, *4*, 6–18. https://doi.org/10.53256/COSE_230201

Poseiro, P. G. G. (2019). *Forecast and Early Warning System for Wave Overtopping and Flooding in Coastal and Port Areas: Development of a Model and Risk Assessment*.

Roelvink, D., Reniers, A., Van Dongeren, A., Van Thiel De Vries, J., McCall, R., & Lescinski, J. (2009). Modelling storm impacts on beaches, dunes and barrier islands. *Coastal Engineering*, *56*(11–12), 1133–1152. https://doi.org/10.1016/j.coastaleng.2009.08.006

Salas Pérez, M. (2014). *Overtopping over a real rubble mound breakwater calculated with SWASH* [Bachelor's thesis, Universitat Politècnica de Catalunya, Escola Tècnica Superior d'Enginyers de Camins, Canals i Ports de Barcelona; Technische Universiteit Delft, Faculty of Civil Engineering and Geosciences]. https://repository.tudelft.nl/record/uuid%3Af6ed9764-943b-4a43-85e3-acc706e75384

Shi, engyan, Kirby, J. T., Tehranirad, B., & Harris, J. C. (2016). *Fully Nonlinear Boussinesq Wave Model with TVD Solver Documentation and User's Manual (Version 3.0)* (No. CACR-11-03). CENTER FOR APPLIED COASTAL RESEARCH Ocean Engineering Laboratory.

Stelling, G. S., & Duinmeijer, S. P. A. (2003). A staggered conservative scheme for every Froude number in rapidly varied shallow water flows. *International Journal for Numerical Methods in Fluids*, *43*(12), 1329–1354. https://doi.org/10.1002/fld.537

Stelling, G., & Zijlema, M. (2003). An accurate and efficient finite-difference algorithm for non-hydrostatic free-surface flow with application to wave propagation. *International Journal for Numerical Methods in Fluids*, *43*(1), 1–23. https://doi.org/10.1002/fld.595

Suzuki, T., Altomare, C., Veale, W., Verwaest, T., Trouw, K., Troch, P., & Zijlema, M. (2017). Efficient and robust wave overtopping estimation for impermeable coastal structures in shallow foreshores using SWASH. *Coastal Engineering*, *122*, 108–123. https://doi.org/10.1016/j.coastaleng.2017.01.009

Suzuki, T., Altomare, C., Verwaest, T., Trouw, K., & Zijlema, M. (2014). TWO-DIMENSIONAL WAVE OVERTOPPING CALCULATION OVER A DIKE IN SHALLOW FORESHORE

BY SWASH. *Coastal Engineering Proceedings*, *1*(34), 3. https://doi.org/10.9753/icce.v34.structures.3

Suzuki, T., Altomare, C., Yasuda, T., & Verwaest, T. (2020). Characterization of Overtopping Waves on Sea Dikes with Gentle and Shallow Foreshores. *Journal of Marine Science and Engineering*, *8*(10), 752. https://doi.org/10.3390/jmse8100752

Suzuki, T., Gruwez, V., Bolle, A., Verwaest, T., & Mostaert, F. (2012). *Numerical modelling of the extreme wave climate in the Belgian harbours: Part 3: Marina of Blankenberge Version 2_0*. WL Rapporten, 769_03_3. Flanders Hydraulics Research & IMDC: Antwerp, Belgium. I/RA/11273/12.045/VGR. IMDC, Antwerp, Belgium.

TAW. (1974). *Wave run-up and overtopping*. Government Publishing Office.

Tuozzo, S., Calabrese, M., & Buccino, M. (2024). An overtopping formula for shallow water vertical seawalls by SWASH. *Applied Ocean Research*, *148*, 104009. https://doi.org/10.1016/j.apor.2024.104009

United Nations. (2022). *Early warnings for all: Executive action plan 2023–2027*. United Nations Digital Library. https://digitallibrary.un.org/record/4001006

Van Der Meer, J., Steendam, G. J., Bruce, T., & Klein Breteler, M. (2022). Admissible post-wave overtopping flow for persons on a horizontal surface. *Journal of Coastal and Hydraulic Structures*. https://doi.org/10.48438/JCHS.2022.0015

Van der Meer, J. W., & Janssen, J. P. F. M. (1994). *Wave run-up and wave overtopping at dikes and revetments* (No. Publication No. 485). Delft Hydraulics.

Van Gent, M. R. A. (1999). *Physical model investigations on coastal structures with shallow foreshores: 2D model tests with and double-peaked wave energy spectra*.

Van Gent, M. R. A., Van Den Boogaard, H. F. P., Pozueta, B., & Medina, J. R. (2007). Neural network modelling of wave overtopping at coastal structures. *Coastal Engineering*, *54*(8), 586–593. https://doi.org/10.1016/j.coastaleng.2006.12.001

Verhaeghe, H., De Rouck, J., & Van Der Meer, J. (2008). Combined classifier–quantifier model: A 2-phases neural model for prediction of wave overtopping at coastal structures. *Coastal Engineering*, *55*(5), 357–374. https://doi.org/10.1016/j.coastaleng.2007.12.002

Victor, L., Van Der Meer, J. W., & Troch, P. (2012). Probability distribution of individual wave overtopping volumes for smooth impermeable steep slopes with low crest freeboards. *Coastal Engineering*, *64*, 87–101. https://doi.org/10.1016/j.coastaleng.2012.01.003

Williams, H. E., Briganti, R., & Pullen, T. (2014). The role of offshore boundary conditions in the uncertainty of numerical prediction of wave overtopping using non-linear shallow water equations. *Coastal Engineering*, *89*, 30–44. https://doi.org/10.1016/j.coastaleng.2014.03.003

Zanuttigh, B., Formentin, S. M., & Briganti, R. (2013). A neural network for the prediction of wave reflection from coastal and harbor structures. *Coastal Engineering*, *80*, 49–67. https://doi.org/10.1016/j.coastaleng.2013.05.004

Zanuttigh, B., Formentin, S. M., & Van Der Meer, J. W. (2014). ADVANCES IN MODELLING WAVE-STRUCTURE INTERACTION THROUGH ARTIFICIAL NEURAL NETWORKS. *Coastal Engineering Proceedings*, *1*(34), 69. https://doi.org/10.9753/icce.v34.structures.69

Zanuttigh, B., Formentin, S. M., & Van Der Meer, J. W. (2016). Prediction of extreme and tolerable wave overtopping discharges through an advanced neural network. *Ocean Engineering*, *127*, 7–22. https://doi.org/10.1016/j.oceaneng.2016.09.032

Zhang, N., Zhang, Q., Wang, K.-H., Zou, G., Jiang, X., Yang, A., & Li, Y. (2020). Numerical Simulation of Wave Overtopping on Breakwater with an Armor Layer of Accropode Using SWASH Model. *Water*, *12*(2), 386. https://doi.org/10.3390/w12020386

Zijlema, M. (2020). Computation of free surface waves in coastal waters with SWASH on unstructured grids. *Computers & Fluids*, *213*, 104751. https://doi.org/10.1016/j.compfluid.2020.104751

Zijlema, M., & Stelling, G. S. (2005). Further experiences with computing non-hydrostatic free-surface flows involving water waves. *International Journal for Numerical Methods in Fluids*, *48*(2), 169–197. https://doi.org/10.1002/fld.821

Zijlema, M., & Stelling, G. S. (2008). Efficient computation of surf zone waves using the nonlinear shallow water equations with non-hydrostatic pressure. *Coastal Engineering*, *55*(10), 780–790. https://doi.org/10.1016/j.coastaleng.2008.02.020

Zijlema, M., Stelling, G., & Smit, P. (2011). SWASH: An operational public domain code for simulating wave fields and rapidly varied flows in coastal waters. *Coastal Engineering*, *58*(10), 992–1012. https://doi.org/10.1016/j.coastaleng.2011.05.015

Annex A- Overtopping at observation points

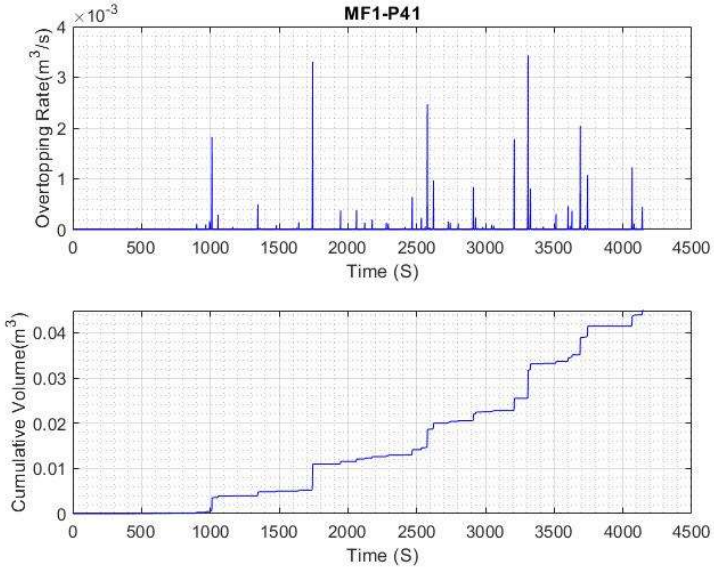

Figure A1- Overtopping instantaneous rate (Top) and cumulative overtopping (Bottom) for MF1 event at Point 41.

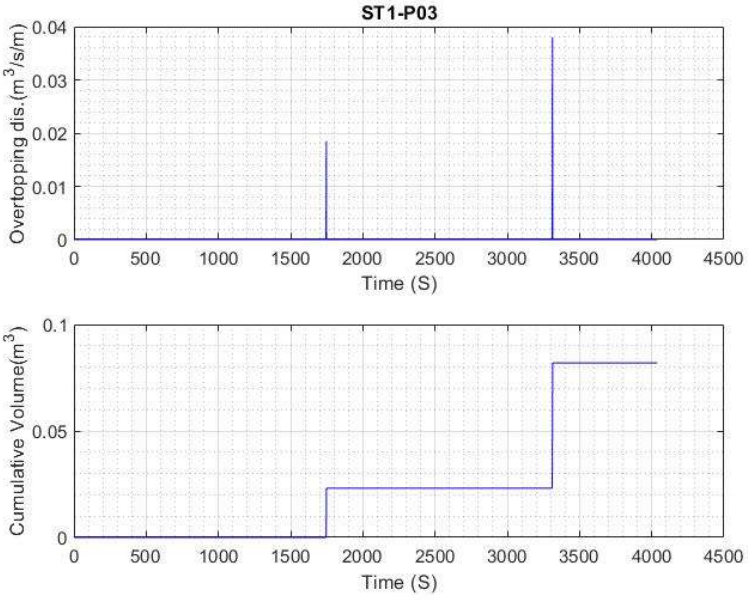

Figure A2- Overtopping instantaneous rate (Top) and cumulative overtopping (Bottom) for ST1 event at Point 03.

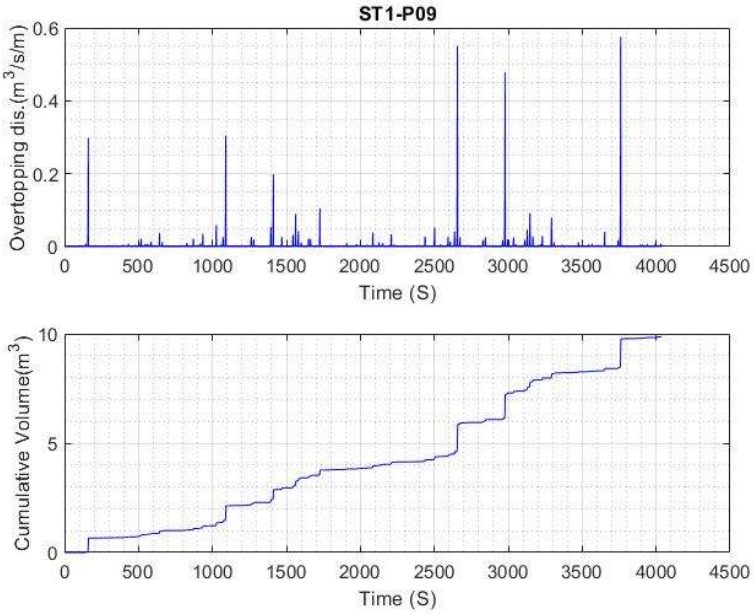

Figure A3- Overtopping instantaneous rate (Top) and cumulative overtopping (Bottom) for ST1 event at Point 09.

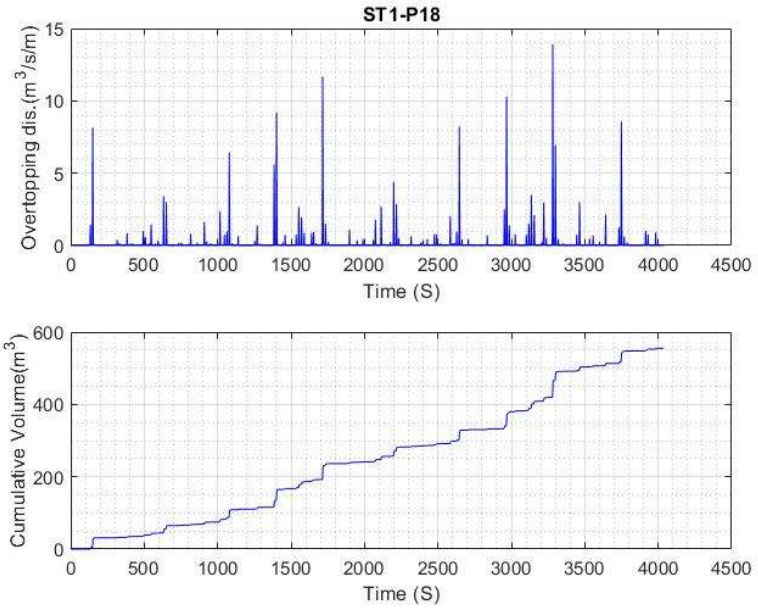

Figure A4- Overtopping instantaneous rate (Top) and cumulative overtopping (Bottom) for ST1 event at Point 18.

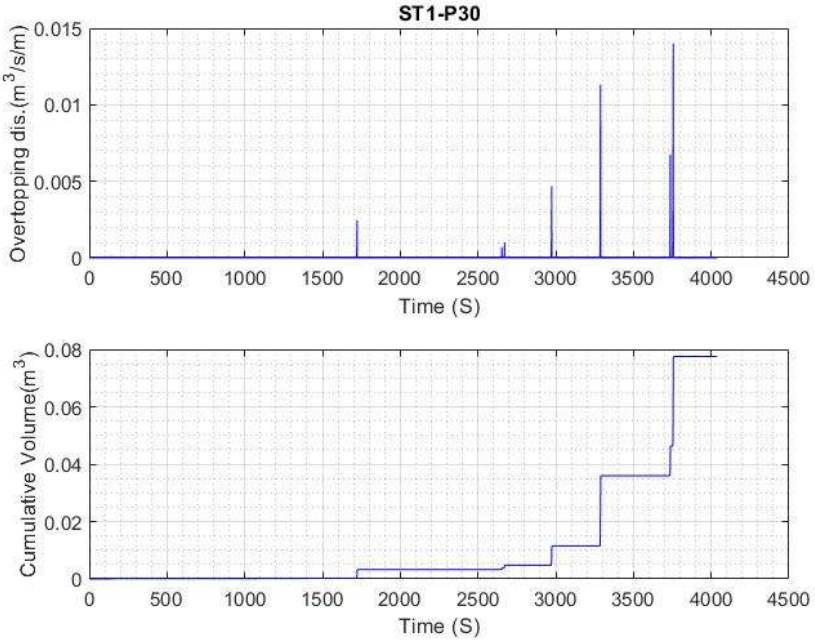

Figure A5- Overtopping instantaneous rate (Top) and cumulative overtopping (Bottom) for ST1 event at Point 30

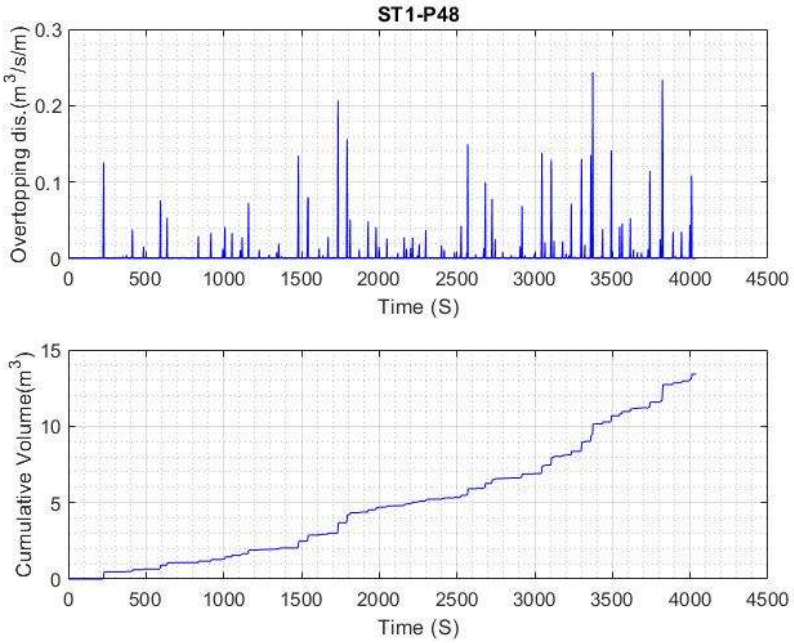

Figure A6- Overtopping instantaneous rate (Top) and cumulative overtopping (Bottom) for ST1 event at Point 48.

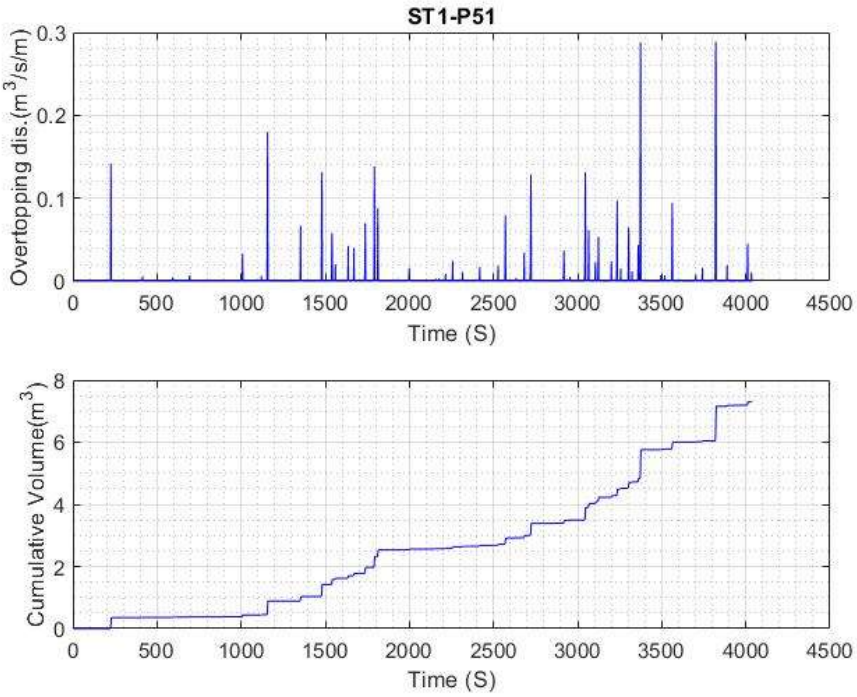

Figure A7- Overtopping instantaneous rate (Top) and cumulative overtopping (Bottom) for ST1 event at Point 51.

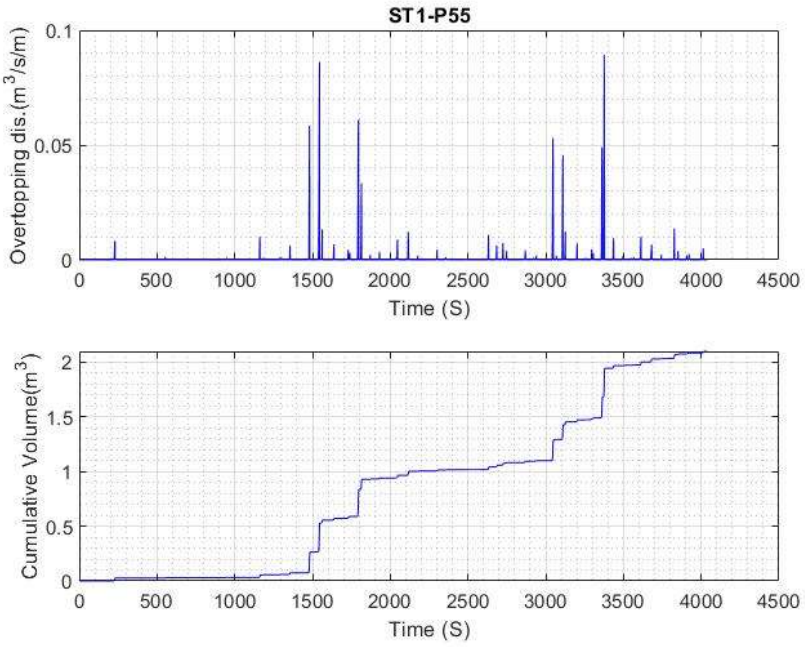

Figure A8- Overtopping instantaneous rate (Top) and cumulative overtopping (Bottom) for ST1 event at Point 55.

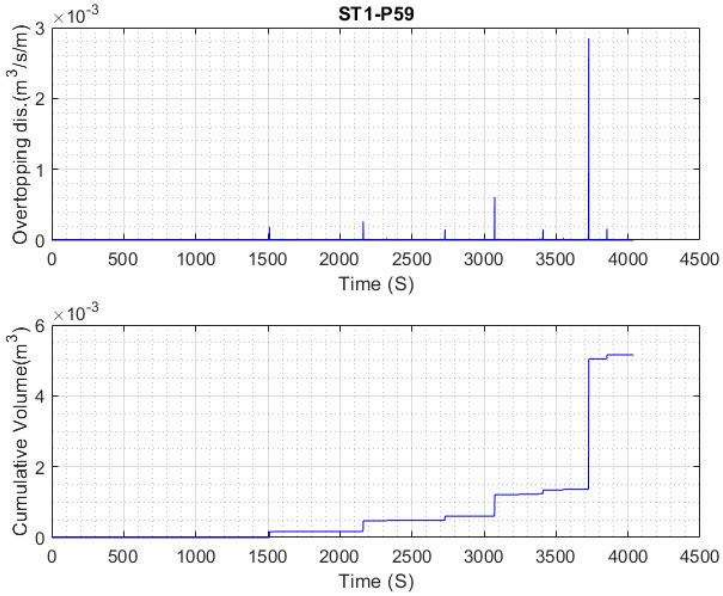

Figure A9- Overtopping instantaneous rate (Top) and cumulative overtopping (Bottom) for ST1 event at Point 59.

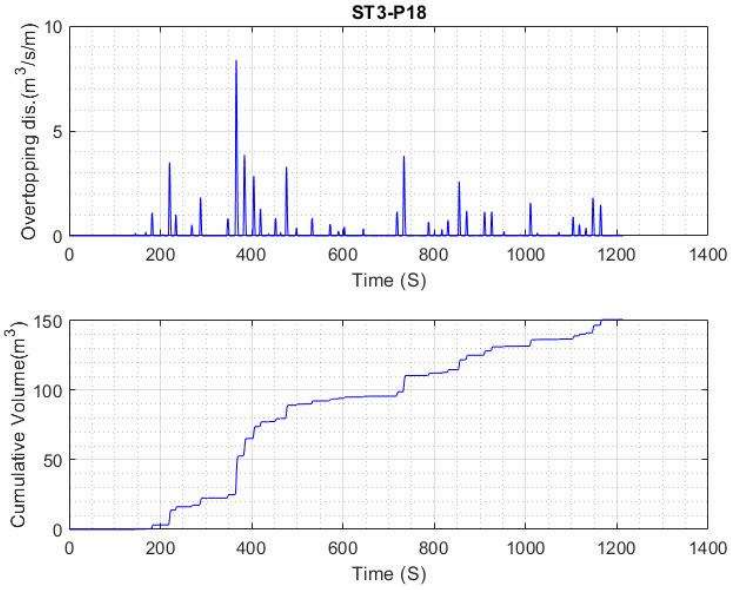

Figure A10- Overtopping instantaneous rate (Top) and cumulative overtopping (Bottom) for ST3 event at Point 18.

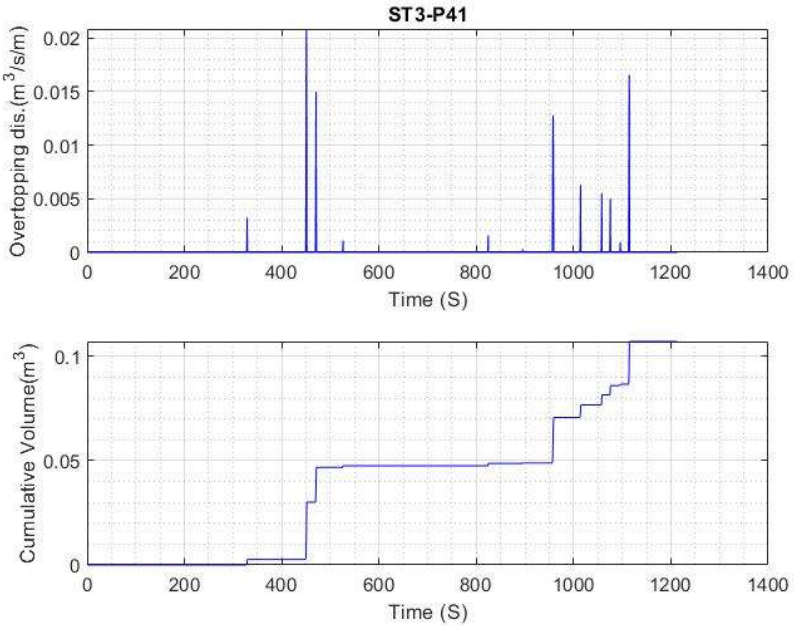

Figure A11- Overtopping instantaneous rate (Top) and cumulative overtopping (Bottom) for ST3 event at Point 41.

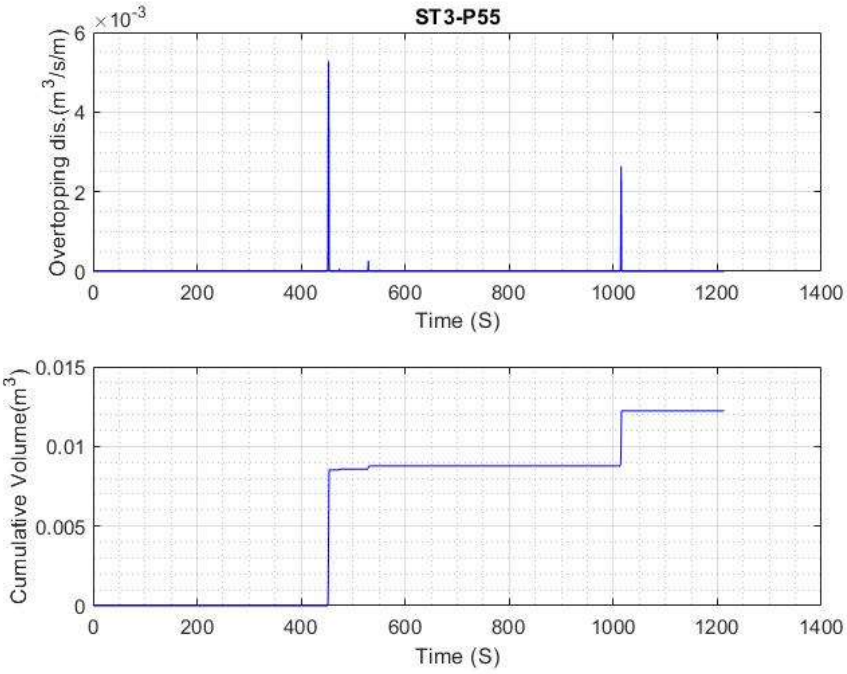

Figure A12- Overtopping instantaneous rate (Top) and cumulative overtopping (Bottom) for ST3 event at Point 55.

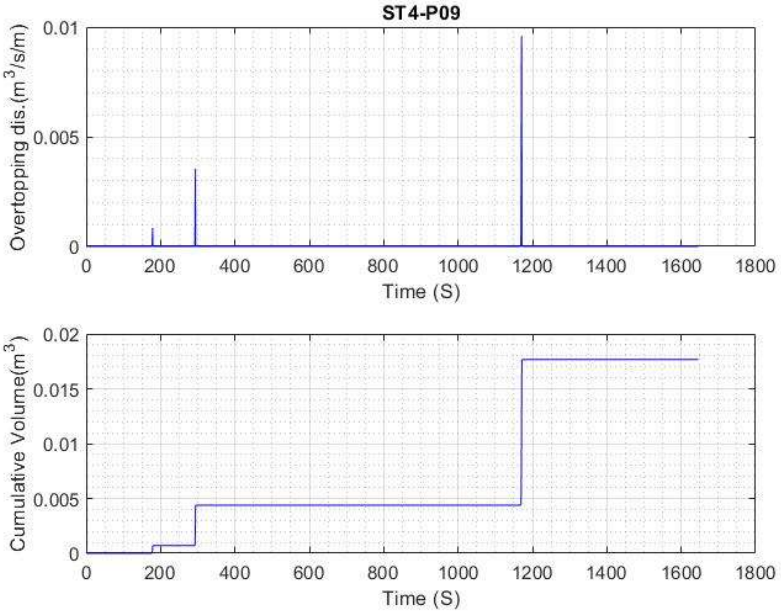

Figure A13- Overtopping instantaneous rate (Top) and cumulative overtopping (Bottom) for ST4 event at Point 09.

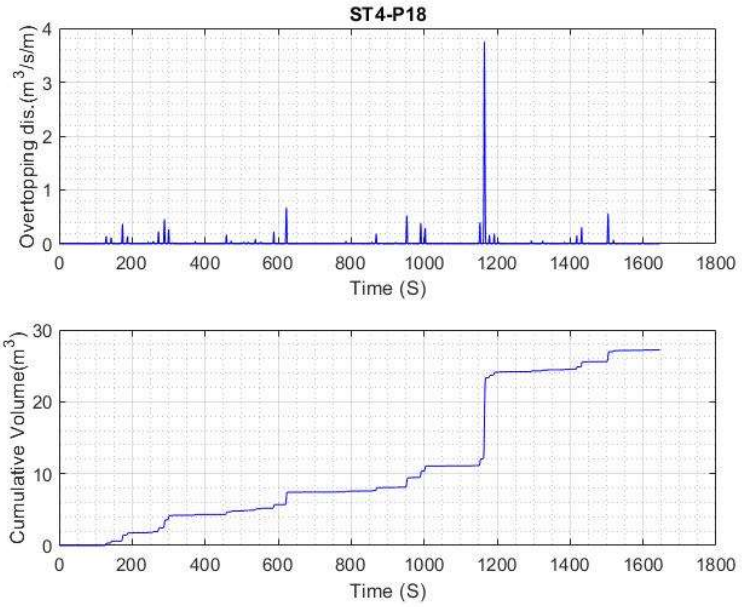

Figure A14- Overtopping instantaneous rate (Top) and cumulative overtopping (Bottom) for ST4 event at Point 18.

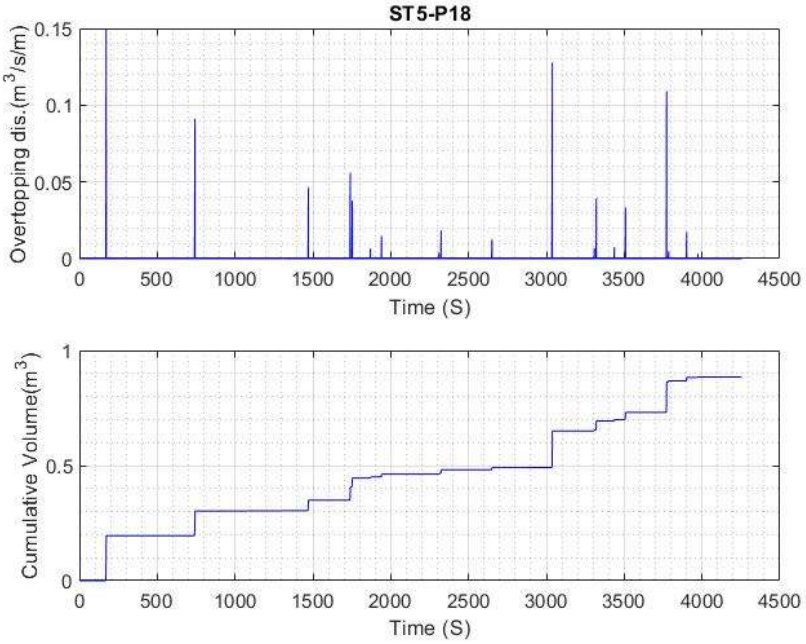

Figure A15- Overtopping instantaneous rate (Top) and cumulative overtopping (Bottom) for ST5 event at Point 18.

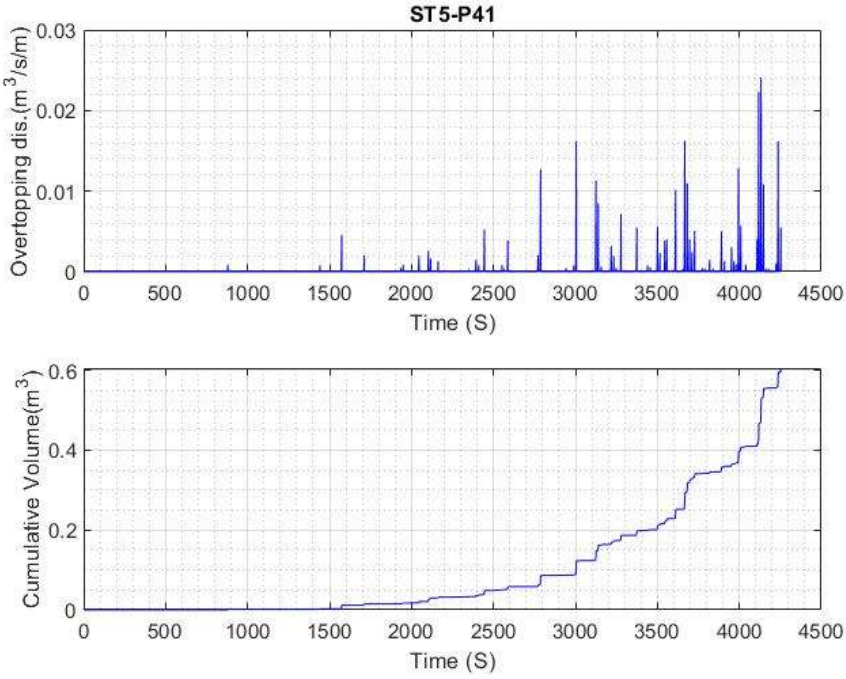

Figure A16- Overtopping instantaneous rate (Top) and cumulative overtopping (Bottom) for ST5 event at Point 41.

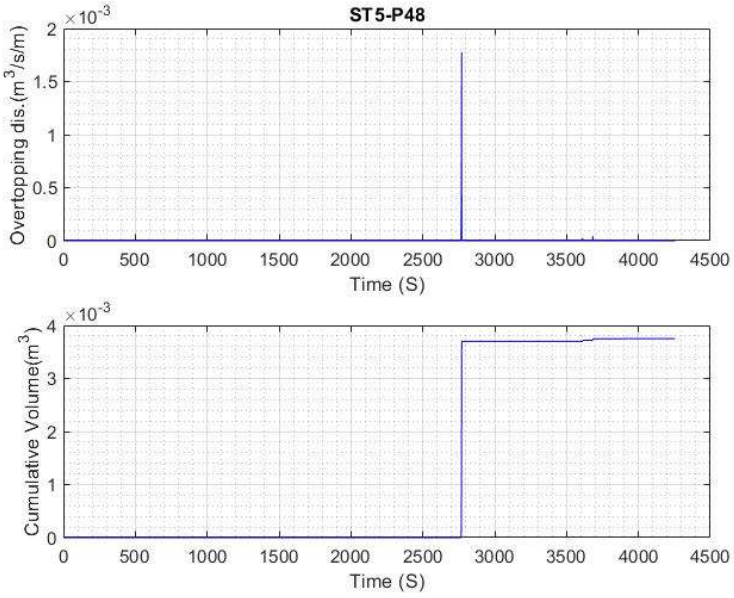

Figure A17- Overtopping instantaneous rate (Top) and cumulative overtopping (Bottom) for ST5 event at Point 48.

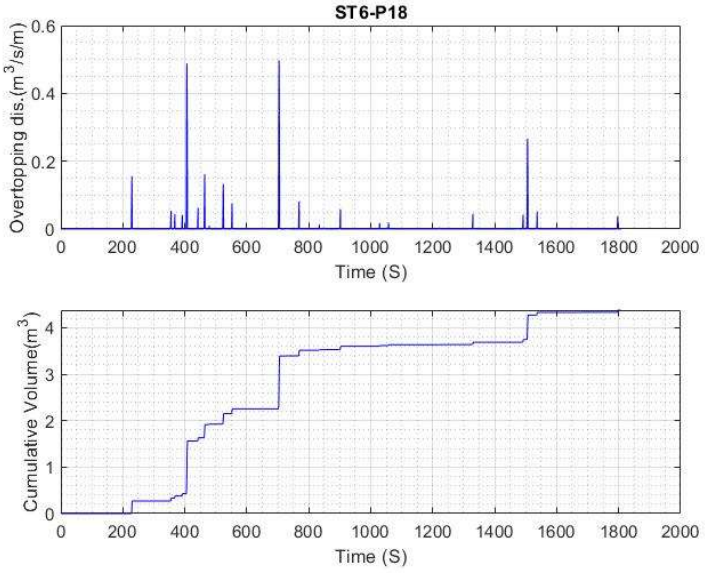

Figure A18- Overtopping instantaneous rate (Top) and cumulative overtopping (Bottom) for ST6 event at Point 18.

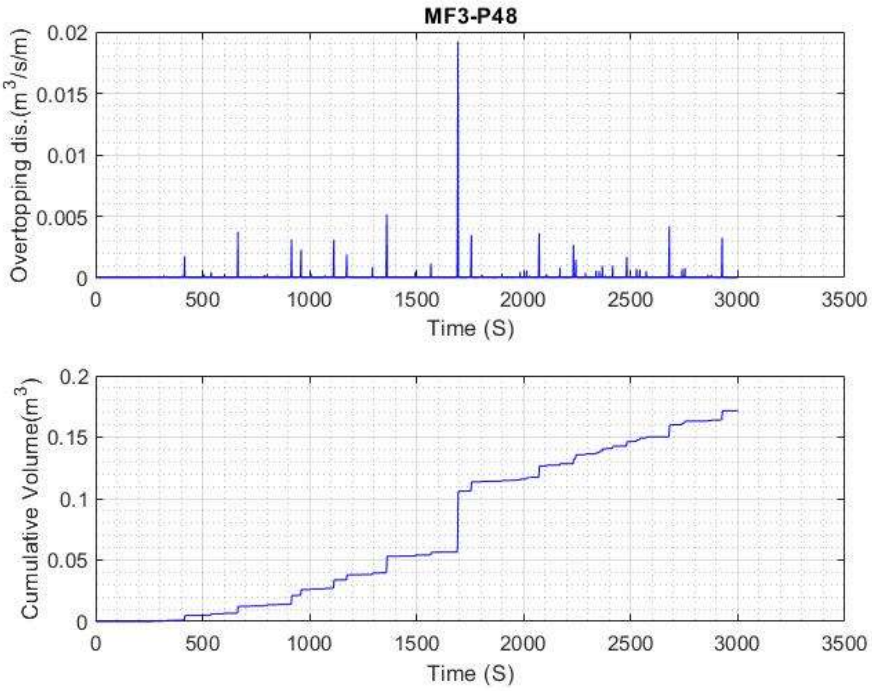

Figure A19-Overtopping instantaneous rate (Top) and cumulative overtopping (Bottom) for ST6 event at Point 48.

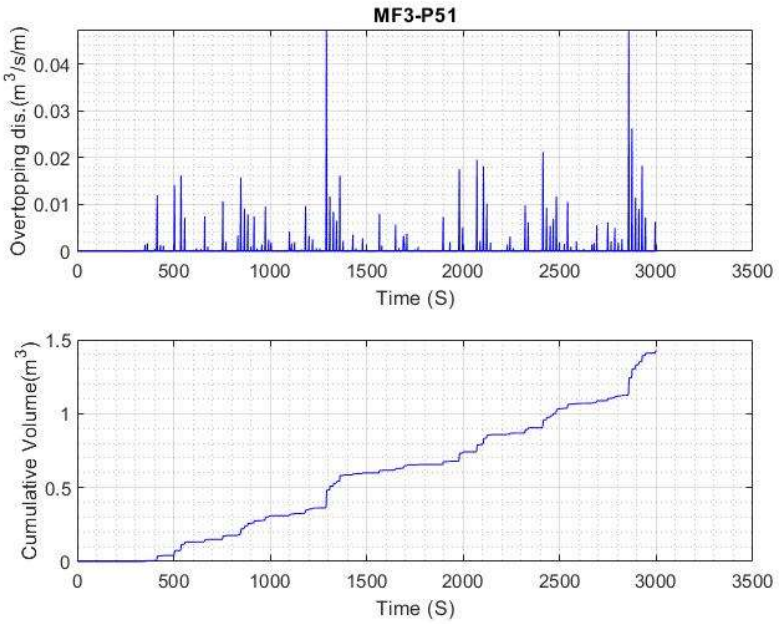

Figure A20- Overtopping instantaneous rate (Top) and cumulative overtopping (Bottom) for ST6 event at Point 51.